OPTIMAL DESIGN AND CONTROL OF COOL THERMAL ENERGY STORAGE SYSTEMS FOR BUILDING DEMAND MANAGEMENT

CUI BORUI

Ph.D

The Hong Kong Polytechnic University

2015

The Hong Kong Polytechnic University

Department of Building Services Engineering

Optimal Design and Control of Cool Thermal Energy Storage Systems for Building Demand Management

Cui Borui

A thesis submitted in partial fulfillment of the requirements

for the degree of Doctor of Philosophy

February 2015

CERTIFICATE OF ORIGINALITY

I hereby declare that this thesis is my own work and that, to the best of my knowledge and belief, it reproduces no materials previously published or written, nor material that has been accepted for the award of any other degree or diploma, except where due acknowledgement has been made in the text.

I also declare that the intellectual content of this thesis is the product of my own work, except to the extent that assistance from others in the project's design and conception or in style, presentation and linguistic expression is acknowledged.

Cui Borui (Signature)

Cui Borui (Name of student)

Department of Building Services Engineering

The Hong Kong Polytechnic University

Hong Kong, P.R. China

ABSTRACT

Abstract of thesis entitled: Optimal Design and Control of Cool Thermal Energy Storage Systems for Building Demand Management

Submitted by : Cui Borui

For the degree of : Doctor of Philosophy

at The Hong Kong Polytechnic University in December, 2014

This thesis presents the investigations on the optimal design and control of cool thermal storage systems for building demand management. The developed strategies include optimal design of active cool thermal energy storage (CTES) for building peak load management, fast power demand response (DR) strategies for buildings involving both active and passive CTES for smart grid applications and optimal design of active CTES for building demand management. These new strategies in different subjects are proposed and validated on a dynamic simulation platform.

A simulation-based optimal design method is developed and used to optimize the capacity of CTES. The quantitative analysis on the life-cycle cost saving potentials of active cold storage systems concerning the operational cost, initial investment and the space cost is also proposed. The optimal capacities of active CTES, monthly/annual operational cost savings and corresponding peak demand set-points are obtained from using the marginal decision rule. Results show that small scale storages can offer substantial annual net cost saving.

Two fast power DR strategies involving both active and passive cool storages are presented. Certain number of operating chiller(s) is shut down at the beginning of the DR event to achieve a significant and immediate power reduction. In the basic fast DR strategy, only chiller power demand reduction is the control objective while in the improved fast power DR strategy, the building indoor temperature during the DR event is the second control objective to control indoor thermal comfort degradation. The results of case studies show that stepped and significant power reduction can be achieved. The power demand reduction and indoor temperature during the DR event can be also predicted accurately.

The life-cycle cost benefit analysis and optimal design of active CTES for building demand management is also proposed. It is assumed that the active CTES is under control of the fast power DR strategy during the DR event. Meanwhile, during the normal days, the active CTES is under control of the storage-priority control to shift peak demand. Based on the different indoor thermal comfort requirements, the optimized capacities of active CTES, the corresponding life-cycle cost saving potentials and the chiller power reduction set-points in the developed fast power DR strategy are then identified. The results show that the optimal capacity of active CTES largely increases with the decrease of the upper limit of indoor temperature set-point.

PUBLICATIONS ARISING FROM THIS THESIS

Journal Papers

2015 **B.R. Cui**. D.C. Gao, S.W. Wang, X. Xue, Effectiveness and Life-cycle Cost-Benefit Analysis of Active Cold Storages for Building Demand Management for Smart Grid Applications, Applied Energy, accepted.

2015 X. Xue, S.W. Wang, C.C. Yan, and **B.R. Cui**, A fast chiller power demand response control strategy for buildings connected to smart grid, Applied Energy, 137: 77-87

2014 **B.R. Cui**, S.W. Wang, C.C. Yan and X. Xue, Evaluation of a Fast Power Demand Response Strategy Using Active and Passive Building Cold Storages for Smart Grid Applications, Energy Conversion and Management, in print.

2014 C.C. Yan, X. Xue, S.W. Wang, and **B.R. Cui**, A novel air-conditioning system for proactive power demand response to smart grid, Energy Conversion and Management, DOI: 10.1016/j.enconman.2014.09.072.

2014 **B.R. Cui,** S.W. Wang, Y.J. Sun, Life-cycle cost benefit analysis and optimal design of small scale active storage system for building demand limiting, Energy, 73: 787-800.

2013 Y.J. Sun, S.W. Wang, **B.R. Cui**, Michael S.C. Yim, Energy performance enhancement of Hong Kong International Airport through chilled water system

integration and control optimization, Applied Thermal Engineering, 60(1-2): 303-15.

Conference Papers

2014 **B.R**. **Cui**, S.W. Wang, C.C. Yan, X. Xue. A compound fast chiller power demand response strategy for buildings. *The 13th International Conference on Sustainable Energy Technologies (SET2014)*, 25-28th August, 2014. Geneva, Switzerland.

2014 **B.R. Cui**, S.W. Wang, and X. Xue. Effects and performance of a demand response strategy for active and passive building cold storage. Submitted to *6th International Conference on Applied Energy (ICAE2014)*, 30, May-2, June 2014, Taipei, Republic of China.

ACKNOWLEDGEMENTS

I would like to express my sincerest appreciation to Professor Shengwei Wang, my supervisor, for his readily available supervision, valuable suggestions, patient encouragement and continuous support during the course of this research. Also, I would like to thank Professor Fu Xiao, my co-supervisor, for her suggestions and support to me over the entire process of my PhD study.

I would also like to thank all colleagues in the research team, especially Dr. Yongjun Sun, Dr. Dian-ce Gao, Dr. Chengchu Yan, Dr. Kui Shan, Dr. Yang Zhao and Dr. Xue Xue. Their talents and diligence always inspire and encourage me to be better.

Finally, I would like to express my deepest appreciation to my girlfriend, Fei Xu, for her comprehensive support and encouragement in the past three years. I would also like to dedicate this thesis to my parents, Jie Cui and Qing Yan, for their unconditional trust and support in my life.

TABLE OF CONTENT

Page

LIST OF FIGURE

LIST OF TABLE

NOMENCLATURE

$a_0 - a_1$	Coefficients
A	Area (m^2)
A_0 *to* A_3	Coefficients
A_h	Heat transfer area of coil pipes in PCM tank (m^2)
A_c	Cross area of coil pipes in PCM tank (m^2)
AHU	Air-handling unit
B	Ratio of the impeller channel depth in the intake position to the depth in the exhaust position
B_0 - B_2	Coefficients
c	Specific heat [kJ/(kg·k)]
$c_0 - c_4$	Coefficients
c_p	Specific heat of PCM [kJ/(kg·k)]
c_{01} - c_{03}, $c_{11} - c_{13}$	Coefficients
C	Thermal Capacitance
CAP	Cooling capacity (kW)
Co	Cost
COP	Coefficient of Performance
CS	Net cost saving
CTES	Cool thermal energy storage
d	Inside radius of tube of PCM tank (m)
$d_0 - d_4$	Coefficients

D,G	Coefficients
DR	Demand response
f	Function
fra	Fraction
Freq	Frequency (Hz)
h	Enthalpy (kJ/kg)
H	Head (kPa or m)
$h_{g,w}$	Enthalpy of water above the reference state (kW/kg)
h_{hyd}	Hydrodynamic losses (kW/kg)
h_{pol}	Polytropical compression work (kW/kg)
h_{th}	Compressor theoretical head (kW/kg)
htc	Heat transfer coefficient [W/(m^2·K)]
H_{pcm}	Melting of freezing latent heat of PCM [kJ/(kg·K)]
HTF	Heat transfer fluid
HX	Heat exchanger
J	Cost function
k	Thermal conductivity [W/(m·K)]
L	Length (m)
Le	Lewis number
M	Flow rate (L/s)
M_{air}	Mass of indoor air (kg)
MCC	Chiller nominal maximum cooling capacity (kW)
M_p	Mass of PCM in PCM tank (kg)

min	Minimum
N	Number
N_{layer}	Layers of tube of PCM tank at radial direction
N_{parts}	Parts of tube of PCM tank at axial direction
NTU	Number of transfer unit
Nu	Nusselt number
P	Power (kW)
PAU	Primary air unit
P_{back}	Pay-back period (year)
PCM	Phase change materials
PD	Peak demand (kW)
PH	Pressure head (kPa or m)
PLM	Peak load management
PLR	Part load ratio
Pow_{low}	Charge set-point (kW)
Pow_{other}	Non air-conditioning power consumption (kW)
Pow_{total}	Total building power consumption (kW)
Pow_{upper}	Peak demand set-point (kW)
Pr	Prandtl number
Q	Cooling capacity (kWh)
Q_{bui}	Heating flux between the indoor air and the building (kW)
Q_{cl}	Cooling load (kW)
Q_{dem}	Cooling demand (kW)

Q_{dis}	Discharge rate of cool thermal energy storage (kW)
Q_{est}	Predicted cooling load (kW)
Q_{loss}	Conduction loss of PCM tank (kW)
Q_{opt}	Optimal storage capacity (kWh)
R	Heat transfer resistance (m^2·K/W)
RadiusF	Inside radius of coil pipe of PCM tank (m)
RadiusN	Boundary of PCM in PCM tank (m)
RA_j	Radius of *j*th PCM layer of PCM tank (m)
R_c	PCM thermal resistance (m^2·K/W)
Re	Reynolds number
SHR	Sensible heat ratio
t	Time duration
T	Temperature (°C)
T'	Temperature after introducing dynamic effects (°C)
T_{ch}	PCM melting or freezing temperature (°C)
T_{eqt}	Equivalent temperature of external heat sources (°C)
u	Velocity (m/s)
u_2	Impeller tip speed (m/s)
U	Heat transfer coefficient of PCM tank [W/(m^2·K)]
V	Volume (m^3)
VFD	Variable frequency drivers
VV	Vapor velocity (m/s)
VV_{r2}	Impeller radial velocity in the exhaust position (m/s)

W_{pi}	Thickness of iron pipe in PCM tank (m)

Subscripts

a	Air
act	Actual
am	Ambient
ann	Annual
b	Building
baseline	Baseline
bui	Building
bypass	Bypass
c	Cost
cd	Condenser
ch	Chiller
char	Charge
chw	Chilled water
cl	Cooling load
coil	Coil
com	Compressor
comp	Component
conv	Convective
ct	Cooling Tower
daily	Daily
dem	Demand

des	Design
dis	Discharge
ef	Effective
est	Estimated
ev	Evaporator
ext	Exhaust?
f	Fluid
flow	Flow rate
fr	Fresh
i	Index
in	Indoor
infil	Infiltration
ini	Initial
inn	Inner
imp	Impeller
inta	Intake
inter	Internal
j	Index
loss	Loss
m	Month
max	Maximum
mean	Mean
min	Minimum

mon	Monthly
n	Index
o	Outdoor
ori	Original
opt	Optimal
ou	Outer
out	Outlet
p	PCM
pr	Pressure
pre	Precooling
pu	Pump
rad	Radiation
rated	Rated
re	Reset
ref	Reference case
rej	Rejection
rtn	Return chilled water
sat	Saturation air
set	Set-point
simu	Simulated
solid	Solid
sto	Storage
sup	Supply chilled water

total	Total
tank	Tank
w	Water

Superscript

k	Sampling time
m, n	Exponentials
p, q	Exponentials

Greek symbols

Π	Efficiency
β	Vane angel
υ	Specific volume
γ	Pre-rotation vane angle
ψ_1, ψ_2	Constants
ς, χ	Constants
ϖ	Coefficient
τ	Time constant
ω	Humidity ratio
$\mathcal{E}$	Heat transfer effectiveness
θ	Capacity flow rate ratio
ΔQ_{bui}	Changing/discharging rate of the building thermal mass (kW)
ΔQ_{demn}	Alteration of the building cooling demand (kW)
$\Delta Q_{pre,c}$	Cooling load alterations due to the precooling (kW)

$\Delta Q_{pre,h}$	Heating load alterations due to the preheating (kW)
$\Delta Q_{set,d}$	Heating/cooling load alterations due to the temperature set-point reset strategies (kW)
$\Delta T_{in,char}$	Temperature set-point differences between the altered cases and the reference case during the charging period (°C)
$\Delta T_{in,dis}$	Temperature set-point differences between the altered cases and the reference case during the discharging period (°C)
α	Ratio of the building outer thermal resistance to the inner thermal resistance
ρ	Density (kg/m^3)
Δt	Time interval (s)
Δx	Space step at axial direction (m)
ΔM_{delt}	Solid or liquid status PCM element mass change (kg)
μ_p	Volumetric storage density of PCM tank (kWh/m^3)
ΔP_{set}	Chiller power reduction set-point (kW)

CHAPTER 1 INTRODUCTION

1.1 Background and Motivations

Due to energy crisis and global warming, the whole world has been paying more attention on the problems of energy and environment. How to reduce the energy consumption and CO_2 emissions while still enhancing life and environment quality becomes the major challenge confronted by the professionals.

Renewable energies are increasingly used in response to the challenges from the depletion of fossil fuels, the dramatic growth of energy demand and global climate change. However, the integration of large amounts of renewable generation, whose capacities depend heavily on weather conditions, e.g. solar density and wind speed, would cause significant stress on the balance of electricity grids. In addition, the imbalance of electricity usage between daytime and night also tends to make the electricity grid be unstable. Any significant imbalance might cause grid instability or severe voltage fluctuations, even grid failures. In order to reduce the fluctuations, additional generating capacities may be needed although they might operate only for a few hours in a year. Therefore, the electricity generation authorities expect balanced use of electricity to achieve optimal generation cost and reduce initial investment. In many countries, the time-of-use electricity price has been adopted to discourage power use at times of peak demand to reduce the generation cost or to avoid grid failure. For consumers, they would benefit in cost saving if altering or reducing the level of

instantaneous demand.

Building sector is one of the major sectors of the energy consumption. According to the 2009 buildings energy data book provided by the U.S. Department of Energy, the buildings sector consumed 74% of U.S. electric energy consumption in 2009, [US, Energy Information Administration, 2010]. While in Hong Kong, the energy consumption of buildings occupied 90% of the total electric energy consumption in 2008, highly surpassing the other sectors, such as industry and transport [Xiao, 2009]. Within the building sector, the heating, ventilation and air conditioning (HVAC) systems are the major contributors to the energy consumption of buildings, which even consume 60% of the building energy in hot climate locations. Furthermore, the energy consumption of HVAC is still increasing with the increasing demand for thermal comfort. Therefore, proper management of the building energy use will be not only essential for the reliable operation of the whole grid but also beneficial in cost saving for the building owners.

During the past few decades, technologies and practices to minimize energy and cost consumption in buildings design and operations have been adopted to with great success. Electricity cost minimization in building operations requires close attention on the efficiency of equipment in buildings, electricity price structures which consider the time and the quantity of electricity used, and the demand response (DR) programs, driven by certain emergency events and provided by regional transmission operators (RTOs) or independent system operators (ISOs).

Table 1.1 summarizes three main technologies for advanced building energy demand management, namely efficiency and conservation, peak load management and demand

response [Motegi et al, 2005]. The term "demand management" is defined as "the planning, implementation and monitoring of those utility activities designed to influence customer use of electricity in ways that will produce desired changed in the utility's load shape, i.e. changes in the pattern and magnitude of a utility's load." [Arteconi et al, 2012].

Table 1.1 Building demand management terminology and operations

	Efficiency and Conservation (Daily)	Peak Load Management (Daily)	Demand Response (Dynamic Event Driven)
Motivation	Economic; Environmental protection; Resource availability;	Time of use savings; Peak demand charges;	Reliability Emergency supply
Operations	Integrated system operations	Demand limiting Demand shifting	Demand shedding Demand shifting Demand limiting

High energy efficiency refers to the reduction in the energy use while providing the same level of services. Energy conservation aims to reduce unnecessary energy use. Both energy efficiency and conservation provide environmental protection and cost savings. Energy efficient operation is a key objective in new building commissioning and retro-commissioning for existing buildings [Wang and Ma, 2008]. Energy efficiency is typically improved by the two important measures: optimal passive designs of the building, including orientation, shape, shading, envelop, glazing, passive system and etc., and optimal active control of devices/systems such as local and supervisory controls [Escrivá-Escrivá, 2011].

Peak load management is usually motivated by high charges for peak demands or time-

of-use rates. Normally, buildings owners are commonly charged for electricity consumption based on energy consumption and peak demand. Demand is defined as the total energy consumed during a billing interval e.g. a month [Sun et al, 2013]. Peak demand is the maximum demand over the billing period. The peak demand charge in buildings tends to be significant, which may account for more than 50% of overall electricity bill. For customers, a more efficient system and money saving can be achieved if they take advantage of different electricity prices during peak and off-peak hours. For utilities, the peak demand of the grids can be accordingly reduced. Therefore, peak load management is usually performed to reduce the peak demand, which results in substantial saving of peak demand cost [Motegi et al, 2005].

Demand response (DR) is event-driven and can be defined as short-term modifications in customer end-use electric loads in response to contractually obligated and voluntary curtailment requested [Escrivá-Escrivá, 2011]. DR is promoted with the emerging of the smart grid. Smart grid with new characteristics, e.g. energy efficiency, low emission, flexibility, reliability, high quality, security, cost-effective, etc., has been considered as a promising solution for future grid in the plans of many countries.

The DR programs published by Regional Transmission Operators (RTOs) or Independent System Operators (ISOs) often give customers load reduction incentives that are separate from, or additional to, their retail electricity rates, which may be fixed (based on average costs) or time-varying. The load reductions are needed and requested when the grid operator thinks reliability conditions are compromised.

Buildings can play an important role in DR programs by actively reducing their power consumption during peak hours. The HVAC systems, which account for the largest

section of the power consumption of the buildings on average, are the main contributor for demand response in buildings. There are several reasons why the HVAC systems can be an excellent demand response resource [Motegi et al, 2005]. First, HVAC systems contribute the largest portion of electricity consumption in buildings. Second, the operation of HVAC systems normally can be temporarily curtailed without immediate and serious impact on building occupants. Third, the inherent physical response capacity of HVAC load can match the fast, short, less frequent DR requirement.

Two main categories of DR strategies for HVAC systems were summarized by Watson et al. [Watson et al, 2006], which are global temperature adjustment and cooling system adjustment. Global temperature adjustment is done by increasing building zone temperature set-points during DR event in summer. Cooling system adjustment includes duct static pressure set-point reduction, fan quantity reduction, chiller quantity reduction and etc. The related studies have been proposed and the performance investigation of the HVAC DR strategies was also conducted.

In recent years, cool thermal energy storage (CTES) is considered as one promising conservation technology to improve the efficiency of building operation. CTES removes heat from a thermal energy storage medium during periods of low cooling demand [ASHRAE, 1993]. CTES can provide higher energy efficiency and energy conservation. As CTES can provide additional cooling capacity during discharging process, the chiller in HVAC system tends to be operated at high part ratio where the efficiency of chiller is high. In addition, CTES system can meet the same total cooling demand during a given period, with a smaller cooling capacity, as a non-storage system.

CTES used for peak load management in buildings is also a very active area [Sun et al, 2013]. Especially, many efforts have been made to develop different strategies with different CTES facilities. In recent decades, CTES system has demonstrated a capability to shift loads from high-peak to off-peak periods, so they have the potential to become a powerful instrument in building demand side management [Arteconi et al, 2012]. For reducing the monthly peak demand or monthly operating cost, different control or design strategies were proposed for CTES systems.

Passive CTES, such as building thermal mass (BTM), has been utilized through implementing global temperature adjustment plus pre-cooling strategies due to the considerable capacities and resistances. The passive CTES is discharged by increasing the indoor temperature set-point and charged by precooling the zones before working hours. Therefore, the thermal capacities of building thermal mass can be utilized to shift the cooling load during DR event for achieving the demand-saving targets while reducing the negative impacts on building indoor thermal comfort.

However, the storage capacities resulted from most previous studies in peak load management were usually quite large, e.g. coping with more than 40% daily cooling load normally, which may require very significant initial costs and spaces. It is in fact that the relationship between operational cost saving potential and capital cost of CTES has not been sufficiently explored. In addition, the computation processes in the previous studies were usually complicated.

Concerning the previous studies on HVAC DR strategies, the developed DR strategies (e.g., normally global temperature adjustment) is hard to provide power demand reduction fast enough during DR events in response to the sudden electricity price rise

or urgent grid reliability problems. Therefore, these strategies may fail to meet certain need, i.e. ancillary services which are those functions required to maintain a balance between generations and loads in near real-time [Kirby, 2006]. Besides, effective demand reduction prediction methods are still inadequate. The accurate short-term prediction of single building electricity consumption can facilitate the electricity load prediction of whole district/regions which is important for optimizing the operation and production of a smart grid and accordingly improve both the grid efficiency and electricity service quality [Soares and Medeiros, 2008].

Once integrated with the HVAC, the active CTES can effectively reduce the building demand for several hours when requested from ISOs or RTOs. The cooling load can be shifted and reduced by discharging the active CTES system for several hours without sacrificing the building indoor thermal comfort too much. The power consumption of HVAC system can be accordingly reduced. Therefore, for the building users, the use of active CTES can increase cost benefits brought by the DR programs. For the ISOs and RTOs, the use of active CTES in buildings can provide longer duration and larger amount of demand response with higher quality. But little research has systematically studied and implemented in the active CTES integrated with the HVAC system to supply demand response.

To address the above issues, , the research in this thesis , therefore, focuses on developing optimal design and control strategies of CTES for building demand management. The major works include optimal design of active CTES for building peak load management, fast power demand response strategy for building involving active and passive CTES and optimal design of active CTES for building demand

management.

1.2 Aim and Objectives

The aim of this study is to develop the optimal design and control strategies of the cool thermal energy storage (CTES) when it is integrated with the building HVAC system for building power demand management. The aim can be accomplished by addressing the following major objectives:

1. Construct a dynamic simulation platform for complex building central chilling systems to dynamically and accurately simulate the whole HVAC system performance and the heat exchange processes in buildings for testing and validating the developed strategies.
2. Develop a simplified active storage tank model with acceptable accuracy and good reliability for analyzing the system performance with different system configurations. The model concerns computation speed and program size when implemented in large scale system simulations.
3. Develop an optimal design method of small scale active CTES for building demand limiting. It is one more meaningful and effective design strategy to optimize storage capacity concerning life-cycle cost saving involving both operational cost saving and capital cost associated to storage capacity. The factors which impact the optimal capacity of active TES, such as electricity price structure and building power consumption profile, should be considered.
4. Develop and validate the fast power demand response strategies for buildings involving active and passive CTES for smart grid applications. The developed

control strategies aim at providing immediate and significant power reduction when requested. It is expected to obtain accurate building power reduction and building indoor thermal comfort level prediction during DR events.

5. Conduct quantitative analysis on the developed fast power demand response strategies. The quantitative relation between costs (including cost concerning indoor thermal comfort degradation and the capital cost of the active storage) and benefits (including average demand shed and the corresponding intrashed variability) can facilitate the decision maker and the interested parties to evaluate the effects of the strategies comprehensively and to make proper choices concerning their interests.

6. Propose economic analysis and optimal design of active CTES in buildings for building demand management. Both benefits from building demand shifting under certain electricity price structure and participating in a DR program provided by grid managers to provide fast demand response are concerned.

1.3 Organization of the Thesis

The thesis is divided into 8 chapters. The main content of each chapter is presented as follow.

Chapter 1 outlines the motivation of the research by presenting the needs of optimal design of CTES for building peak load management, fast power demand response strategy for building involving CTES and economic analysis of CTES for building demand management. The aim and main objectives are also included in the chapter.

Chapter 2 presents a comprehensive literature review of the related existing studies on the developments and applications of optimal design and control of CTES for building demand management. The chapter also describes the research gaps which are intended to be bridged in this thesis.

Chapter 3 describes the complex central chilling systems in three studied buildings with different scales, including a supper high-rise commercial building, a middle scale shopping center and a small scale building located in Hong Kong Polytechnic University (PolyU) campus. Based on the central chilling systems, the dynamic simulation platforms are constructed. The major components and their interconnections are presented to test the developed strategies. The developed optimal design and control strategies of CTES for building demand management are tested on this platform to analyze and evaluate their performances.

Chapter 4 presents a simplified physical dynamic model of coils storage tank for analyzing the system performance with different configurations. The accuracy, reliability, computation speed and control stability are carefully considered during the development of this model.

Chapter 5 presents a simulation-based optimal design method for active CTES systems used for demand limiting control under time-of-use plus peak demand charge electricity price structure. The marginal decision rule is introduced to determine the optimal capacity of CTES for achieving maximum annual net cost saving under demand limiting control. The peak demand set-points of each month are determined to maximize peak demand reduction corresponding to the optimal capacity of CTES. The optimal capacity of CTES concerns the life-cycle cost saving potentials involving both operational cost-

saving and capital cost associated to capacity of CTES. The performance of the developed optimal design method, including the resulted storage capacity and the corresponding cost saving potential, is evaluated and the main factors that determine the results are also discussed in the case studies.

Chapter 6 focuses on development and validation of fast power demand response strategies for buildings involving both active and passive CTES. The strategies aim to provide immediate demand response by altering the real-time energy use when requested to support the demand response of buildings connected to smart grids. The fast power demand response strategies are developed by two steps. At the first step, only demand reduction is the control objective and the corresponding impacts on building indoor thermal comfort is discussed. At the second step, the primary control objective is to control the level of indoor thermal comfort degradation and the second control objective is to control the power reduction under set-point during the DR event. Accurate demand reduction and building indoor thermal comfort prediction methods are also developed. A set of parameters are introduced to characterize the demand reductions under control of the developed strategy. The quantitative analysis on the developed strategy concerning the required active storage capacity, the indoor thermal comfort and the quantity as well as quality of power reduction during the DR event is also presented.

Chapter 7 presents the economic analysis when using active CTES for building demand management including demand limiting during the normal day and fast demand response during the DR event. The optimal design method, presented in Chapter 3, is used to optimize the capacity of CTES and determine the corresponding life-cycle cost

saving potentials. The acceptable building indoor thermal comfort degradation is one important limitation to restrict the achievable demand response capacity.

Chapter 8 summarizes the main contributions of the work conducted in this PhD projects, and gives recommendations for future research on the subject areas concerned.

CHAPTER 2 LITERATURE REVIEW

This chapter provides a comprehensive review on the existing studies associated with CTES and HVAC demand response strategies. Section 2.1 presents an introduction of CTES, including types, storage medium and characteristics of CTES as well as the advantages of CTES. In Section 2.2, the previous studies on the design and control of CTES systems for peak load management are summarized, such as conventional control and optimal design and control of active and passive CTES. The HVAC demand response strategies are introduced in Section 2.3, including conventional HVAC demand response strategies as well as the performance and effect investigation of HVAC demand response strategies. A summary of this chapter is given in Section 2.4.

2.1 Cool Thermal Energy Storage Systems

2.1.1 Introduction

Cool thermal energy storage (CTES) systems normally remove heat from a thermal storage medium during periods of low cooling demand [ASHRAE, 1993]. The stored cooling is later used to meet an air-conditioning (AC) or process cooling load. The cool storage medium can be chilled water, ice, or a eutectic salt phase change material. Early refrigeration systems used blocks of ice cut from frozen lakes as stored cooling. With the advent of mechanical refrigeration, most stored cooling systems were replaced by instantaneous cooling systems sized to meet the maximum expected load at any time.

Interest in CTES for commercial applications grew in the 1970s and 1980s, when

electric utility companies recognized the need to reduce the peak demand on their generation and distribution systems. For many utilities, the peak system demand is driven by the air-conditioning load on the hottest days of the year [ASHRAE, 1993]. They realized that if cooling could be generated and stored during off-peak periods for later use, more on-peak generating capacity, as an expanded cooling capacity, would become available [Elleson, 1997]. Furthermore, off-peak capacity would be utilized more efficiently.

Many utility companies began to offer financial incentives in the form of specialized rates, peak demand charges, rebates, and subsidies to encourage customers to shift their on-peak power demand and energy consumption to off-peak periods. This encouragement has resulted in rapid growth in the popularity of CTES for air-conditioning in buildings since the primary benefit of cool storage is its ability to substantially reduce operating costs [Elleson, 1997].

CTES technology is an effective means of shifting peak electrical loads as part of the strategy for energy management in buildings. Such systems can help the electrical utilities reduce on-peak loads and increase the load during off-peak periods [Hasnain, 1998]. The building operating cost saving is achieved because cool storage systems reduce the expensive on-peak electric power demand, use less expensive nighttime power to do the same job instead.

The CTES has the following advantages:

- This shifting of load improves the utilization of base load generating equipment, thereby reducing the reliance on peaking units which have higher operating costs.

- The electric utilities benefit from a reduction in peak and accordingly reduce the reliance on peaking units which have higher operating costs, and customers also benefit with lower electricity bills, depending upon the electricity price structure, as the CTES system allows customers to take advantage of lower off-peak rates for electric energy and reduced peak demand billing charges. By using cool storage, the cooling system could be operated during the off-peak night time hours when the cooling load is low. The required cooling during day time could then be supplied by discharging the cool storage medium rather than operating the chillers. Therefore, benefits can be received by both the consumer (lower energy cost, better space temperature control) and the utility (higher load factor, lower capital investment in new generating equipment) [Hasnain, 1998].

- In addition, a cool storage system meets the same total cooling load in a given period as a non-storage system but with a smaller cooling capacity. Often, the money saved by downsizing chillers can offset the cost of adding a cool storage medium. Some cool storage technologies facilitate further cost reductions by making the use of lower supply air and supply water temperatures practical and cost effective. Air and water distribution equipment can be downsized when supply temperatures are reduced and operating differentials are increased [ASHRAE, 1993].

- By decoupling chiller operation from instantaneous load, cool storage systems also increase chiller efficiency due to lower condensing temperatures during nighttime operation [ASHRAE, 1993].

2.1.2 Types and storage medium

CTES can be further divided into "active" and "passive" storage systems which are formed in different ways to provide different functions. "Active" denotes that thermal storage systems, such as ice storage, require an additional fluid loop to charge and discharge the storage or to deliver cooling to the existing chilled water loop [Henze et al, 2004]. The passive means that the use of CTES as well as melting and freezing of CTES medium are realized without resort to mechanical equipment, e.g. the use of building thermal capacitances through nighttime pre-cooling is "passive" [Zhu et al, 2009].

Active CTES

Active CTES can be classified according to the type of thermal storage medium and the way the storage medium used. Normally, active CTES media include chilled water, ice, Eutectic salts (PCM). These media mainly differ in their storage capacities, the change in temperature or phase change temperature of the material at which cooling is stored, the required refrigeration equipment type and etc., as listed in Table.1.2. Chilled water (Water) systems offer the lowest energy storage density, and are the least complex. But the cost of water system is the lowest. Ice systems offer the highest energy storage density but the required refrigeration equipment is different from the other, e.g. chillers for lower chilled water temperature are needed for ice making resulting lower chiller coefficient of performance (COP). The Eutectic salts (PCM) storage has relatively large latent heat capacity compared with water storage systems. It also allows the conventional refrigeration equipment, e.g. chillers, to meet the charging temperature requirement offering higher COP. It is therefore more convenient and economically

beneficial to employ PCM storage systems in buildings. These medium determines how large the capacity of storage system will be and the corresponding configuration of the HVAC system and components. The details of the above medium are shown in the following [Ibrahim and Rosen, 2002].

Chilled water active CTES: Employing chilled water to store cool energy is a well-known method in many countries to save energy by shifting power consumption from the peak hours in the day to the night-times [Mackie and Reeves, 1998]. Under ideal conditions, the water is stored inside the tank in stratified layers for later use in meeting cooling needs. During the discharge mode, chilled water is supplied from the bottom of the tank and is returned to the top of the tank at low flow rates to minimize the mixing of the layers. The cooling capacity of the system depends on the temperature differential across the stratified storage tank. Chilled water active CTES uses conventional water chillers, operating under the same general conditions for storage as for conventional AC systems. During the past decade, many different types of chilled water CTES designs were developed and employed in the field prior to the successful evolution of thermally stratified system [Yau and Rismanchi, 2012]. Primarily designs were in the manner to avoid temperature mixing of chilled water with return water. However, they often require more complex tank configurations and piping systems which are more expensive.

However, the practice of Chilled water CTES has proved much more difficult than the theory. The first problem is storage volume. Each cubic meter can only provide 5.8 kWh of cooling if the temperature rise of 5°C is used. Therefore, the volume requirements are enormous and tend to discourage the use of chilled water storage. The second design

consideration in Chilled water CTES systems is the need to isolate the cold water from the return warm water. Various methods were employed to maintain separation between the stored supply water and the warmer stored return water. Mixing cannot be allowed otherwise cooling capacity will be lost [Hasnain, 1998]. Thirdly, complex tank configurations or piping systems, which are expensive and difficult to operate, is required.

Ice active CTES: Among all the available CTES systems, the use of ice due to its high latent heat of fusion (333 kJ/kg) was considered as the most popular technique during the past decade, especially when the available space is limited. To store cooling in ice, chiller is required to provide charging fluids at temperature below the normal operating range of conventional chiller. Therefore, special ice-making equipment instead of standard chillers for low temperature service is used.

Table 2.1 Primary features of active CTES media [Hasnain, 1998]

	Chilled Water	Ice	Eutectic salts (c)
Specific heat (kJ/kg•K)	4.19	2.04	-
Latent heat of fusion (kJ/kg)	-	333	80-250
Chiller type	Standard water	Low temperature secondary coolant	Standard water
Tank volume	0.089-0.169 m^3/kWh	0.019-0.023 m^3/kWh	0.048 m^3/kWh
Storage installed cost	$8.5-$28/kWh	$14-$20/kWh	$26-$83/kWh
Charging temperature	4-6˚C	-6 - -3˚C	4-6 ˚C
Chiller charging efficiency	5.0 - 5.9 COP	2.9 - 4.1 COP	5.0 - 5.9 COP
Discharging temperature	1– 4 ˚C	1- 3˚C	9- 10˚C
Discharging fluid	Water	Secondary coolant	Water
Maintenance	High	Medium	Medium

With ice as the storage medium, there are several technologies available for charging and discharging the storage:

Ice harvester systems feature an evaporator surface on which ice is formed and periodically released into a storage tank which is partially filled with water. During the charging period, the ice is formed on the plate's surface of the evaporator. A circulating pump brings the water at a temperature at 0°C on the outer surface of the evaporator, which is fed internally with liquid refrigerant. During the discharging period, the chilled water that circulates through the storage tank for further reducing the water temperature to cope with the load [Chan and Chow, 2006].

Ice slurry systems store water or water/glycol solutions in a slurry state (a partially frozen mixture of liquid and ice crystals that looks like slush). The ice is formed by passing the solution through the pipes submerged in an evaporating refrigerant. The evaporating refrigerant cools the solution and produces a suspension of ice crystals. The small ice particles are pumped or dropped directly into the storing tank.

In the external melt ice-on-coil systems, the ice is formed on the outer surface of the heat exchangers coils submerged in an insulated open tank of water [Lee and Jones, 1996]. During the charging procedure, a liquid refrigerant or a glycol solution circulates inside the heat exchanger coils and produces ice on the outer surface of the coil. During the discharging process, the returned water from the load circulates while passing through the ice tank and cooled down by direct contact with the ice [Shi, 2005].

In the internal melt ice-on-coil storage systems, the heat transfer fluid such as the glycol solution circulated through winding coils submerged in tanks filled with water. During charging, the glycol solution with lower temperature (-6°C to -3°C) flows through the

coils inside the tank and produces ice on the coil's outside surface [Zhu and Zhang, 2001]. The storage is discharged by circulating warm coolant through the pipes and melting the ice from the inside. The cold coolant is then pumped through the building cooling system or used to cool a secondary coolant that circulates through the building's cooling system.

An encapsulated ice storage system consists of numbers of spheres or rectangular plastic capsules of water immersed in a secondary coolant such as ethylene glycol in a steel or concrete tank. In the United States, rectangular containers of approximately 0.017 m^3 and 0.0042 m^3 size and dimpled spheres of 100 mm diameter capsules are available. The capsules are usually made of a high-density polyethylene that is able to bear up the pressure due to the water expansion. During the charging period, a low temperature solution (-6°C to -3°C) passes through the tank and freezes the water inside the capsules. In the discharging period, the warm solution returns from the load to the tank and melts the ice [Erek and Dincer, 2009].

A major drawback of ice CTES is that the chiller evaporator temperature must be lower than that for a chilled water CTES, so chiller capacity and COP are decreased. For water CTES, the evaporation temperature of an ordinary chiller is in the vicinity of 0 $^{\circ}$C. For ice CTES, however, evaporator temperatures are often below -10°C so that the capacity and COP are reduced to about 56% and 72% of those of water CTES system respectively.

Eutectic salts (PCMs) active CTES: There are a large number of materials, which can be identified as phase change materials (PCMs) from the point of view of melting temperature and latent heat of fusion [Pasupathy et al, 2008]. PCM can be divided into

organic and inorganic categories. Organic materials are further divided into paraffin and non-paraffin (e.g. fatty acids). Inorganic materials consist of compounds and eutectics.

In CTES applications, the PCMs can be integrated into building covering materials such as concrete, gypsum wallboard and plaster, as part of building structures for lightweight or even heavy weight buildings to increase the thermal mass. Here, the PCM is used as the storage media for passive CTES. They can also be installed in water circuits or air circuits of HVAC systems as thermal energy storage tank to provide functional purposes. In this case, the PCM is used as the storage media for active CTES.

Eutectic salts is one main kind of PCMs and another commonly used medium to store cooling energy in active CTES. A eutectic material is a composition of two or more components, which melts and freezes congruently forming a mixture of the component crystals during crystallization [Oró et al, 2012]. Normally, the material is encapsulated in plastic containers that are stacked in a storage tank through which water is circulated. The most commonly used mixture for thermal storage freezes at around 8°C. Therefore, the eutectic salts can be charged with typical conventional chilled water temperature of 4 to 7°C. This allows the addition of storage to existing systems with no modifications to existing chillers and few changes to existing distribution systems. Eutectic salt systems can be arranged in chiller upstream or chiller downstream configuration. The chiller upstream arrangement can be used with full storage operating strategies or where no further cooling of the storage discharge is required. The chiller downstream configuration allows the water leaving storage to be cooled by the chiller to the required supply temperature [ASHRAE, 1993].

Passive CTES

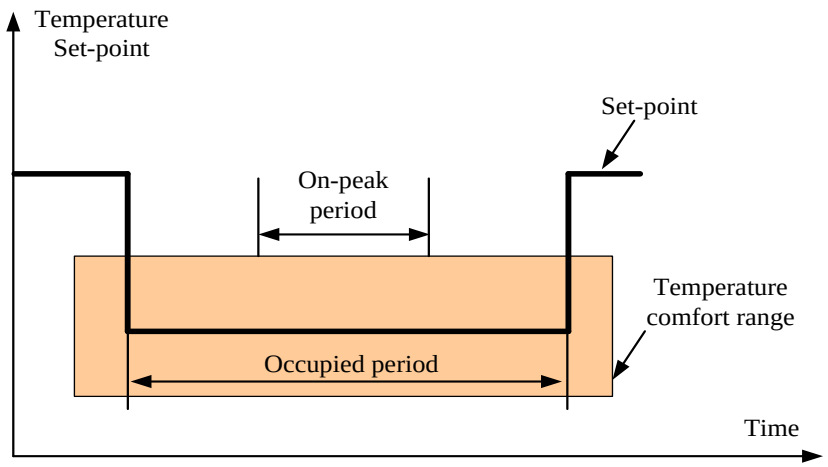

Fig.2.1 Conventional night setup control strategy

The BTM as TES is mainly used for load shifting. In conventional control strategies, the thermal storage of a building is not utilized for reducing operating costs, as shown in Fig.2.1. When the building is not occupied, the thermostat is set up to a higher temperature for cooling since the equipment is generally off during these periods. The start algorithms determine the time for turning equipment on so that the building becomes occupied. The goal of these algorithms is to minimize the pre-cooling time. During occupied hours, the zone conditions are typically maintained at constant set-points. For these conventional night setup/setback strategies, the assumption is that BTM works to increase operating costs. A massless building would require no time for pre-cooling and would have lower overall cooling loads than actual buildings. However, under proper circumstances, use of a BTM as a TES for building demand management can significantly reduce operational costs, even though the total cooling load may increase [Braun, 2003].

At any given time, the cooling requirement for a space is due to convection from internal gains, i.e. lights, equipment and people and interior surfaces. Since a significant

fraction of the internal gains is radiated to interior surfaces, the state of BTM dictates the cooling requirement. Pre-cooling of the building during unoccupied times reduces the overall convection from exposed surfaces during the occupied period as compared with night setup control and can accordingly reduce day-time cooling requirements. The potential for storing cooling energy within the structure and furnishings of conventional buildings is significant when compared to the daily cooling load requirements. Typically, internal gains are on the order of 3-7 W per square foot of floor space. The thermal capacity for typical concrete buildings structures is on the order of 2-4Wh/$^{\circ}$F per square foot of floor area (12-24Wh/$^{\circ}$C •m^2). Thus, for an internal space, the energy storage is on the order of 1hr for every $^{\circ}$F (0.5°C) of pre-cooling of the BTM [Braun, 2003].

For use in passive CTES, the PCMs in buildings can provide different functions for different applications. They can be used for enhancing the free cooling of buildings, building peak demand shifting, solar energy utilization, waste heat recovery, etc. PCMs are normally integrated into building envelops (i.e. walls, roofs, and floors), being part of building structures to increase the building thermal mass [Zhu, 2010].

During daytime, the PCM undergoes a melting process by absorbing part of heat flowing though the building structure. During night, the PCM solidifies and releases the stored heat into surrounding environments when outdoor or indoor temperature falls. Therefore, they can prevent the indoor environment from overheating during daytime in hot summer and provide heat for space heating during night in cold winter [Zhu, 2010].

Due to the ability to provide high energy storage density and the characteristics to store cooling at relatively constant temperatures, PCMs as passive TES media in buildings

have attracted increasing attention for developing low energy or energy efficient buildings. Many scientists, environmentalists and international communities are now taking an interest on the applications of PCMs in buildings to enhance their thermal and energy performance.

However, the successful use of PCMs in buildings depends on many factors, such as the type and quantity of PCMs used, the encapsulation method used, the location of PCMs in building structures, building design and orientation, equipment design and selection, climate condition, utility rate policy, occupancy schedule, system control and operational algorithms, etc. To properly use PCMs in buildings, a good knowledge on the energy performance and dynamic characteristics of PCM is needed.

2.2 Design and Control of Cool Thermal Energy Storage for Peak Load Management

2.2.1 Introduction

Owners of (commercial) buildings are commonly charged for electric power based upon energy consumption [Sun et al, 2013] (i.e. kWh) and peak demand. Demand is defined as the energy consumed during a demand interval and peak demand is the maximum demand over a specified billing period, e.g. a month. The cost of peak demand in commercial buildings is usually more than 50% of the overall electricity bill. Peak load management has been conducted in many buildings to minimize the impact of peak demand charge [Motegi et al, 2005].

Although electricity rate structures from utilities differ from each other, a common feature can be found that large price differences exist between different periods. For the

period with a lower electricity price, it is usually denoted as ‘‘off-peak period’’. In contrast, the period with a higher price is usually denoted as ‘‘on-peak period’’. The price difference is a direct and effective incentive which encourages building owners to alter their load profiles using different peak load management methods, e.g. load shedding and load shifting.

For decades, peak load management in (commercial) buildings has been a very active area of the research and development in the heating, ventilation and air conditioning (HVAC) field. Most of them aim at minimizing overall operating cost through reducing peak demand. Generally, the methods for peak load/demand management can be categorized into three groups: demand shedding, demand shifting and demand limiting.

Demand shedding is a method that is commonly used by both power supply and demand sides. For the power supply side, load shedding is used by a utility company in order to avoid a total blackout of the power system when the demand for electricity exceeds the power supply capacity of the network. For the power demand side, load shedding is used by a grid management to reduce peak demand in a building via turning off non-essential electrical load, e.g., part of lighting or hot water heaters [Huang and Huang, 2000]. Demand shifting aims at taking advantages of electricity rate difference between different periods via shifting on-peak demand to off-peak hour. For CTES systems, the cooling stored in off-peak hours is used to partially/completely offset the on-peak demand. Demand Limiting refers to shedding loads when pre-determined peak demand limits are about to be exceeded [Motegi et al, 2005]. Demand limits can be placed on equipment (such as a chiller or fan), systems (such as a CTES system), or a whole building. Loads are restored when the demand is sufficiently reduced. This is typically

done to flatten the load shape when the monthly peak demand is pre-determined. Demand shifting is achieved by changing the time that electricity is used.

CTES system is suitable for peak load management in buildings by shifting cooling demands from peak periods to off-peak periods. Recently, many research works have been done to develop different strategies with different CTES facilities. The CTES system has successfully demonstrated its potentials to be a powerful instrument in building peak load management.

2.2.2 Design and control of active cool thermal energy storage

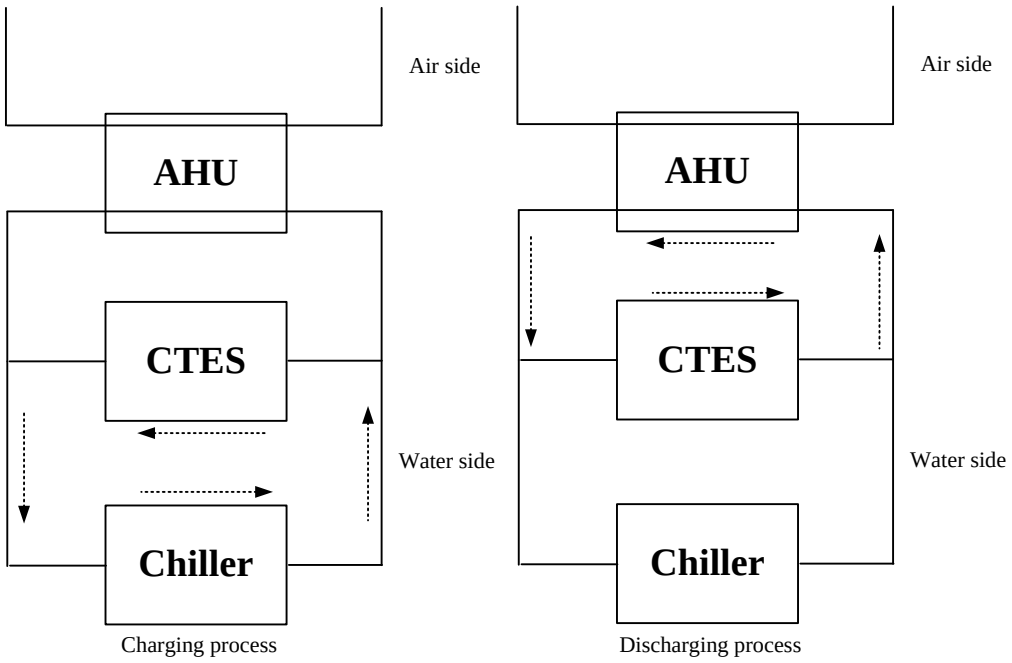

Fig.2.2 Schematic of charging and discharging processes using active CTES

Typical cooling charging and discharging processes of active CTES are shown in Fig. 2.2. In the cooling charging process, the cooling produced by chillers in the off-peak period is directly stored in CTES. In the on-peak period, the cooling is discharged from

CTES to partly/completely offset the mechanical cooling demand from end users.

The control strategies of active CTES can be categorized into two groups: the near optimal control strategies based on simple heuristic rules and the optimal control strategies.

Conventional control of active cool thermal energy storage

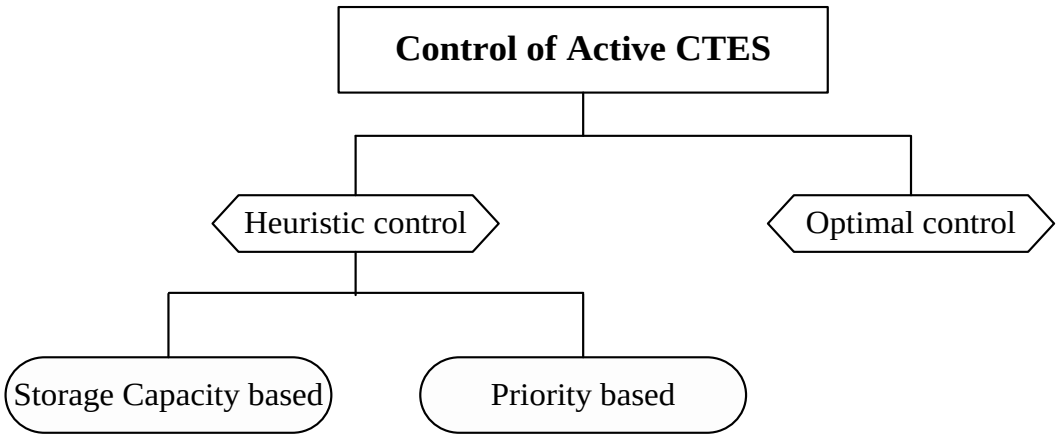

Fig.2.3 Classification of control strategies of active CTES

These near optimal control strategies using heuristic rules mainly consists of storage capacity based control and priority based control [Sun et al, 2013], as shown in Fig. 2.3. According to whether the storage system can fully offset the load in on-peak period, the storage capacity based control is further divided into full storage control and partial storage control, as shown in Fig.2.4.

For full storage control, the entire on-peak cooling load is shifted to off-peak period. A system designed for full storage typically operates at full capacity during on-peak period. The chillers do not run during on-peak hours, and all cooling loads are met from CTES. Relatively larger capacity of chiller and CTES are normally required under full

storage control. Full storage control is most attractive where on-peak demand charges are high or where the on-peak period is relatively short [Elleson, 1997].

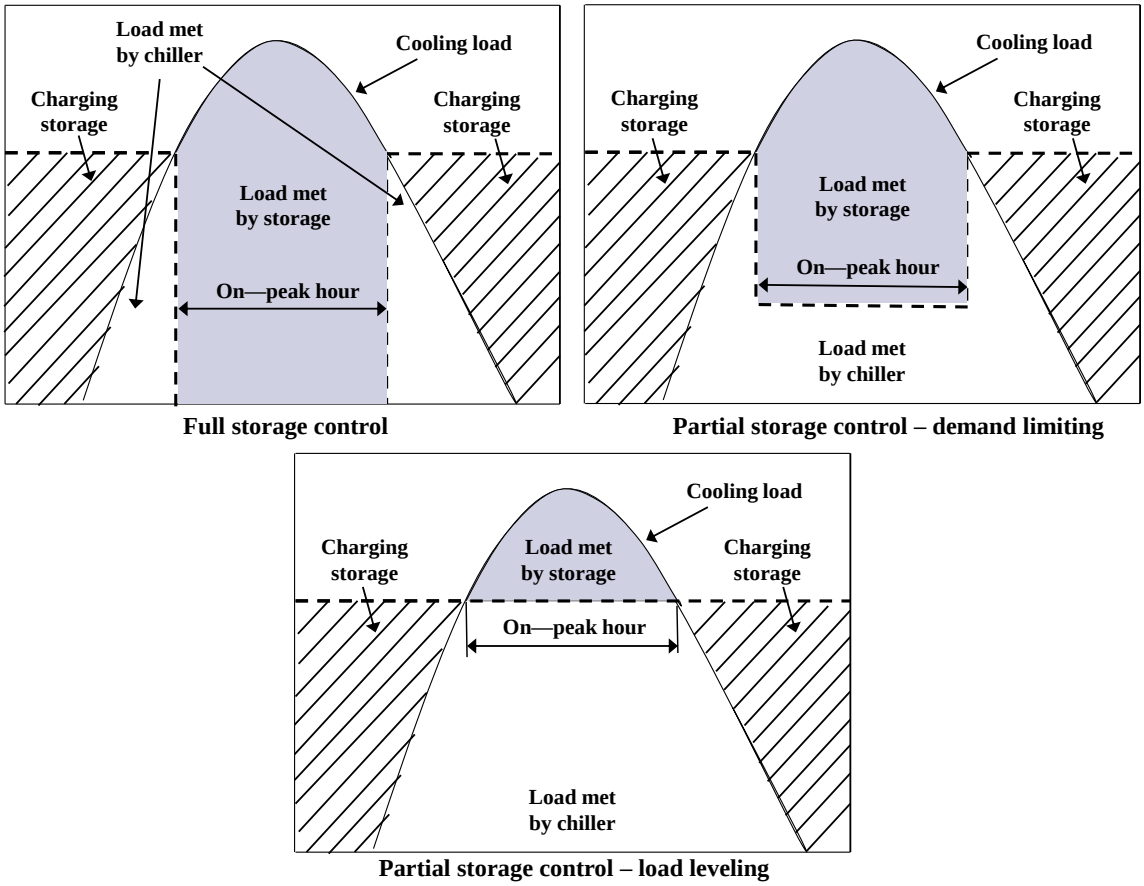

Fig.2.4 Storage capacity based control strategies

A portion of the on-peak cooling load is met by storages under partial storage control, with the remainder of cooling load met by the chiller [ASHRAE, 1993]. Partial storage control can be further subdivided into load-leveling and demand-limiting control. A load-leveling system typically operates with the chiller running at full capacity for 24h on the design day. When the load is less than the chiller output, the excess cooling is stored in the CTES system; when the load exceeds the chiller capacity, the additional requirement is discharged from storage. Load-leveling control is particularly attractive

for applications where the peak cooling load is much higher than the average load. In a demand-limiting partial storage system, the chiller operates at a reduced capacity or demand level during on-peak period. In some cases, the chiller may be controlled to keep the power demand below a given level of the billing meter.

In terms of which system (chiller or storage) has the priority to satisfy the on-peak cooling load, the priority based control is further divided into chiller-priority control, storage-priority control and constant-proportion control [Sun et al, 2013].

Chiller-priority control is one of the simplest control strategies for load/demand shifting using active CTES. In this control, the chiller runs continuously under conventional chiller control (direct cooling) while the storage provides the remaining cooling capacity if required [Henze et al, 1997]. The principle is described as shown in Eq. 2.1. Where, Q_{dis} represents charging or discharging rate (positive value is charging value rate and negative value is discharging rate); Q_{cl} is cooling load; CAP_{ch} is cooling capacity of chiller; The upper script k means the kth sampling time.

$$Q_{dis}^{k} = \begin{cases} Q_{max}^{k} & \text{if } k \text{ is off} - \text{peak} \\ 0 & \text{if } k \text{ is on} - \text{peak and } CAP_{ch} \leq Q_{cl}^{k} \\ -(Q_{cl}^{k} - CAP_{ch}) & \text{if } k \text{ is on} - \text{peak and } Q_{cl}^{k} < CAP_{ch} \end{cases} \quad (2.1)$$

The constant-proportion control implies that the storage meets a constant fraction *fra* of the cooling load under all conditions. Thus, the storage and the chiller have the same priority in providing cooling. Normally, this simple control provides a greater demand reduction than chiller-priority control sine the chiller capacity fraction used for a particular month will track the predetermined constant fraction. The principle is described as Eq. 2.2:

$$Q_{dis}^{k} = \begin{cases} Q_{dis,max}^{k} & \text{if } k \text{ is off} - \text{peak} \\ \max\left(-fra \cdot Q_{cl}^{k}, Q_{dis,min}^{k}\right) & \text{if } k \text{ is on} - \text{peak} \end{cases} \quad (2.2)$$

Storage-priority control, opposite to chiller-priority control, requires melting as much storage media as possible during the on-peak period. It is generally defined as the control strategy that aims at fully discharge the available storage capacity during the on-peak period. The principle is described as Eq. 2.3.

$$Q_{dis} = \begin{cases} Q_{dis,max}^{k} & \text{During off} - \text{peak hours} \\ Q_{cl}^{k} & \text{During on} - \text{peak hours and } Q_{cl}^{k} \leq -Q_{dis,min}^{k} \\ Q_{dis,min}^{k} & \text{During on} - \text{peak hours and } -Q_{dis,min}^{k} < Q_{cl}^{k} \end{cases} \quad (2.3)$$

Since the trade-off between energy increase and peak demand reduction is not considered in these heuristic control strategies, the final cost saving may not be optimal [Sun et al, 2013]. In contrast, the optimal control strategies, which belong to the second control strategies of active CTES, aim at minimizing the operating cost. In these control strategies, the trade-off between energy increase and peak demand reduction needs to be well considered [Sun et al, 2013].

Optimal design and control of active cool thermal energy storage

The optimal control strategies of active CTES focus on finding the best charging and discharging rates (i.e. $Q_{dis,i}$ in Eq.2.4) in different time, which minimize the overall operating cost. In other words, the optimal control strategies become a global searching problem with practical constraints. Techniques, such as particle swarm optimization and dynamic programming, have been adopted in solving these searching programs [Henze et al, 1997].

$$J = J\left(Q_{dis,1}, Q_{dis,2}, \dots, Q_{dis,n}\right) = \min(f_c) \quad (2.4)$$

where, $Q_{dis,1}$, $Q_{dis,2}$,... $Q_{dis,n}$ represent optimal charging and discharging rates in different time.

A particle swarm algorithm [Lee et al, 2009] is applied to determine the optimal ice storage system capacity and its optimal control strategy considering CO_2 emission as an additional cost. The objective function for the optimization was life-cycle cost including energy cost and initial cost. The results of the case study show that about 19% annual cost saving could be achieved when the storage system coped with around 50% daily cooling load of typical design day.

A load shifting control strategy [Henze et al, 1997] was developed in which the charging and discharging rates were optimized in discrete time. The strategy was planned at every time step over a fixed look-ahead time window utilizing newly available information. The study analyzed various predictor models with respect to their performance in forecasting cooling loads and ambient conditions for exploration of the potential of optimal control of active CTES system. It was found that the proposed controller could bring substantial daily cost saving under the premise of existence of complex rate structure.

A rule-based control strategy [Drees and Braun, 1996] was proposed, which combined elements of storage-priority and chiller-priority strategies. This rule-based strategy could be easily implemented within a small micro-processor controller and only required measurements of the building cooling load, building electrical usage and the state-of-charge of the storage. Remarkable seasonal cost saving could be achieved by implementing this rule-based optimal control strategy.

A simpler optimal control method was also developed [Braun, 2007] for charging and

discharging of active CTES systems when real-time pricing (RTP) electric rates were available. This method required little plant specific information and relatively low-cost measurements, i.e. cooling load and storage state of charge. The control method was evaluated for ice storage systems using a simulation tool for different combinations of storage sizes, buildings, locations, RTP rates and cooling plants. The simulation results show that the simplified method worked well in all the above cases

A neural network based on optimal controller for ice storage systems was constructed and its performance was measured by Massie et al [Massie et al, 2004]. The controller learned equipment responses to the environment and determined the necessary control settings first. It then determined the control actions involving the chiller operation and ice tank charge/discharge rates that minimized the total operating cost. Substantial daily costing saving could be obtained through implementing the optimal control strategy under RTP.

A preliminary study on the model predictive control (MPC) of active CTES was conducted [Ma et al, 2009]. The MPC for the chiller operation was designed in order to optimally store the cooling energy in a water tank by using predictive knowledge of building loads and weather conditions. The study addressed the real-time implementation and feasibility issues of the MPC scheme by using a simplified hybrid model of the system. The simulation results show that the daily electricity cost saving was more than 24.5% of that resulted from heuristic control.

For optimal design of active CTES, Ashok and Banerjee [Ashok and Banerjee, 2003] presented a methodology to determine the optimal capacity of chilled water CTES system and corresponding operating strategy under different electricity price structures.

The optimal operating strategy for chilled water CTES was obtained by minimizing the total operating cost including the annualized life-cycle cost of the tank and accessories. A trade-off between the capital cost of chilled water CTES and operational cost saving was achieved. A case study for a typical office showed that 38% peak demand reduction could be achieved under optimal control strategy.

Arkin and Navon [Arkin et al, 1997] developed two models for optimal design and optimal scheduling of AC systems with CTES. One was used to select optimal capacities of associated chillers and ice storage tanks through minimization of the objective function. The other one was used to determine the optimal scheduling of chiller operation cycle by minimizing the objective function concerning the electricity cost per cycle. Considerable annual operating cost saving could be achieved with quite large storage capacity and corresponding initial cost in a case study [Navon and Arkin, 1997].

Chen and Sheen [Chen and Sheen, 1993] developed a mathematical model to determine the proper capacity of a eutectic salt CTES system and corresponding optimal control strategy. The ratio of storage capacity to the maximum daily cooling load was set as a function of the off-peak time period. It was found that around 41% of the electrical peak demand could be reduced and 56% of the energy consumption was shifted from peak period to off-peak period by storage system under conventional control strategy, i.e. tank-priority operation, in the case study.

2.2.3 Control of passive cool thermal energy storage

The potential for storing cooling energy within building structure and furnishings is

significant. Opportunities for reducing operating costs through use of BTM for cooling are due to four factors [Braun, 2003]: demand cost reduction, energy cost reduction, reduced mechanical cooling resulting from the use of cool nighttime air for ventilation pre-cooling and improved mechanical cooling efficiency due to increased operation in more favorable part-load and ambient conditions. However, the above benefits are balanced with the increase in total cooling requirement caused by the use of the BTM. Therefore, the saving, associated with demand shifting and demand shedding, depends upon both the control strategies and the specific applications.

Normally, the charging of BTM is done by pre-cooling while the discharging of BTM is done by adjusting building indoor temperature set-point during occupied period, as shown in Fig.2.5. Pre-cooling is the most commonly used approach for charging BTM [Yin et al, 2010]. Pre-cooling in the building occupied and unoccupied periods are different due to the indoor thermal comfort. The indoor room temperature can be lower in the unoccupied period in which the occupant's thermal comfort is of no concern. In contrast, the lowest charging temperature during the occupied period has to stay in the thermal comfort range, as shown in Fig. 2.5.

As the operating cost minimization was considered, more complicated pre-cooling control strategies were needed in terms of selecting proper pre-cooling temperature set-point and charging time to prevent increasing the overall energy cost [Ma et al, 2012]. Sun et al. [Sun et al, 2012] conducted a study to discuss the impacts of pre-cooling temperature and duration on peak demand in two different types of buildings, i.e. buildings integrated with or without Phase Change Material (PCM), with and without use of the developed peak demand limiting method.

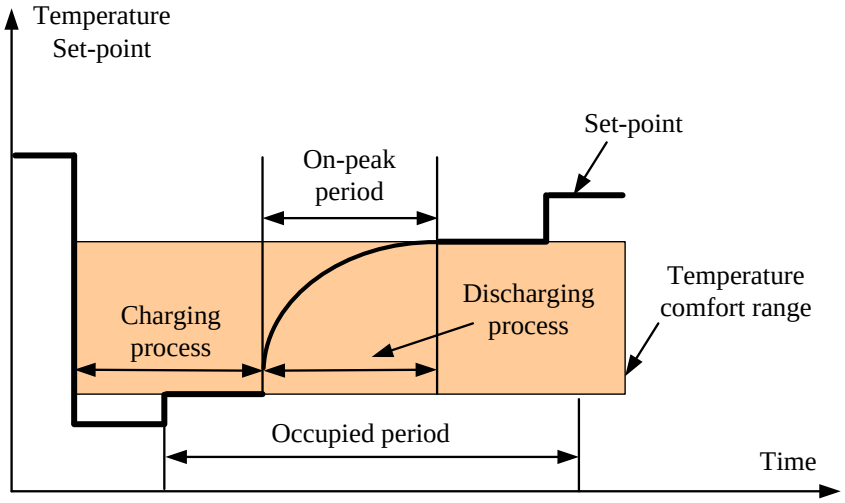

Fig.2.5 Temperature set-points in charging and discharging processes

A method of minimizing monthly electricity bill by taking the relationship between peak demand reduction and energy rise into considerations also provided [Sun et al, 2010]. This study fully considered the relationship between demand reduction and energy rise to achieve monthly cost saving. The results of case studies showed that the proposed strategy could substantially reduce the monthly electricity cost.

A pre-cooling case study was conducted at the Santa Rosa Federal Building in [Xu et al, 2004]. It was found that a simple pre-cooling control reduced more than 80% peak load in a 3 hours on-peak period. The pre-cooling control simply maintained zone temperatures at its lowest limit of the comfort range during the occupied hours before the on-peak period. In the on-peak hour, the zone temperatures floated up to its highest limit of the comfort range.

In order to discharge the stored cooling from BTM to achieve at targeted power demand reduction for operating cost saving, the room temperature set-point trajectory needs to be optimized. The studies have been conducted on cooling discharging control via room temperature set-point adjustment.

Different approaches [Lee and Braun, 2008] were proposed, such as semi-analytical (SA) and load weighted-averaging (WA) methods. They were used to estimate the building zone temperature set-point trajectories which determined the discharging rate of the cooling stored in building thermal mass for reducing the daily cooling load. These methods were also evaluated in another paper [Lee and Braun, 2008].

An inverse model was developed in [Braun et al, 2001] and was then used to estimate the savings associated with different zone temperature adjustment strategies. The impacts of different climatic conditions, building constructions, utility rate structures on the cost saving potential of the control strategies were also analyzed.

The primary factors that impact the optimal control passive CTES have been identified in one study [Cheng et al, 2008]. The optimal control strategies were determined with the objective of minimizing total energy and demand cost using an integrated optimization and building simulation tool. A fractional factorial analysis is employed to investigate how cost saving are affected by several building and system characteristics, electricity price structure, and climates. The results show that the electricity price structure, cooling load and building mass level are more important factors.

A passive CTES model was developed to demonstrate a fundamental trade-off between savings and losses and to show how the CTES can emerge in predictive control scheme [Ma et al, 2012]. This basic trade-off existed when realistic building models and performance indices were used. The results show that the both the energy conversion and the energy distribution problems can be solved using an MPC scheme. More importantly, it was demonstrated that the MPC method used in passive CTES was able to coordinate a variety of established feasible solutions for energy savings in real

building.

With regard to PCMs' integration with buildings, the control strategies are similar to the demand shifting control using BTM. Such integrations largely enhance buildings' storage capacities, e.g. SSPCM [Sun et al, 2013]. A simplified physical dynamic model of building structure integrated with shaped-stabilized phase change material (SSPCM) was developed [Zhu et al, 2010]. The parameters of the simplified model were identified using genetic algorithm (GA) on the physical properties of the PCM layer and wall. Simulation test was also conducted to investigate the impacts of SSPCM and different control strategies on the energy consumption and electricity cost at typical summer conditions in two climates [Zhu et al, 2011]. The test results show that the use of SSPCM in building envelopes could reduce the electricity cost significantly under two electricity pricing structures by using demand shifting control and demand limiting control respectively.

The potential of peak cooling load shifting by using the PCMs in buildings was numerically studied [Halford and Boehm, 2007]. The PCM was installed within the ceiling and wall insulation to assist in delaying the peak air-conditioning demand. The results showed that the use of PCMs can help to achieve 11-25% and 19-57% reduction in peak cooling load as compared to the 'mass but no phase change' case and 'insulation only' case, respectively, where the 'mass but no phase change' case meant that the systems had the mass of the PCM but the PCM was not allowed to change phase while the 'insulation only' case referred to a purely resistive wall.

The effects of the peak demand reduction using the PCM ceiling board in an office building in Tokyo, Japan were examined [Kondo and Ibamoto, 2006]. During the

charging period, the cooled air from the air-handling unit (AHU) flew into the ceiling chamber space and cooled down the PCM ceiling board. During the peak reduction period, the air from the room returned to the AHU via the ceiling chamber space. The results from simulations show that the maximum cooling load using the PCM ceiling board was reduced by 9.4% as compared to the conventional rock wool ceiling board. The overall running cost was 96.6% lower than that of the rock wool ceiling board due to the use of discounted cheap electricity price during nighttime.

To estimate the load reduction potential of phase-change wallboards in office buildings, a numerical study using RADCOOL was conducted [Stetiu and Feustel, 1998]. The results show that the use of PCM wallboards coupled with mechanical night ventilation in office buildings can offer the opportunity for system downsizing in climates where the outside air temperature drops below 18 ˚C at night. About 28% peak cooling load reduction can be achieved for a prototype IEA building located in California climate condition.

2.2.4 Control of combined active and passive cool thermal energy storage

Some studies were also conducted to study the impact of combined use of active and passive CTES. The control utilizing passive CTES is performed through pre-cooling and the building indoor temperature set-point reset. The control using active CTES is conducted through charging and discharging the storage medium. Thus, the control of using both active and passive CTES requires considering the pre-cooling control, indoor temperature set-point reset and charging/discharging control of active storage [Sun et al, 2014]. Compared with control using either active or passive CTES, the control using both of them is more complicated.

The combined usage of both building thermal mass and thermal energy storage (TES) under optimal control was investigated [Henze et al, 2004]. An algorithm named ‘‘Iterative Sequential Optimization’’ was developed, as shown in Fig.2.6. In the figure, the symbols T, Q_L, u and J_L represent temperature, cooling load, charging/discharging rate and cost function. Subscripts *Z*, *SP*, *UB*, *LB*, *OPT* and *init* are zone, set-point, upper boundary, lower boundary, optimal value and initial value. Basically, the optimization is performed in two major steps. In the first step, with a specified charging and discharging rate profile, a series of optimal room temperature set-points $\{T_{Z,SP}\}$ resulting in minimum utility cost is identified using the quasi-newton method. In the second step, the obtained cooling load Q_L and the previously identified $\{T_{Z,SP}\}$ are used to determine a new optimal charging and discharging rates $\{u\}$ and a new optimal utility cost using dynamic programming. This cycle is repeated until the optimal cost J_L converges. The simulation results show that the saving of the combined use of active and passive CTES was larger than the saving of either active or passive CTES used, but less than the sum of the individual saving. This statement was made based on the pre-condition that the optimal controller was given perfect weather forecasts and the building model used perfectly matched the actual building. Henze et al. [Henze et al, 2004] explored the impacts of the prediction uncertainty on the strategy’s cost saving performance. It was found that the overall cost saving performance with the weather forecast uncertainty was only marginally inferior compared with the case when weather perfectly predicted. In order to investigate the impacts of building model error on the cost saving performance of the developed control, another simulation study conducted [Liu and Henze, 2004] under the condition of perfect weather prediction. The impacts of five categories of building modeling mismatches were studied and evaluated.

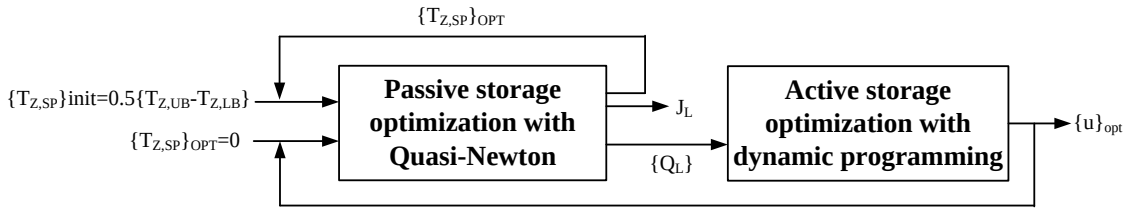

Fig.2.6 Iterative sequential optimization of electricity consumption cost

The relationship between operating cost savings and energy consumption in the combined utilization of active and passive building thermal storage under "time-of-use" electricity structure also was investigated [Henze, 2005]. A reinforcement learning controller for optimal control of active and passive building CTES was developed [Liu and Henze, 2007]. The reinforcement learning controller learned to charge or discharge the storage tank based on the feedback it received from past control actions. The analysis showed that the reinforcement learning control was a feasible method to find a near-optimal control strategy for the active and passive building CTES. However, the cost saving obtained by the reinforcement learning control method was less than that resulted from the model-based control method.

A parametric analysis to assess the effects of building mass, utility rate, building location, thermal comfort, chiller capacities and economizer on the cost savings of optimal control for active and passive building CTES was conducted [Zhou et al, 2005]. The results of this study show that heavy-mass buildings, strong-incentive time-of-use electricity utility rates and large on-peak cooling loads would likely lead to abundant cost savings resulting from optimal storage control.

One experimental analysis of model-based predictive optimal control active and passive CTES was conducted in [Henze et al. 2005]. A novel supervisory controller successfully

was used by three steps including short-term weather prediction, optimization of control strategy over the next planning horizon and post-processing of the optimal strategy to generate the control command for the current time step that can be executed in the real systems. The results show that more electricity cost saving compared to that under control of heuristic controls is achieved even when the optimal controller is given imperfect weather forecasts.

2.3 HVAC System Demand Response Strategies

2.3.1 Introduction

The integration of large amount of increasing renewable energy resources may cause significant stress on the balance of electricity grids because these sources are volatile, intermittent and uncontrollable. In response to the dramatic growth of power demand and the use of renewable energies, smart grid is considered as a promising solution in improving the power reliability and sustainability. The need for demand response is accordingly increased.

Demand response (DR) can be defined as: “Changes in electric usage by end-use customers from their normal consumption patterns in response to incentive payments designed to induce lower electricity use at times of high wholesale market prices or when system reliability is jeopardized” [Department of Energy US, 2006]. A demand response resource participating in an organized wholesale energy market administered by an RTO or ISO has the capability to balance supply and demand as an alternative to a generation resource [U.S. Federal Energy Regulatory Commission. 2011]. The demand response programs are established by utilities, regional transmission operators (RTOs)

or independent system operators (ISO). These programs give customers additional incentives that are separate from their retail electricity rate.

Currently, effective peak demand reduction according to real-time price structure cannot be achieved immediately for all customers [Department of Energy US, 2006]. Conventional metering and billing systems for most customers are not adequate for charging time-varying rates and most customers are not used to making electricity decisions on a daily or hourly basis. Consequently, fostering demand response through incentive-based programs will help improve efficiency and reliability while price-based demand response grows. Normally, individual contract is needed for demand response program to make customer to do obligated and voluntary power curtailment. In addition, demand response programs usually involve complicated preliminary decisions such as determining the baseline in a way that does not promote higher consumption during non-event periods [Surles and Henze, 2012].

Many researches and applications have been investigated and conducted on different demand response strategies. DR strategies refer to control methodologies that enhance load shedding or load shifting during times when the electric grid is near its capacity or electricity prices are high. The goal of DR strategies is to meet the demand saving targets while minimizing any negative impacts on the customers. The specific operations in the DR strategies include demand shedding, demand shifting and demand limiting [Motegi et al, 2005]. Demand limiting and shifting can be utilized for demand response when the reliability issues are predicted and communicated to each demand response resource (DRR) in advance. DR can also be accomplished with demand shedding, which is a temporary reduction or curtailment of peak electric demand within shorter period of

response time.

Buildings play important roles in smart gird according to its substantial power consumption and accordingly have significant flexibility in DR. The largest portion of energy use in buildings is for the provision of heating, ventilation and air conditioning (HVAC), which accounts for 50% of whole building energy consumption on average [EMSD, 2012]. Therefore, HVAC systems are the most crucial systems affecting power consumption in buildings.

HVAC systems can be an excellent resource for DR savings for the following reasons. First, HVAC systems comprise a substantial portion of the electric load in (commercial) buildings. Second, the "thermal flywheel" (passive CTES such as BTM) effect of indoor environments allows HVAC systems to be temporarily unloaded without immediate impact on the building occupants. Third, it is common for HVAC systems to be at least partially automated with energy management and control systems (EMCS). In addition, most of the DR programs aim to short-term but aggressive demand saving. On the other hand, a long-term event may be triggered by an electricity price change and may require log-term but moderate demand saving. The characteristic of HVAC DR strategy better suit short-term DR event when the BTM and active CTES are used to largely reduce power consumption during the short-term DR event without serious impact on the building user.

The electricity loads in HVAC systems are relatively difficult to predict due to the dynamic characteristics of the working condition (e.g., outdoor weather conditions and variable internal gains). However, the prediction of the demand responses for different building is very important because accurate prediction not only support the generation

planning and operation scheduling of a grid, but also allow the building user to understand their power demand potentials in benefiting themselves [Zhou et al, 2013].

HVAC-based DR strategies recommended for a given building is based on building type and system configuration. For instance, the thermal capacities of building thermal mass are very different in different buildings and the CTES in the building can be used to shift cooling load. Based on these factors, the best DR strategies are those that achieve the aforementioned goals of meeting electricity demand-saving targets while minimizing negative impacts on building thermal comfort.

2.3.2 Conventional strategies

Since BTM can significantly affect the building cooling load due to their considerable capacities and resistances that may result in the reduction and delay of the external heat fluxes, the charging and discharging controls of BTM, including pre-cooling and zone temperature reset strategies, are the most popular HVAC DR strategies [Xu and Haves, 2006].

A preliminary case study to demonstrate the potential of utilizing BTM for demand reduction in an office building in California was conducted [Xu and Haves, 2006]. The average change rate of zone temperature was about one degree per hour. In the worst-case zone, the temperature rise was approximately two degree per hour. The results show that demand-limiting strategy reduced the chiller power by 80~100% from 2 p.m. to 5 p.m. without causing any thermal comfort complaints and nighttime. Precooling was found to have varied effects on the magnitude of the peak in the following day. The occupant comfort was maintained in the precooling tests as long as the room temperature was within the range of (21.1°C to 25.6°C).

The pre-cooling strategies optimization procedure for buildings with the demand response quick assessment Tool (DRQAT) in a hot climate was proposed [Yin et al, 2010]. A series of simulations were conducted to identify the optimal pre-cooling strategies with the calibrated simulation models. The "pre-cooling with exponential temp set up" and "pre-cooling with step temp set up" strategies turned out to be better DR strategies compared to the "Pre-cooling with linear temp set up" strategy. The predicted average demand shed during the DR event by DRQAT matched well with the measured data during the Auto-DR event days in the 7 of 9 field test buildings.

The indoor thermal comfort is one important issue for the pre-cooling control. In order to further investigate the effects of pre-cooling on the occupants' indoor thermal comfort, a web-based comfort survey was conducted in the field tests of two large scale commercial buildings with heavy mass [Xu et al, 2005]. The results indicated that the occupant comfort was maintained in the pre-cooling periods and the following discharging periods.

On study case in New York was conducted by [Kiliccote et al, 2006]. The adopted HVAC DR strategy was global temperature set-point adjustment. In the reference building, the duration of the DR period was set as three hours. The initial recommendation method was to increase the set-point 3°F for moderate demand reduction and an additional 3°F for further demand reduction. Iterations of the temperature gradient were depending on the simulated temperatures within the zone. The estimated peak demand savings derived from different present DR programs offered by the local utility and New York Independent System Operator was compared and discussed.

Besides, zone temperature reset strategies, other HVAC DR strategies includes duct static pressure set-point reduction, fan speed limit, fan speed limit, fan quantity reduction, supply air temperature increase, raising chilled water supply temperature set-point, chiller power limiting, chiller operating number of chiller and etc. One paper presented a review of different HVAC DR strategies that used in commercial buildings [Watson et al, 2006]. The strategies discussed in this paper were based on the results of three years of automated demand response field tests in which 28 buildings, including office building, high school, museum, laboratory data center, supermarket and etc., with an occupied area totaling more than 11 million ft^2 were tested. The average value of demand saving intensity over one hour was also shown.

One study proposed a HVAC DR strategy based on occupancy prediction and real time occupancy monitoring via a sensor network of cameras [Erickson and Cerpa, 2010]. The Moving Window Markov Chain occupancy model utilizing Markov Chains was defined. With defined the occupancy model and the availability of an occupancy monitoring system, it could be possible to implement occupancy based HVAC DR strategy. The strategy aggregates multiple predictions processes to find the likelihood of a section to be occupied. The comfortable temperature was used only if the occupied at least ten minutes. The simulation tests results show that 20.0% potential energy saving was achieved while still maintaining acceptable indoor thermal comfort.

To analyze the benefits of demand response programs for the individual residential building, a detailed simulation program was developed [Katipamula and Lu, 2006]. A simplified first-principle-based thermal load model was developed and used to simulate the HVAC load response. The demand reduction, indoor temperature rise and the cost

for energy consumption were evaluated when different indoor temperature reset strategies, including constant temperature control, total curtailment and precooling controls. The results suggested that the curtailment control strategy provided the largest demand reduction. However, the resulted demand reduction brought the loss of indoor thermal comfort immediately. Precooling provided almost same demand reduction as that provided by the curtailment strategy but consumed more energy and cost more. With the precooling control strategy, there is no thermal comfort loss.

2.3.3 Performance investigation

Regional Transmission Operators (RTOs) and Independent System Operators (ISOs), such as Midwest ISO, New York ISO (NYISO), ISO New England (ISONE) and etc., have encouraged demand response resources (DRRs) to provide ancillary reserves [Chen and Li, 2011]. Ancillary services are those functions required to maintain a balance between generations and loads in near real-time [Kirby, 2006]. The ancillary services include regulating reserve, spinning reserve, non-spinning reserve, replacement reserve and etc. They are distinguished by the required response speed, duration, and frequency of deployment. For instance, the regulation reserve provides the continuous minute-to-minute balancing of generation and load under normal conditions. Spinning reserve is required to respond to event immediately and must fully respond within ten minutes. Non-spinning reserve does not need to respond immediately but is still required to fully respond within 10 minutes. Replacement reserve begins responding in 30 to 60 minutes. Traditionally generators have dominated supplying ancillary services through injecting power to the grids.

A number of research studies were also conducted to investigate the performance and

effects of ancillary services provided by the HVAC systems.

How ancillary services can be obtained by using the power demand flexibility in HVAC systems was described by Hao et al [Hao et al, 2012]. The building thermal and power consumption of HVAC system models were constructed to simulate the systems in a building in Florida in the study. The control objective is to control the fan power tracking the time-varying signal. The results show that 15% of fan power capacity can be provided for regulation services while maintaining indoor temperature deviation no more than ±0.2 °C. Based on the results, the author concluded that the HVAC systems in 90,000 medium-sized commercial buildings can provide the entire regulation service needed by the ISO without noticeable change in indoor air quality.

A pilot project to investigate the performance of demand response in buildings which participated in the ISO's ancillary services market as non-spinning reserves product was conducted [Kiliccote et al, 2010]. A DR strategy utilizing 4 ºF temperature set-point adjustments with one degree increments was used. During the DR period, forecasted target demand shed level and the actual demand shed were compared and the temperature set-points adjustments were accordingly made. The hourly demand and load curtailment potential can be forecasted and were then submitted to the ISO as available resource. One demonstration to determine whether the HVAC systems could deliver demand response that met the requirements of non-spinning reserves was set out in California [Kiliccote, 2013]. Four DR strategies, each indicating a global temperature adjustment method, were conducted. The power demand during DR event was forecasted and compared with the measured power demand. It was found that the accuracy of the forecasted power demand influenced the accuracy of the delivered DR.

Another demand response spinning reserve project was carried out to demonstrate of how use equipment in building to provide spinning reserve [Eto et al, 2006]. The magnitude of the demand shed of AC system was set as a function of time of day and expected weather conditions. The method of forecasting response had a confidence level of greater than 95 percent and an accuracy of greater than 90 percent. The results also show that the curtailment of AC systems power consumption in a manner similar to the deployment of spinning reserve could be accomplished without a single customer complaint. In addition, the speed of curtailment of AC system power consumption can be fully conducted faster than the ramping up of spinning reserve from generators in supply side.

A paper presented the direct control of HVAC unit to adjust their power consumption to follow the ancillary services signals from grid [Lu, 2012]. The ancillary services signals are used to decide the operation of HVAC unit under different outdoor temperature profiles and different indoor temperature set-points. The baseline aggregated HVAC power output was estimated from the modeled averagely power consumption profile based on outdoor temperature forecast. The operation of HVAC unit was numerically simulated and their capacity to provide ancillary services was evaluated. The simulation results indicated that approximately 1000 HVAC unit with rated capacity of 6 kW and 4°C dead-band could provide 24 hours of ancillary services by the developed control method. It was also found that a narrow room temperature dead-band limits the capacity of the HVAC unit to provide ancillary services.

A HVAC DR control method was proposed in one study [Lin et al, 2013]. The ancillary services signals were tracked by varying the cooling demand in commercial building in

real-time. The bandwidth limitation of the ancillary services signals, which allows the HVAC system to provide fast power reduction without serious effect on the building indoor thermal comfort. The control objective is the air flow rate to instantaneously reduce the power consumption of chiller and fan. The calculated results show that the commercial buildings in the U.S. can provide 47 GW of regulation reserves with virtually no significant thermal comfort degradation.

A novel air-conditioning system with proactive demand control for daily demand shifting and real time power balance in the developing smart grid was proposed [Yan et al, 2014]. The simulated integrated system consisted of a chilled water CTES together with a temperature and humidity independent control (THIC) air-conditioning systems, which could effectively enable a building with flexibility in the changing its power consumption patterns. Two types of demand response strategies such as demand side bidding (DSB) strategy and demand as frequency controlled reserve (DFR) strategy were implemented in respond to the day-ahead and hour-ahead power change requirements of the grid, respectively. A case study was conducted in a simulation platform to demonstrate the application of the proposed system in an office building. The results show that considerable energy and cost saving can be achieved for both the electricity utilities and building owners.

2.4 Discussions

Based on the above developed design and control strategies of CTES for peak load management, the peak load can be successfully reduced and the electricity cost can be accordingly saved. The developed HVAC DR strategies, such as global temperature

adjustment, can achieve the targeted demand reduction within short time delay during short periods. However, it also can be found that the related research is still inadequate in the following aspects:

For peak load management, storage capacities resulted from the most previous studies were usually quite large, e.g. coping with more than 40% daily cooling load normally, which may bring very substantial initial cost. More attention should be paid to the relationship between operational cost saving potential and capital cost of CTES systems. In addition, the computation processes in the previous studies were usually complicated. Therefore, an optimal design method of relative small scale active CTES system for building to achieve maximum life-cycle cost saving is required.

For HVAC demand response strategies, except passive CTES such BTM discussed in the above researches, the active CTES storage is seldom used. But the active CTES can actually play an important and active role in building power demand response. For instance, power reduction normally cannot be a constant value, which is not convenient for grid to do prediction, under control of the zone temperature reset strategies by discharging BTM**.** Active CTES can not only enable more capabilities of the building power demand response by discharging cooling energy, but can also modulate the power profile individual HVAC system to result desired power reduction, i.e. steady power reduction.

In addition, the HVAC DR strategies such as global temperature adjustment and air flow rate reduction normally cannot provide fast enough demand response to meet the requirements of ancillary services in most of the previous studies. These strategies could not reduce the power consumption of HVAC systems immediately because of the

inevitable delays caused by the thermal mass of buildings [Shi et al, 2005] and control process. Normally, it may take more than 20 minutes to generate obvious power reduction after building indoor temperature set-point is increased. Besides, effective demand reduction prediction methods are still inadequate.

Therefore, more research work is required to develop more updated and advanced and appropriate optimal design and control strategies of CTES, including optimal design of CTES for building peak load management, fast power demand response strategy for building involving CTES and economic analysis of CTES for building demand management, which have more desirable and satisfactory performance in practical applications. The developed strategies presented in this thesis will achieve better performance.

2.5 Summary

This chapter provides a literature review of the previous related works about developments and applications of optimal design and control of CTES for building demand management, including optimal control of active CTES for peak load management, optimal control of passive CTES for demand response and etc. The evaluation and discussion of the current studies have been also presented.

CHAPTER 3 BUILDING SYSTEMS AND DYNAMIC TEST PLATFORM

The dynamic simulation platform, namely virtual building system in this thesis, performs the real-time simulation of buildings and their HVAC systems. It is mainly used to analyze and test the developed strategies in terms of control, thermal comfort and energy performances under dynamic operating conditions. Based on the test results, the design and control strategies with satisfactory performance are selected prior to their in-site implementations.

Some well-designed commercial simulation software packages, e.g. Energy Plus and DOE-2, are readily available for constructing dynamic platform for buildings and HVAC systems. However, the difficulties of integrating the water distribution system, air distribution system and building load calculation into a compound and intact system prevent constructing such effective dynamic simulation platform. In addition, the system configurations, including cooling system, water and air distribution systems configurations, in the above software packages are complex and complicated. The positive effects of the above software packages for detailed dynamic control and design strategies in large scale system simulations, which concern computation speed, are limited.

TRNSYS is selected in this study to construct the dynamic simulation platform because it is a complete and extensible simulation environment for the transient simulation of multi-zone building systems. TRNSYS is also capable of conducting the building

cooling load calculation, water system simulation and air system simulation with one single simulation package.

This chapter mainly describes the simulated buildings and their central chilling systems. Energy performance and system efficiency tests are conducted in the dynamic simulation platform to evaluate the developed optimal design and control strategies for building demand management in this thesis.

The buildings and their HVAC systems are described in Section 3.1. Based on the complex chilling systems, the dynamic simulation platforms are constructed in Section 3.2. Except for PCM storage tank model, models of the major components in HVAC systems and their interconnections used to construct the complex dynamic simulation platforms are introduced. A summary of this chapter is given in Section 3.3.

3.1Description of Buildings and Systems

For evaluating the developed optimal design and control strategies for building demand management, three real buildings with different sizes and different chilling systems are introduced. These three buildings have different scale of cooling load and energy consumptions of HVAC systems. The buildings and the associated HVAC systems will be simplified and simulated in the developed simulation platforms.

3.1.1 International Commerce Center and its HVAC system: a large scale building

International Commerce Center

A schematic picture of International Commerce Centre (ICC) building is shown in Fig.3.1. This building is super high-rising of meter high above the ground with 440,000

m^2 construction areas, including a basement of four floors, a block building of six floors and a tower building of 112 floors, located in Kowloon, Hong Kong. The basement, about 24,000 m^2, is mainly used for car parking and public transportation. The block building, from the ground floor to 5th floor, has a gross area of about 67,000 m^2 and mainly serves as commercial center involving restaurants, exhibition halls and shopping market.

Fig.3.1 Profile of International Commerce Center (ICC)

The tower building has an area of 230,000 m^2. The 6th and 7th floors in it serve as the mechanical floor (M1) to accommodate chillers, pumps, cooling towers and etc. The 8th floor is a refugee floor. The commercial office floors are located in the 9th to 98th floors. Each floor is with the length of 66 m and the width of 65 m. Among the commercial office floors, the 41st and 77th floor are the refugee floors, and the 42nd

(M2), 78th (M3) and 99th (M4) floor are used as mechanical floors to accommodate mechanical equipment such heat exchangers, pumps, primary air unit (PAU) and etc. A six-star hotel is located from the 100th to 118th floors.

The whole building is constructed primarily of reinforced steel concrete. External walls are mostly glass curtain. The floor structure is 125mm slab of reinforced steel concrete. The vertical transportation systems and air-handling unit (AHU) plants are located in the core of each floor with a quasi-rectangle of 45 m by 41 m.

HVAC system

Six identical centrifugal chillers are installed to supply cooling to the building. The design cooling capacity of each chiller is 7,230 kW. All the chillers are supplied with high voltage of electricity (10,000 V). The nominal power of the compressor in the chiller is 1,345 kW at the full load condition. Each chiller is associated with one constant condenser water pump and one constant primary chilled water pump.

The heat generated by the compressor is taken off by the refrigerant. The heat dissipated from the chiller condensers is rejected by the 11 evaporative water cooling towers with a nominal capacity of 51,709 kW. Two different types of cooling towers, i.e. CTA and CTB, are used due to the consideration of plume abatement. CTA are the towers without heating coil while CTB refers the cooling towers with a heating coil installed at the air exhaust of each tower. Each CTA cooling tower has a heat rejection capacity of 5,234 kW and a nominal power consumption of 152 kW at the design condition. The rated air and water flow rates of CTA tower are 157.2 m^3/s and 250L/s respectively. Each CTB tower has a heat rejection capacity of 4,061kW and a nominal power of 120 kW at the

design condition. The rated air and water flow rates of CTB tower are 127.0 m^3/s and 194L/s respectively.

For each floor in the building, two AHUs located in the core are used to handle the mixture of re-circulated air from offices and fresh air which is delivered to the AHU through the shaft in the core by PAUs located in the mechanical floors. The PAUs are used to cool down the temperature of fresh air to 16.5 $^{\circ}C$ which is the machine dew point. The PAUs and AHUs are equipped with VFDs for energy efficient operation. The major specifications the main HVAC equipment, such as fans of AHUs and PAUs, chillers, cooling towers and pumps, are summarized in Table 3.1.

Table 3.1 shows the specification of the main equipment in the water-cooled HVAC system. The designed power of the whole system is 16,503 kW. The chillers consume the largest proportion of power consumption. The ratio of nominal power consumption of each chiller to the designed power of whole system is 43.7%. The second largest electricity power consumer is the fans in the PAUs and AHUs. It contributes about 27.7% of the designed power of whole system. The nominal power of pumps and fans in the cooling tower consume around 20.5% and 8.1% of the designed power of the whole system respectively.

The nomenclatures in Table 3.1 are defined as following. N_{comp} is the number of components, M is the flow rate. MCC is the chiller nominal maximum cooling capacity. Q is the heat transfer rate, P is the power consumption, η is the efficiency. The subscripts a, w, cd, ev and rej represent air, water, condenser, evaporator and rejection respectively.

Table 3.1 The specifications of the main equipment in the HVAC system of ICC

Chillers	N_{comp}	$N_{w,ev}$ (L/s)	$M_{w,cd}$ (L/s)	MCC (kW)	P (kW)	P_{total} (kW)
WCC-06-01 to 06	6	345.0	410.1	7,230	1,346	8,076
Cooling towers	N_{comp}	M_w (L/s)	M_a (m^3/s)	Q_{rej} (kW)	P (kW)	P_{total} (kW)
CTA-06-01 to 06	6	250.0	157.2	5,234	152.0	912.0
CTB-06-01 to 05	5	194.0	127.0	4,061	120.0	600.0
Pumps	N_{comp}	M_w (L/s)	H (m)	η(%)	P (kW)	P_{total} (kW)
CDWP-06-01 to 06	6	410.1	41.6	83.6	202.0	1,212
PCHWP-06-01 to 06	6	345.0	31.6	84.5	126.0	756.0
SCHWP-06-01 to 02	1(1)*	345.0	24.6	82.2	101.0	101.0
SCHWP-06-03 to 05	2(1)*	345.0	41.4	85.7	163.0	326.0
SCHWP-06-06 to 08	2(1)*	345.0	30.3	84.2	122.0	244.0
SCHWP-06-09 to 11	2(1)*	155.0	39.9	78.8	76.9	153.8
PCHWP-42-01 to 07	7	149.0	26.0	84.9	44.7	312.9
SCHWP-42-01 to 03	2(1)*	294.0	36.5	87.8	120.0	240.0
SCHWP-42-04 to 06	2(1)*	227.0	26.2	84.3	69.1	138.2
PCHWP-78-01 to 03	3	151.0	20.6	84.3	36.1	108.3
SCHWP-78-01 to 03	2(1)*	227.0	39.2	85.8	102.0	204.0
Air-side PAU fan	29	-	-	-	-	513
Air-side AHU fan	152	-	-	-	-	4600

Design total power load			
	Chillers	8,076 kW	43.7%
	AHU and PAU fans	5,113 kW	27.6%
	Pumps	3,796 kW	20.5%
	Cooling tower fans	1,512 kW	8.2%
	Total	18,497 kW	100 %

3.1.2 A commercial center and its HVAC system: a midscale building

A commercial center

A four-storey shopping center, located on Tsing Yi Island, Hong Kong, is also used as the reference building in this study, as shown in Fig.3.2. The area of the air-conditioned space is about 45,000 m^2. It includes two parts: train station and shopping mall in which the HVAC system operating schedules are different. The annual electrical consumption of the whole building is around 23,000,000kWh.

Fig.3.2 A commercial center

HVAC system

Four chillers with nominal power consumption of 700 kW and two chillers with nominal power consumption of 280 kW are used in this building. The nominal power of the eight chilled water pumps is 110 kW each. The eight condenser water pumps have the nominal power of 185 kW each.

3.1.3 PolyU Phase 5 building and its HVAC system: a small scale building

PolyU Phase 5 building

Fig.3.3 PolyU Phase 5 building

The Phase 5 building, located in the Hong Kong Polytechnic University (PolyU) campus, is used as the reference building in this study, as shown in Fig.3.3. It mainly consists of offices, classrooms and computer rooms. The total area is approximately 11000 m^2, in which about 8500 m^2 is air-conditioned. The building annual electrical consumption is about 5,000,000kWh.

HVAC system

The central chiller plant consists of four air-cooled chillers. Two of them have the cooling capacity of 1050 kW each with the nominal power consumption of 338.3 kW. The other chiller has a cooling capacity of 262 kW with a nominal power consumption of 50 kW. The fourth chiller has a nominal cooling capacity of 473 kW with a nominal power consumption of 101kW. The constant speed pumps also include three types of different nominal power consumptions. Two of them are 30 kW while the third and fourth pumps are 15 and 18.5 kW respectively.

3.2 Development of the Dynamic Simulation Platform

3.2.1 Outline

The simulation platforms based on the complex chilling systems mentioned before is developed based on TRNSYS, which is extensible simulation environment for the transient simulation of system, including multi-zone buildings. It is often used by researchers to develop and validate the new developed energy concepts. The application scope includes simple hot water system, design and simulation of different types of buildings and the equipment in the buildings. The control strategies, occupant behavior, alternative energy systems (solar, photovoltaic, wind hydrogen systems), etc.

The most important factor in TRNSYS is its open, modular structure. The source code of the kernel as well as the component models is delivered to the end users. The existing models are simplified to make them fit the user's specific needs. The DLL-based architecture allows users and third-party developers to easily add custom component models, using all common programming languages (C, C++, PASCAL, FORTRAN,

etc.). The TRNSYS can easily connect to other software or packages, i.e. Matlab and Microsoft Excel, through pre-processing, post-processing or interactive calls during the simulation.

The detailed applications of TRNSYS include:

1. Low or zero energy buildings and HVAC systems with advance design characteristics, such as natural ventilation, double facade, slab heating or cooling and etc.;
2. Solar systems (solar thermal and PV);
3. Renewable energy systems;
4. Cogeneration, fuel cells;
5. Anything that requires dynamic simulation;

When developing the simulation platform, the studied real buildings and their HVAC system will be firstly simplified and modeled. Then, a detailed thermal storage tank model is developed and integrated in the developed simulation platform. The models of the building envelop and the HVAC components (e.g. chillers, pumps, cooling towers, AHUs) are all detailed physical models, which can simulate the dynamic heat and mass transfer process.

3.2.2 Simulation test platform based on the real building

A simplified dynamic simulation platform is constructed based on the real building using TRNSYS as shown in Fig.3.4. It is a typical primary constant- secondary variable chilled water system. In the primary loop, each chiller is associated with a constant speed pump to produce the chilled water. In the secondary loop, the variable speed

secondary water pump is employed to distribute the chilled water to the terminal units. The primary loop and the secondary loop are decoupled by a bypass line.

The simulation platform mainly consists of the models of building envelop and main components of a central air-conditioning system, such as the chillers, AHUs and etc. Since this research mainly focuses on optimal design and control strategies of CTES for building demand management, the thermal balance is of major concern and the pressure flow balance in the water and air distribution loops have not been considered. A global AHU is used instead of multiple different AHUs for different zones in practice to simulate the outlet water and outlet air states. Both primary and secondary pumps have the nominal powers which are in accord with those of the pumps in the real HVAC systems. The chillers also have the nominal power consumptions and cooling capacities which also agree with those of the chillers in the real HVAC systems.

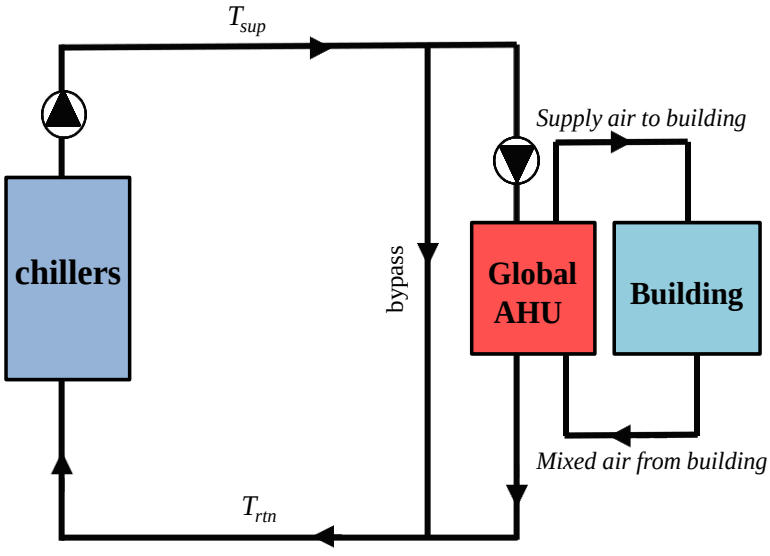

Fig.3.4 Simulation platform configuration

The multi-zone building model in TRNSYS 16 is employed to simulate the thermal

behaviors of the buildings. The load from the equipment, occupants and lighting system in the buildings as well as weather data are considered in the simulation platforms as input files. The weather condition used in the thesis is the data of typical year in Hong Kong. The air flow rates and AHU inlet air dry-bulb temperatures of each individual zone are simulated according to the weather data and internal heat gain of each zone provided together with some reasonable and acceptable assumptions.

Some assumptions used are presented as follows：

1. The room design air dry-bulb temperature is 23°C with a 50 humidity ratio;
2. A minimum ratio of the fresh air to supply air is assumed as 20%;
3. The air dry-bulb temperature leaving AHUs is controlled under the set-point which can be different from season to season with a 95% humidity ratio.
4. The set-point of the chilled water temperature at the outlet of the chillers was set at 7°C.

The simulated system structure and the interactions of the original components, such as the chiller, AHU and pump, in the simulation platform are the same with the actual complex chilling systems.

3.2.3 Simulation test platform integrated with PCM storage

In order to study and evaluate the effect of thermal storage tank on the conventional building HVAC system, a detailed PCM storage tank model is developed and integrated in the simulation platform. The detailed description of the developed storage tank model will be presented in Chapter 4.

The PCM storage has large latent heat capacity compared with water storage systems. It

also allows the conventional chillers to meet the charging temperature requirement. It is therefore more economically beneficial to employ PCM storage systems in buildings.

Fig. 3.5 shows the improved HVAC system integrated with the PCM storage tank. This is a typical chiller downstream configuration, allowing the return chilled water from building to be cooled by the PCM storage tank before entering the chiller. During the discharging process, the valve b is opened to modulate the return chilled water with high temperature as the discharge flow rate to the tank. During the charging process, the valve a is opened to modulated the supply chilled water with low temperature to charge the tank.

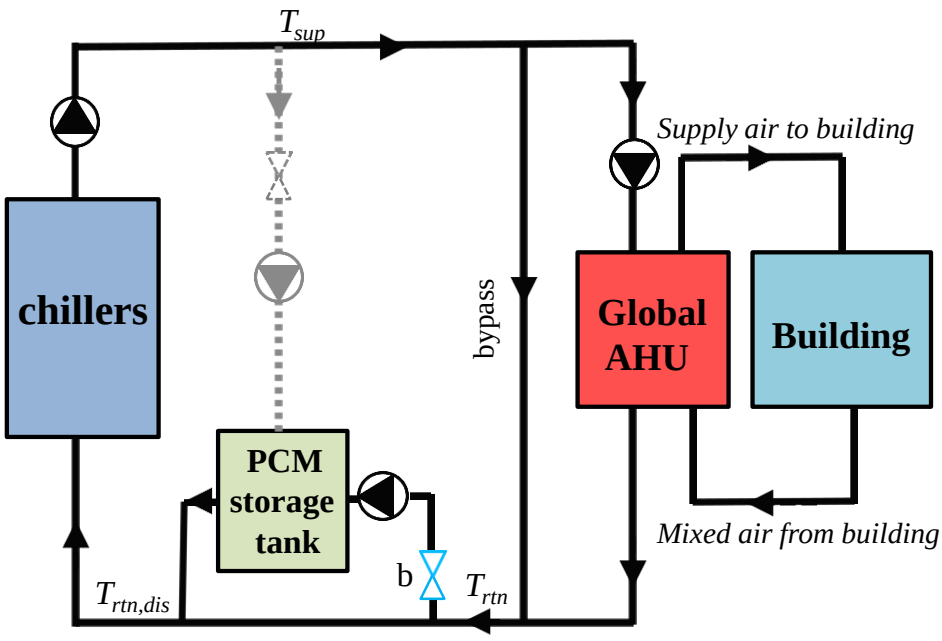

(a) Discharging process

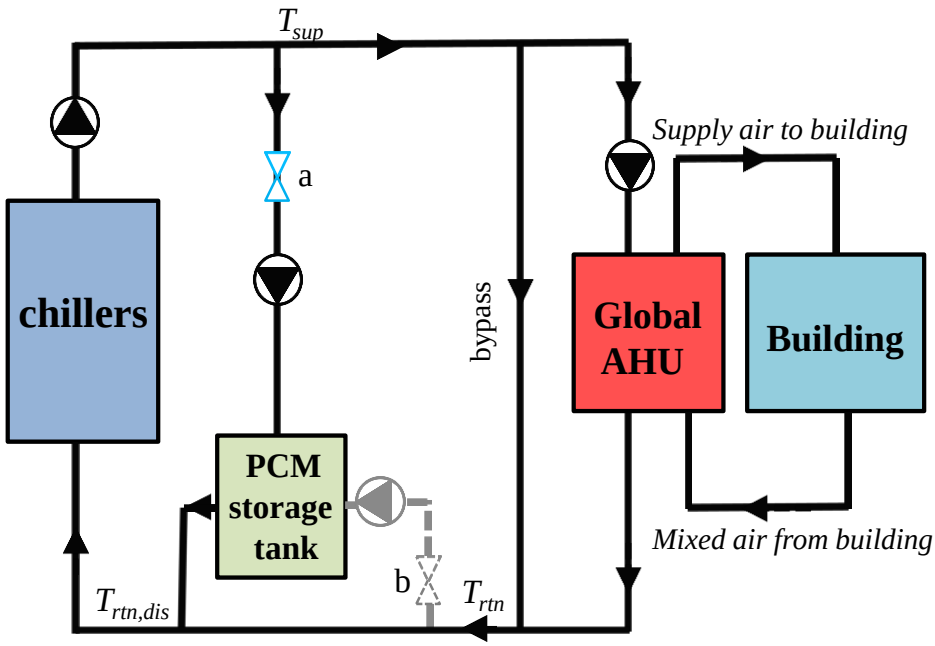

(b) Charging process

Fig.3.5 Chiller downstream PCM storage system configuration

The chilled water temperature at the outlet of the chillers was set at 7°C during normal operation while it was set at 5.5 °C during storage charging period. The reason for setting different supplied chilled water temperature is that if the temperature of charging fluid is lower, the PCM with lower freezing and melting temperature can be selected. The heat transfer effect will be better during discharging process.

It is worth noticing that Different PCM storage system configurations actually, to some extent, affect heat transfer efficiency and consequently the results of the applied control strategy. But this thesis focuses on an optimal control and design methods of CTES considering the performance of the whole system. In addition, the simulation results of all the case studies are based on the same configuration. Therefore, the influence of different PCM storage system configurations is not considered in this thesis and the qualitative conclusions of the paper are not affected.

3.2.4 Models of the major HVAC components

The models of major components, except for PCM storage tank, used to construct the complex dynamic simulation platforms were summarized as followed.

Chiller

The chiller model was developed in [Wang et al, 2000]. It is used to simulate the chiller power performance dynamically under various operation conditions. The simulation is based on the impeller tip speed, impeller exhaust area, impeller blades angel and other 13 coefficients and constraints. The compression process in compressor, heat transfer process in evaporator and condenser are simulated in this chiller model. The compressor model is based on the Euler turbo-machine equation, energy balance equation and mass conversion equation. The Euler equation is shown in Eq. 3.1. Eq. 3.2 and Eq.3.3 describe the energy balances in the impeller control volume and compressor control volume. The inlet losses, friction losses and incidence losses are considered in the two control volumes. Eq. 3.4 and Eq. 3.5 show such hydrodynamic losses ($h_{hyd,com}$ *and* $h_{hyd,imp}$) respectively.

$$h_{th} = u_2\left[u_2 - (\frac{\pi^2}{8})^2 VV_{r2}\left(ctg\beta + B\frac{\upsilon_{inta}}{\upsilon_{ext}}tg\gamma\right)\right] \tag{3.1}$$

$$h_{th} = h_{pol,com} + h_{hyd,com} \tag{3.2}$$

$$h_{th} = h_{pol,imp} + h_{hyd,imp} + \frac{VV_{imp,ext}^2}{2} \tag{3.3}$$

$$h_{hyd,com} = \varsigma\left[1 + \psi_1(\frac{\upsilon_{inta}}{\upsilon_{ext}}\frac{1}{cos\gamma})^2 + \psi_2(\frac{\upsilon_{inta}}{\upsilon_{ext}}tg\gamma)^2\right]C_{r2}^2 \tag{3.4}$$

$$h_{hyd,imp} = \varsigma\left[\chi + \psi_1(\frac{\upsilon_{inta}}{\upsilon_{ext}}\frac{1}{cos\gamma})^2 + \psi_2(\frac{\upsilon_{inta}}{\upsilon_{ext}}tg\gamma)^2\right]C_{r2}^2 \tag{3.5}$$

where, h_{hyd} is the hydrodynamic losses and h_{th} is the compressor theoretical head. u_2 is the impeller tip speed. B refers to the ratio of the impeller channel depth in the intake position to the depth in the exhaust position. β is the vane angel. h_{pol} means the polytropical compression work. υ_{inta} and υ_{ext} are the specific volumes in the impeller intake and exhaust positions respectively. $VV_{imp,ext}$ is the vapor velocity in the impeller exhaust position. γ is the pre-rotation vane angle. VV_{r2} is the impeller radial velocity in the exhaust position. ψ_1, ψ_2, ς, χ are the introduced constants. Subscripts *imp* and *com* indicate the impeller and compressor respectively.

The chiller power is calculated using Eq. 3.6. It is calculated based on the internal compression power (P_{inter}) which is variable and the power losses (P_{loss}) which is constant. Where, ϖ is a coefficient.

$$P = P_{loss} + \varpi \cdot P_{inter} \tag{3.6}$$

The classical heat exchanger efficiency method is used to simulate the evaporator and condenser. The thermal storage units are used to represent the dynamic responses of the chiller to the changes of the temperature in the inlet. Eq. 3.7 and 3.8 are used to show the models of the two heat exchangers. The first-order differential method is used to model them.

$$CAP_{flow,ev}\frac{dT'_{ev,inta}}{d\tau} = c_w M_{w,ev}(T_{ev,inta} - T'_{ev,inta}) \tag{3.7}$$

$$CAP_{flow,cd}\frac{dT'_{cd,inta}}{d\tau} = c_w M_{w,cd}(T_{cd,inta} - T'_{cd,inta}) \tag{3.8}$$

where, T is the temperature and T' is the temperature after introducing dynamic effects. CAP_{flow} is the capacity flow rate. c_w is the specific heat of water . Subscript "*ev*" is evaporator while "*cd*" means condenser. τ is the time.

Cooling tower

The cooling tower model simulates the states of the outlet air and outlet water of the cooling tower, which is based on Braun's effectiveness model [Braun et al, 1989]. The model estimates the status of air at the outlet position and the status of cooling water from inlet of the cooling tower and the control signal to the fan. The control signal is normally linearly converted to fan frequency in the simulation.

As shown in from Eq.3.9 to 3.11., this cooling tower model is built based on the steady-state of energy and the mass balances on the incremental volume. The heat and mass transfer processes in the cooling tower is simulated by the effectiveness of the cooling tower ($\mathcal{E}_{ct}$). The actual heat transfer is then calculated in terms of the effectiveness as shown in Eq.3.12 to 3.15. The number of transfer unit (NTU) is calculated by Eq.3.16. The Empirical formulas as shown in Eq. 3.17 and 3.18 are used to predict the required air flow rate (M_a) and power consumption of the cooling tower (P_{ct}), respectively.

$$\frac{d\omega_a}{dV} = -\frac{NTU}{V_{total}}(\omega_a - \omega_{sat,w}) \tag{3.9}$$

$$\frac{dh_a}{dV} = -Le\frac{NTU}{V_{total}}[(h_a - h_{sat,w}) + (h_a - h_{sat,w})(1/Le - 1)h_{g,w}] \tag{3.10}$$

$$\frac{dT_w}{dV} = \frac{d_{h_a}/dV - C_{pr,w}(T_w - T_{ref})d\omega_a/dV}{[M_{w,i/}M_a - (\omega_{a,o} - \omega_a)]C_{pr,w}} \tag{3.11}$$

$$Q_{ct} = \varepsilon_{ct}M_a(h_{sat,w,i} - h_{a,i}) \tag{3.12}$$

$$h_{a,o} = h_{a,i} + \varepsilon_{cl}(h_{sat,w,i} - h_{a,i}) \tag{3.13}$$

$$\omega_{a,o} = \omega_{sat,w,ef} + (\omega_{a,i} - \omega_{sat,w,ef})exp(-NTU) \tag{3.14}$$

$$T_{w,o} = T_{ref} + \frac{M_{w,i}(T_{w,i} - T_{ref})c_{pr,w} - M_a(h_{a,o} - h_{a,i})}{M_{w,o}C_{p,w}} \tag{3.15}$$

$$NTU = c[\frac{M_w}{M_a}]^{1+n} \tag{3.16}$$

$$M_a = M_{a,des}[c_{01} + c_{02}\left(\frac{Freq}{Freq_{des}}\right) + c_{03}(\frac{Freq}{Freq_{des}})^2] \tag{3.17}$$

$$P_{ct} = P_{a,des}[c_{11} + c_{12}\left(\frac{Freq}{Freq_{des}}\right) + c_{13}(\frac{Freq}{Freq_{des}})^2] \tag{3.18}$$

where, ω_a is the air humidity ratio, $\omega_{sat,w}$ and $\omega_{sat,w,ef}$ are the saturation air humidity ratio and effective saturation air humidity ratio with respect to the temperature of the water surface, respectively. *Le* means the Lewis number. V_{total} is total volume. T_w is the water temperature. T_{ref} is the reference temperature of liquid water with zero enthalpy. h_a is the enthalpy of the moist air per mass of dry air. $h_{sat,w}$ is the saturation air enthalpy with respect to the water surface temperature. $h_{g,w}$ is the enthalpy of water above the reference state. M_a and M_w are the mass flow rates of dry air and water, respectively. $M_{a,des}$ and $P_{ct,des}$ are the air flow rate in cooling tower on the design condition and power consumption. *Freq* is the fan operating frequency. c_{01} - c_{03} and c_{11} – c_{13} are the coefficients.

Pump

The variable speed pump model was developed in [Wang, 1998]. It includes a steady-state frequency inverter, a steady-state pump and a dynamic actuator of the inverter. Eq.3.19 and 3.20 are used to calculate the power and pressure of pumps respectively. The coefficients in these two equations can be by identified by regression of historical operation data.

$$P_{pu}(Freq, M_w) = \sum_{p=0}^{m}\sum_{q=0}^{n} G_{pq}\, Freq^p M_w^q \tag{3.19}$$

$$PH_{pu}(Freq, M_w) = \sum_{p=0}^{m}\sum_{q=0}^{n} D_{pq}\, Freq^p M_w^q \tag{3.20}$$

where, PH_{pu} and P_{pu} are the pump pressure head and power consumption respectively. *Freq* is the frequency input to the pump. M_w means the water flow rate. *G* and *D* are the coefficients identified by least square method using historic operation data. *m, n, p, q* are exponentials, which are subject to the equations: m=n=4, p+q <=4.

AHU coil

The AHU coil model is simulates the air and water states at outlet. In this thesis, the physical model developed in a dynamic approach is used [Wang, 1998]. A first-order differential equation, shown in Eq. 3.21, is used to represent the dynamics of a coil with lumped thermal mass. The dynamic equation based on the energy balance ensures that the energy is conserved. The air and water temperatures at outlets ($T_{a,out}$, $T_{w,out}$) are calculated by Eq. 3.22 and 3.23 respectively, by the heat balances in both sides. The heat transfer calculation uses the classical heat transfer effectiveness and NTU methods. The classical method to calculate the effect of the fins in the air side on the thermal resistance is used.

$$C_{Coil}\frac{dT_{coil}}{d\tau} = \frac{T_{a,inta}-T_{coil}}{R_1} - \frac{T_{coil}-T_{w,inta}}{R_2} \tag{3.21}$$

$$T_{a,out} = T_{a,inta} - \frac{SHR(T_{a,inta}-T_{coil})}{R_1 C_a} \tag{3.22}$$

$$T_{w,out} = T_{w,inta} - \frac{T_{coil}-T_{w,inta}}{R_2 C_w} \tag{3.23}$$

where, C_{coil} is the overall thermal capacity of the coil. C_a and C_w are the capacity flow rates of air and water respectively. T_{coil} is the mean temperature of the coil. $T_{a,inta}$ and $T_{w,inta}$ are the air and water temperatures at intake positions. R_1 and R_2 are the overall heat transfer resistances at air and water sides. *SHR* is the sensible heat ratio.

3.3 Summary

This chapter presents the developed simulation platform involving the buildings, the HVAC systems and the PCM storage tank. The platforms are developed based on three real buildings with necessary simplifications. The outline of developed dynamic simulation platform and the models of the major components, i.e. chiller, cooling tower, pump, AHU coil and heat exchangers, in HVAC systems are given. The performance of the developed control strategies will be tested and evaluated on the platforms concerning power consumption and energy efficiency.

It worth noticing that the simulation platform used multiple dynamic models, such as chiller, AHU coil, pump and etc., which are calibrated with the field data in a real building. Therefore, the simulation platform can, to some extent, show the possible and reasonable real building performance, such as cooling demand and energy consumption. But the whole simulation platform is not calibrated with the actual data in a actual specific building or HVAC system, some scenarios and problems, i.e. dynamic characteristics of devices, in reality may not be reflected as expected.

CHAPTER 4 PCM STORAGE TANK MODEL DEVELOPMENT AND VALIDATION

For the model-based design and control strategy, the component models are essential for the control system to test and evaluate the system performance under different control settings and time-changing working conditions. For the detailed simulation of the active CTES, a simplified PCM storage tank model with acceptable accuracy and good reliability is developed concerning computational speed and program size when implemented in large scale system simulations. It can be employed to simulate the actual PCM storage tank for testing the performance of optimal design and control strategies of CTES for building demand management presented in Chapter 5-7.

Section 4.1 presents the introduction and the need of the simplified PCM storage tank model. The design of the developed PCM storage tank is introduced in Section 4.2. The corresponding mathematical model is presented in Section 4.3. The validation of the developed PCM storage tank model is conducted in Section 4.4. The active CTES properties and system configuration are described in Section 4.4. A summary is given in Section 4.5.

4.1 Introduction

To properly use CTES, a good knowledge on dynamic characteristics and energy performance of the CTES is essential, which can help the operators fully understand the response characteristics and potential energy/cost saving due to the use of CTES. It

could also help the operators adopt proper design options and concepts in the decision making process during the initial planning and design stages. In addition, advanced control and operational algorithm to maximize system operating efficiency is also possible to be utilized. Therefore, a reliable CTES model with acceptable accuracy is an important basis for the thermodynamic characteristic and energy performance analysis particularly for operational performance evaluation and control applications.

In general, purely data-driven models cannot always ensure the stable performance prediction although they are simple. Detailed physical models always require high computational costs and memory demands as well as a lot of iterations, which maybe prevent their applications in the large scale system simulation although they are effective. For large scale system simulations, the models utilized in the system should preferably have simplified structures with certain physical significance to ensure the stable performance prediction and acceptable accuracy over a wide range of operation conditions. The models should require less training and calibration efforts with readily historical operation data. The models should also need less computational cost and memory demand. According to these criteria, simplified models are the better choice for implementation in large scale system simulations. In this study, a simplified PCM storage tank model with acceptable accuracy and good reliability is developed concerning computation speed and program size when implemented in large scale system simulations.

PCM is selected as the storage media. If water storage is used, a large storage capacity is needed because the sensible heat capacity of water is relatively small. If ice storage is used, chillers for lower chilled water temperature are needed for ice making resulting

lower chiller COP. The PCM storage has relatively large latent heat capacity. It also allows the conventional chillers to meet the charging temperature requirement offering higher chiller COP. It is therefore more convenient and economically beneficial to employ PCM storage systems in buildings.

4.2 PCM Storage Tank Design

A schematic diagram of coil pipes configuration for cool storage system is shown in Fig.4.1. Where, the *RadiusF* means the inside radius of coil pipe filled with heat transfer fluid. The *RadiusN* means the boundary of PCM. The storage tank is a rectangular container, which consists of horizontal parallel curved pipes which are submerged in quiescent PCMs.

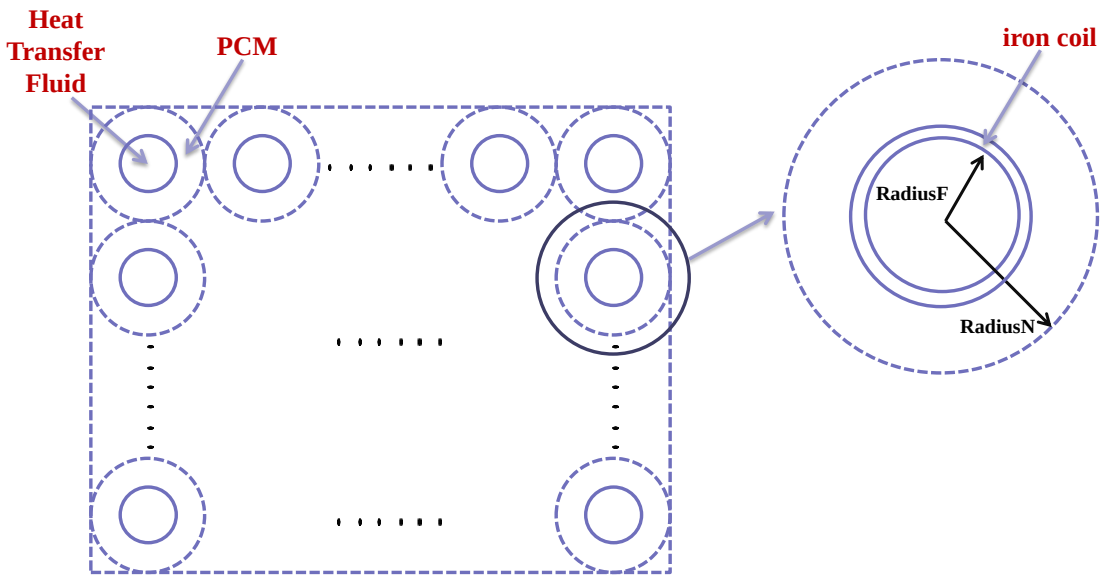

Fig.4.1 The schematic diagram of coil pipes PCM storage tank configuration

For simplifying the tank modeling and analysis, some assumptions were made as following:

1) The physical-thermal properties in both PCM and heat transfer fluid are constant.

2) The heat transfer fluid (HTF) and PCM in liquid status are both incompressible;

3) Axial conduction of the PCM and HTF are negligible as well as the natural convection in the liquid portion of PCM;

4) Axial conductions of the container walls are negligible;

5) All the pipes in the tank were independent of each other;

6) The initial temperature of HTF and PCM are set equally;

4.3 Mathematical Model

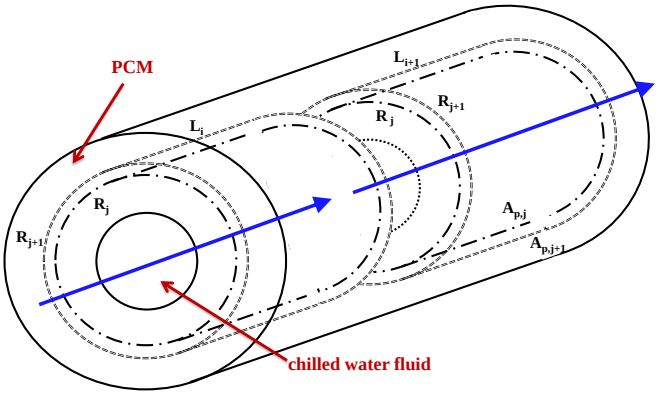

(a) PCM surrounding the tubes

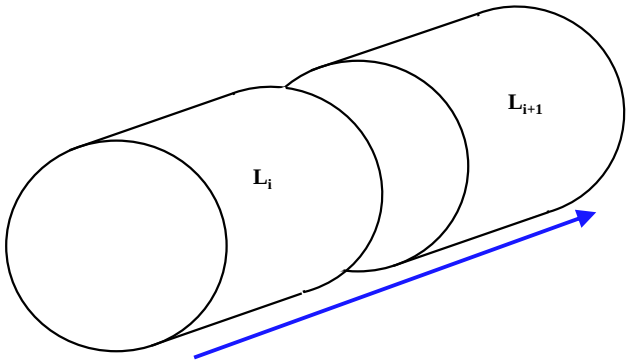

(b) Chilled water in tubes

Fig.4.2 Control volumes of PCM surrounding tubes and chilled water in tubes

Since some assumptions were made to simplify the mathematical model: the axial conduction of the PCM and HTF are negligible; the effect of the density difference between the solid and liquid PCM is not considered; no heat transfer enhancement methods, such as additives and fins, are introduced in the design of PCM storage model. Therefore, the simple finite method can be used. The control volume element is one cylinder composed by coil pipe and PCM surrounding the pipes. In this model, the chilled water in the tube is divided into N_{parts} "part" (cylinder) at axial direction as shown in Fig.4.2. The PCM surrounding each chilled water "part" is further divided into N_{layers} "layers" (hollow cylinders) at radial direction.

$$L_i = \frac{L}{Nparts} \tag{4.1}$$

$$RA_j = \frac{(RadiusN-(RadiusF+W_{pi}))}{Nlayers} \times j + RadiusF \tag{4.2}$$

where, L_i means the length of ith part ($1 \le i \le N_{parts}$) and RA_j means the radius of jth PCM layer ($1 \le j \le N_{layers}$). L is total length of PCM storage tank. W_{pi} means thickness of iron pipe.

According to energy balance of each segment of HTF and PCM, the charging and discharging processes are described in the following equations:

4.3.1 Sensible heat change stage:

For heat transfer fluid:

$$\frac{T_{f,i}^{k+1}-T_{f,i}^{k}}{\Delta t} = \frac{h \cdot A_h}{c_f \cdot \rho_f \cdot A_c}\left(T_{p,i,1}^{k+1} - T_{f,i+1}^{k+1}\right) - u \cdot \frac{T_{f,i+1}^{k}-T_{f,i}^{k}}{\Delta x} \tag{4.3}$$

where, $T_{f,i}$ means the temperature of HTF element in ith part at axial direction (°C) and k represent kth sampling time. $T_{p,i,1}$ means the temperature of PCM which is in first layer

of *ith* part at axial direction (°C), *htc* means heat transfer coefficient (W/m^2·K), A_h denotes the heat transfer area of coil pipes (m^2), A_c is cross area of coil pipes (m^2), *u* means flow velocity of HTF (m/s), c_f means HTF specific heat (kJ/kg·K), ρ_f means HTF density (kg/m^3), *x* is location at axial direction (m), Δt is time interval and Δx is space step at axial direction.

For first layer PCM:

where, $T_{p,i,2}$ means the temperature of PCM element which is in *i*th part at axial direction and in second layer at (°C), $M_{p,1}$ means first layer PCM mass (kg), C_p means PCM specific heat (kJ/kg·K), $R_{c,1}$ is PCM thermal resistance between *1*th and *2*th layers (m^2·K/W), $A_{p,1}$ is lateral surface area of *1*th layer PCM.

$$\frac{T_{p,i,1}^{k+1}-T_{p,i,1}^{k}}{\Delta t}=\frac{htc\cdot A_h}{c_p\cdot\frac{M_{p,1}}{N_{parts}}}\left(T_{f,i}^{k+1}-T_{p,i,1}^{k+1}\right)-\frac{T_{p,i,1}^{k+1}-T_{p,i,2}^{k}}{c_p\cdot R_{c,1}\cdot A_{p,1}\cdot\frac{M_{p,1}}{N_{parts}}} \tag{4.4}$$

For PCM in j layer (when $1<j<N_{layers}$):

$$\frac{T_{p,i,j}^{k+1}-T_{p,i,j}^{k}}{\Delta t}=\frac{\left(T_{p,i,j-1}^{k+1}-T_{p,i,j}^{k+1}\right)}{c_p\cdot R_{c,j}\cdot A_{p,j-1}\cdot\frac{M_{p,j}}{N_{parts}}}-\frac{\left(T_{p,i,j}^{k+1}-T_{p,i,j+1}^{k+1}\right)}{c_p\cdot R_{c,j+1}\cdot A_{p,j+1}\cdot\frac{M_{p,j}}{N_{parts}}} \tag{4.5}$$

For PCM in the last layer:

$$\frac{T_{p,i,N}^{k+1}-T_{p,i,N}^{k}}{\Delta t}=\frac{\left(T_{p,i,N}^{k}-T_{p,i,N-1}^{k+1}\right)}{c_p\cdot R_{c,N}\cdot A_{p,N-1}\cdot\frac{M_{p,N}}{N_{parts}}} \tag{4.6}$$

where, $N = N_{layers}$.

4.3.2 PCM phase change stage:

For heat transfer fluid:

$$\frac{T_{f,i}^{k+1}-T_{f,i}^{k}}{\Delta t}=\frac{htc\cdot A_h}{c_f\cdot\rho_f\cdot A_c}\left(T_{ch}-T_{f,i+1}^{k+1}\right)-u\cdot\frac{T_{f,i+1}^{k}-T_{f,i}^{k}}{\Delta x} \quad (4.7)$$

For first layer PCM in phase change stage:

$$H_{pcm}\cdot\frac{\Delta M_{delt}}{\Delta t}=htc\cdot A_h\cdot\left(T_{f,i}^{k+1}-T_{ch}\right)-\frac{T_{ch}-T_{p,i,2}^{k}}{R_{c,1}\cdot A_{p,1}} \quad (4.8)$$

where, T_{ch} means PCM melting or freezing temperature, ΔM_{delt} means solid or liquid status PCM element mass change. H_{pcm} means melting or freezing latent heat of PCM (kJ/kg·K).

For PCM in the middle layer:

$$H_{pcm}\cdot\frac{\Delta M_{delt}}{\Delta t}=\frac{T_{p,i,j-1}^{k+1}-T_{ch}}{A_{p,j-1}\cdot R_{c,j}}-\frac{T_{ch}-T_{p,i,j+1}^{k+1}}{A_{p,j+1}\cdot R_{c,j+1}} \quad (4.9)$$

For PCM in the last layer:

$$H_{pcm}\cdot\frac{\Delta M_{delt}}{\Delta t}=\frac{T_{ch}-T_{p,i,N-1}^{k+1}}{A_{p,N-1}\cdot R_{c,N}} \quad (4.10)$$

The heat transfer coefficient of the HTF (*htc*) inside the tubes is determined from Eq.4.11 to 14 [Wu et al, 2012]. Where, k_f is the thermal conductivity of HTF. Nu_f is the Nusselt number of HTF. *Re* is the Reynolds number. *Pr* is the Prandtl number. *d* is the inside radius of tube.

$$htc=\frac{k_f\cdot Nu_f}{d} \quad (4.11)$$

$$Nu_f=0.023Re^{0.8}\cdot Pr^{0.4}, \text{ when } Re>2300 \quad (4.12)$$

$$Nu_f=3.66+\frac{0.0534(Re\cdot Pr\cdot d/L)^{1.15}}{1+0.0316(Re\cdot Pr\cdot d/L)^{0.84}}, \text{ when } Re\leq 2300 \quad (4.13)$$

The thermal resistance of the PCM between *j*th and *j+1*th layers ($R_{c,j}$) is determined from Eq.4.14. Where, k_p is the thermal conductivity of PCM.

$$R_{c,j} = \frac{\ln(R_{j+1}/R_j)}{2 \cdot \pi \cdot k_p \cdot L_i} \tag{4.14}$$

The initial and boundary conditions of the above equations are stated in the following:

$$T_{f,0,k} = T_{f,inta} \tag{4.15}$$

$$T_{f,i,0} = T_{p,i,j,0} = T_{ini} \tag{4.16}$$

where, $T_{f,inta}$ is temperature of HTF at the intake and T_{ini} is the initial temperature of PCM and chilled water in coils.

The charge/discharge rate of the cool CTES (Q_{dis}) is determined by Eq. 4.17:

$$Q_{dis} = A_c \cdot u \cdot c_f \cdot \rho_f \left(T_{f,inta} - T_{f,out}\right) \tag{4.17}$$

where, $T_{f,inta}$ and $T_{f,out}$ are the chilled water temperatures at the intake and outlet of the tubes respectively. A_c is the cross area of the tube. u is the flow velocity of chilled water in the tube. c_f is the specific heat of chilled water. ρ_f is the density of chilled water.

The thermal conduction loss depends on the surface of the tank, the heat transfer coefficient of the tank wall, and the temperature as well as conductivity of the medium surrounding the tank. The conduction loss for a given tank can be calculated by Eq. 4.18.

$$Q_{loss} = U \cdot A \cdot (T_{am} - T_{mean}) \tag{4.18}$$

where, Q_{loss} is the conduction loss. U is the heat transfer coefficient. A is the tank surface area. T_{mean} is the mean temperature of PCM. T_{am} is the ambient temperature surrounding the tank. The overall conduction loss is assumed to be 5% of storage capacity per day (note: the normal range given is between 1% and 5% in [ASHRAE, 1993]).

PCM tank volumetric thermal storage density:

$$\mu_p = \frac{M_p \cdot H_{pcm}}{V_{tank}} \tag{4.19}$$

where, μ_p is volumetric storage density of PCM storage tank (kWh/m^3). V_{tank} is the tank volume. It is worth noticing that this parameter can be an important indicator to verify the PCM tank design.

4.4 Model Validation

This sub-section presents the validation of the developed PCM storage tank model. The two main outputs concerned are the charge/discharge rate and the mean PCM temperature in the tank. The validation is conducted through comparing the above two model outputs with the results from an experimental study [Castell et al, 2011]. The main parameters used in the PCM storage tank model include heat transfer surface, PCM density, thermal-properties of HTF and PCM, etc. and the values of these parameters are those in the experiment as shown in Table 4.1.

As shown in Fig.4.3, the $T_{PCM,simu}$ and $Q_{dis,simu}$ are the simulated mean PCM temperature and discharge rate respectively. The $T_{PCM,act}$ and $Q_{dis,act}$ are the actual mean PCM temperature and discharge rate respectively. The mean absolute error (MAE) of $T_{PCM,simu}$ and $Q_{dis,simu}$ are 1.68 ˚C and 0.07 kW respectively. The mean absolute percentage error (MAPE) of $T_{PCM,simu}$ and $Q_{dis,simu}$ are 12% and 10% respectively. The root mean square error (RMSE) of $T_{PCM,simu}$ and $Q_{dis,simu}$ are 1.99 ˚C and 0.11 kW respectively. By comparing the model outputs and the corresponding experimental results, it can be found that the outputs of the PCM storage tank model well match the experimental data,

indicating that the model accuracy is acceptable.

Table 4.1 Parameters used in the PCM storage tank model

PCM	Latent heat (kJ/kg)	145
	Melting point (˚C)	-27
	Specific heat (kJ/kg·K)	1.99
	Density (kg/m^3)	1320
HTF	Specific heat (kJ/kg·K)	2.8
	Density (kg/m^3)	1315
PCM storage tank	Tank diameter (m)	0.29
	Tank height (m)	0.35
	Pipe length (m)	5.46
	Pipe internal diameter (m)	0.008
	Heat transfer surface (m^2)	0.98

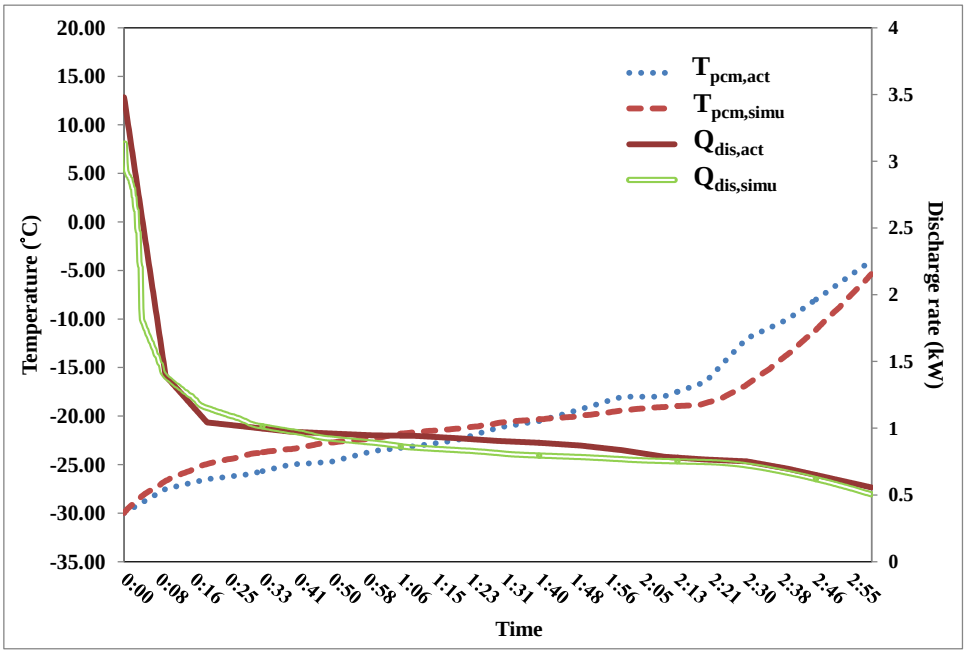

Fig.4.3 Outputs from tank model *vs* results from experiment

4.5 PCM storage properties

The PCM material selected in this study is E8 from a UK manufacturer [PCM Products Ltd. Sales Literature, www.pcmproducts.net]. The thermal properties and the price of PCM as well as storage tanks are listed in Table.4.2.

Table 4.2 Thermal-physical properties and price of PCM and PCM tank

PCM (E8)	Phase change temperature(°C)	8 °C
	Density (kg/m^3)	1469
	Specific heat (kJ/kg•K)	0.67
	Thermal conductivity (W/m•K)	0.43
	Latent heat (kJ/kg)	140
	Unit storage capacity (kWh/m^3)	57
PCM storage tank	capacity of unit volume (kWh/m^3)	35
	Price (HKD/m^3)	30000

4.6 Summary

The tank model is an essential part in storage system simulation platform for analyzing the system performance with different system configurations. In this study, a simplified physical dynamic model of coils storage tank, of acceptable accuracy and good reliability, is developed concerning computational speed and program size when implemented in large scale system simulations. The design and mathematical equations of the model are introduced. The validation is conducted through comparing the two

main outputs of the model, including the discharge rate and the mean PCM temperature in tank, with the results from an experimental study. The validation results demonstrate that the model has acceptable accuracy and reliable performance. The thermal-physical properties as well as the price of PCM and PCM tank are listed, which are used in the later strategies to estimate the required volume and cost of used PCM storage tank.

CHAPTER 5 OPTIMAL DESIGN OF ACTIVE COOL THERMAL ENERGY STORAGE FOR BUILDING PEAK LOAD MANAGEMENT

A simulation-based optimal design method of active CTES for building peak load management is developed in this section. A quantitative analysis on the life-cycle cost saving potentials concerning the operational cost, initial investment and the space cost is presented. Using the actual load profiles of three real buildings with different sizes, the life-cycle cost saving potentials under the peak demand limiting control are investigated under Hong Kong electricity price structure. By using the marginal decision rule, the optimal storage capacities of active CTES, monthly/annual operational cost savings and corresponding peak demand set-points are obtained.

In sub-section 5.1, the necessity of life-cycle cost benefit analysis of active CTES is discussed. Sub-section 5.2 outlines the proposed storage capacity optimization method, including the PID limiting control and the law of diminishing marginal utility and marginal decision rule. The test and validation of the proposed capacity optimization method of active CTES is conducted through cases studies and analysis in sub-section 5.3. The summary is given in sub-section 5.4.

5.1 Necessity of Life-cycle Cost Benefit Analysis of Active Cool Thermal Energy Storage

Demand limiting control (or demand limiting operation) is one of the three most common cold storage system operation modes, i.e., full load shifting, load leveling and demand limiting control. In high density regions, such as Hong Kong, the space assigned for chiller plant rooms is usually very valuable so that it is not feasible to use large storage systems in chiller plant rooms for large scale daily cooling load shifting. However, the on-peak demand cost usually contributes over 50% to the monthly electric bills for large users in Hong Kong according to the electricity price structure of China Light and Power (CLP), a local power company in Hong Kong. Effective reduction of monthly peak demand is therefore desired for reducing the monthly electricity bill.

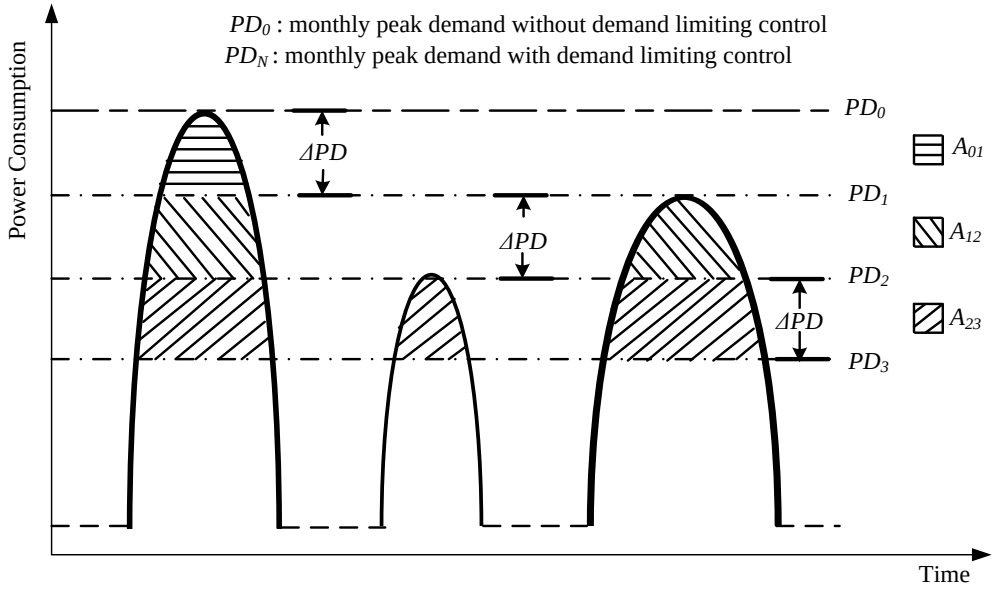

Fig.5.1 Impacts of different monthly peak demand set-points on shifted energy

Fig.5.1. illustrates the quantitative relation between the energy shifted and the monthly peak demand reduction. The total electrical energy, which needs to be shifted at a lower

monthly peak demand level, is much higher than that when reducing the same amount of monthly peak demand at higher level (i.e.: $A_{01}<A_{12}<A_{23}$). Where, the monthly peak demand without demand limiting control is represented by PD_o. PD_1, PD_2 and PD_3 are three levels of monthly peak demand if demand limiting control is used. A_{01}, A_{12} and A_{23} are amounts of the electrical energy to be shifted from Level 0 to Level 1, from Level 1 to Level 2 and from Level 2 to Level 3, respectively. It can be observed that the required storage capacity (Q_{sto}) increases progressively when the desired monthly peak demand reduction increases as shown in Fig.5.1 and Fig. 5.2.

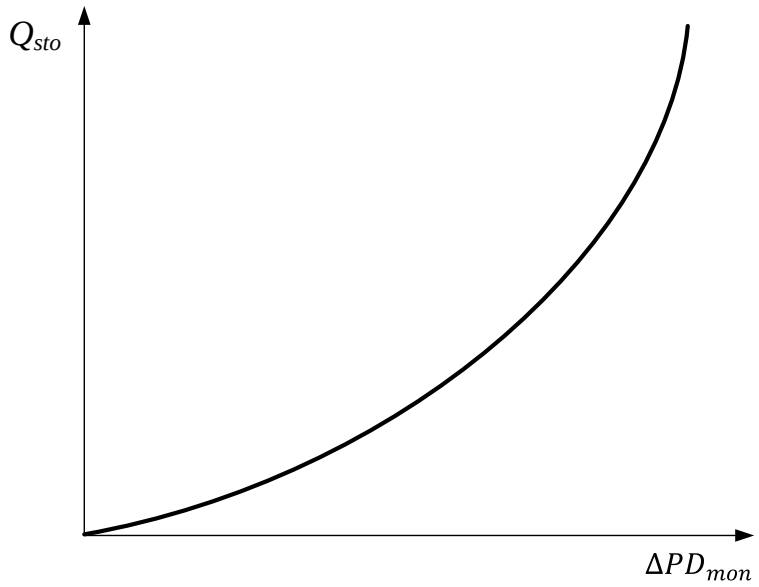

Fig.5.2 Peak demand reduction *vs* storage capacity

Although the operational cost saving increases as the storage capacity increases, the capital cost also rises at the same time. Therefore, there should be a compromised storage capacity when the average annual system cost, which includes annualized capital cost of the storage system and the annual space rent, is considered. Fig.5.3. illustrates the effects of storage capacity on maximum annual net cost saving. Q_{opt} is the optimal

storage capacity that leads to the maximum annual net cost saving over the life cycle when the difference between annual operating cost saving and average annual system cost is maximum. If an inappropriately low capacity is selected, the limited storage capacity will result in low annual net cost saving, while if an inappropriately high capacity is selected, the annual net cost saving will also be low or even negative because the annual average system cost approaches and will finally exceed the annual operational cost saving, i.e. at Point A. This section presents a method, which identifies optimal storage capacity and the corresponding monthly peak demand set-points for maximizing the annual net cost saving.

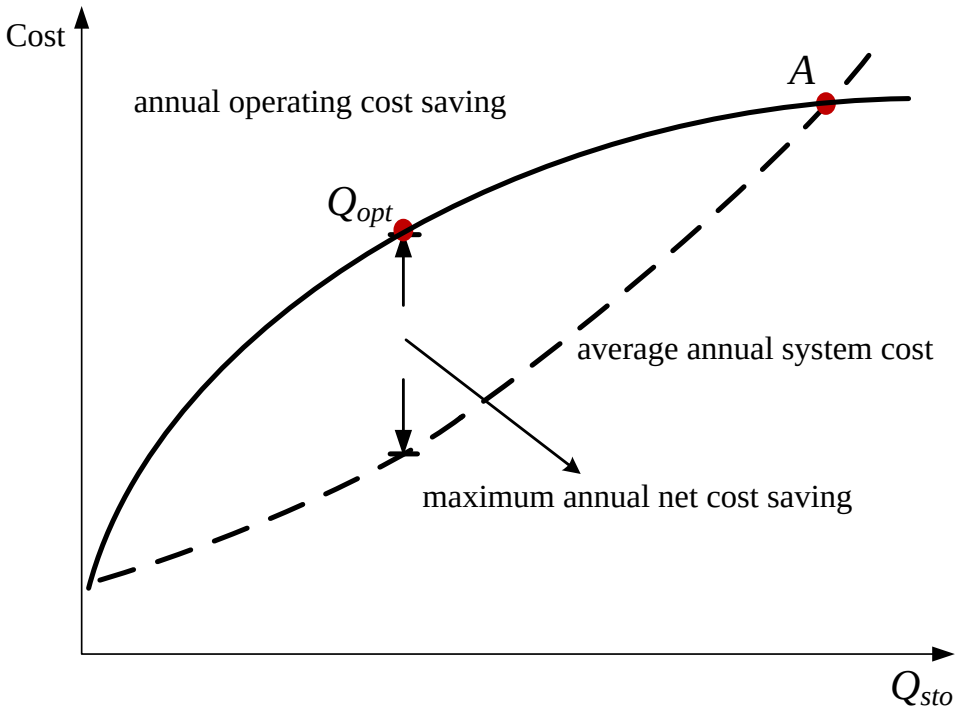

Fig.5.3 Effects of storage capacity on net cost saving

5.2 Storage Capacity Optimization Method

The storage capacity optimization method is introduced in this sub-section. The

discharging and charging of active storage tank is controlled by the PID limiting control method which is introduced in sub-section 5.2.1. The marginal decision rule is presented in sub-section 5.2.2 and is used to determine the optimal storage capacity for achieving maximum annual net cost saving under demand limiting control, which is performed in sub-section 5.2.3.

5.2.1 PID limiting control

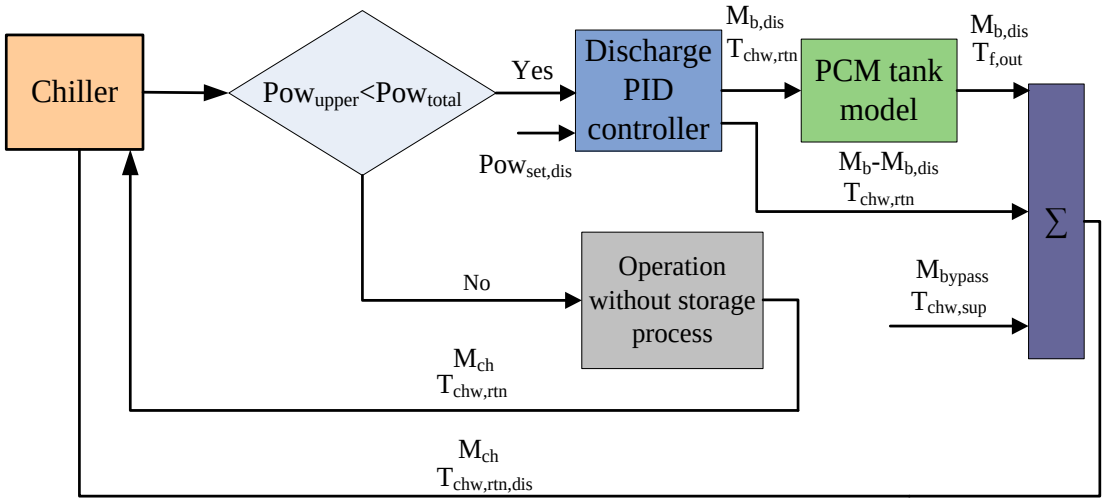

Fig.5.4 Schematic of PID control algorithm during discharging

The PID demand limiting algorithm for reducing the daily peak demand is shown in Fig.5.4 and the corresponding system diagram is shown in Fig.5.5. Typical monthly non air-conditioning power consumption (Pow_{other}) and the air-conditioning load (Q_{cl}) are used as the inputs in the dynamic simulation platform. The control variable is the total building power (Pow_{total}). When the total building power consumption exceeds the peak demand set-point (Pow_{upper}), the discharge PID controller will be activated to limit the power consumption within the target set-point ($Pow_{set,dis}$). Part of the return chilled water from building (M_b), as the HTF (heat transfer fluid, chilled water to tank

particularly in this study), passes through the tank to release the heat (i.e. storage discharging). The valve opening is controlled by the PID controller to adjust the amount of chilled water flow ($M_{b,dis}$) passing through the storage. A larger temperature difference between PCM in tank and chilled water, normally 4 to 5 ˚C, can be therefore maintained.

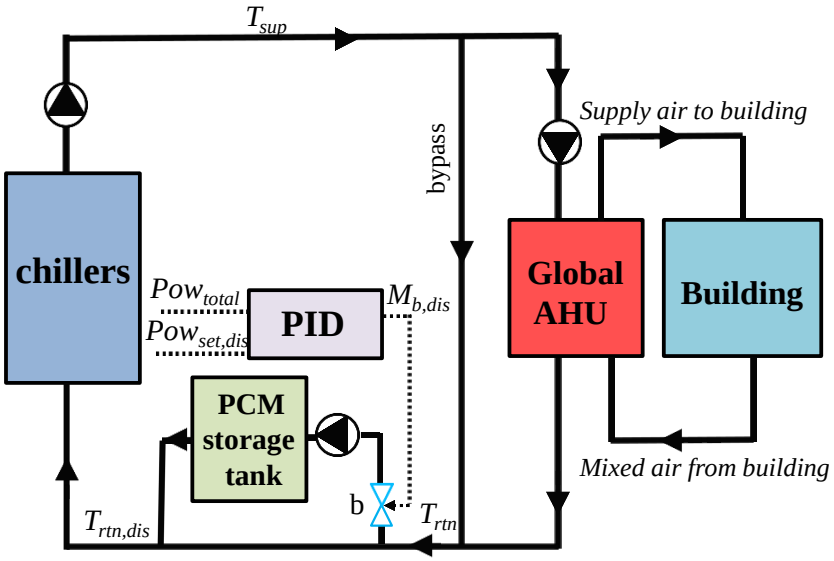

Fig.5.5 System diagram of PID control during discharging

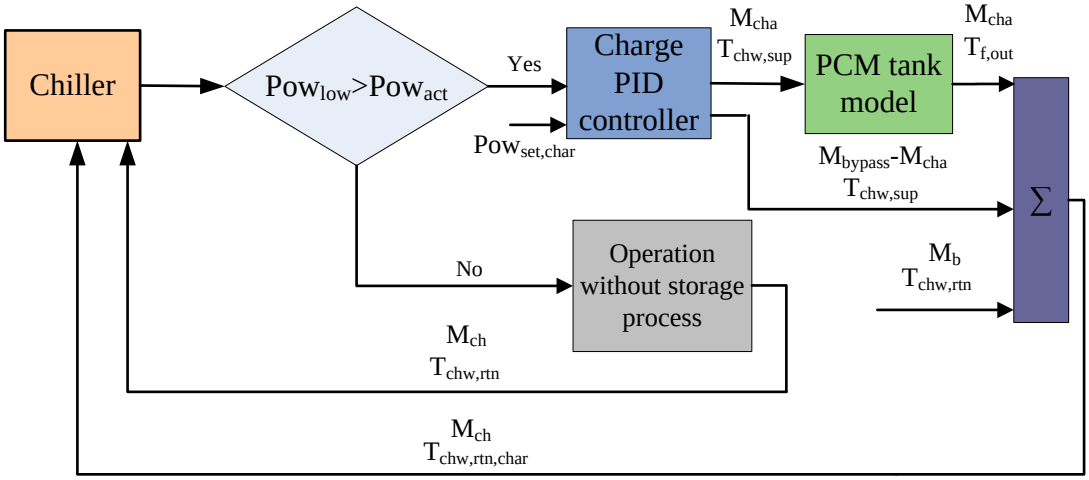

Fig.5.6 Schematic of PID control algorithm during charging

Similarly, another PID controller will be activated to control of the proportion the supply chilled water from main pipe as charging flow rate to cool the PCM when the Pow_{total} is lower than the charge set-point (Pow_{low}) as shown in Fig.5.6. The system diagram of PID control during charging is shown in Fig.5.7.

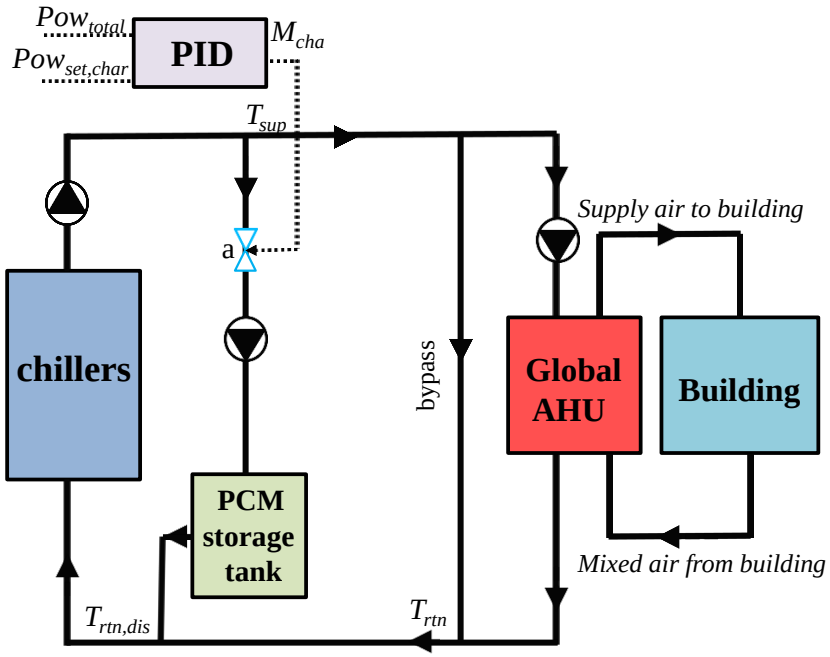

Fig.5.7 System diagram of PID control during charging

5.2.2 Law of diminishing marginal utility and marginal decision rule

In economics, the expression “marginal” is a key term and always means “additional” or “extra” [Samuelson and Nordhaus, 2010]. “Marginal utility” denotes the additional utility gets from the consumption of an additional unit of a product or service, where “utility” is benefit or satisfaction. The “marginal cost” is the amount by which an additional unit of product or service increases to its total cost. It is the cost of consuming one more unit of a product or service.

The “law of diminishing marginal utility” states that, as the consumption of a product or service increases, there is a decline in the marginal utility that derived from consuming each additional unit of that product [Rittenberg and Tregarthen, 2009]. Although keeps increasing as more good or service consumed, the total utility or benefit will grow as a slower and slower rate. To determine the quantity of any activity that will maximize its net benefit, marginal decision rule is selected [Rittenberg and Tregarthen, 2009]. If the marginal utility exceeds the marginal cost, the quantity of product should be increased while if the marginal utility is less than the marginal cost, the quantity should be reduced. Net benefit is maximized at the point at which marginal benefit equals marginal cost.

5.2.3 Optimal storage capacity and annual net cost saving identification

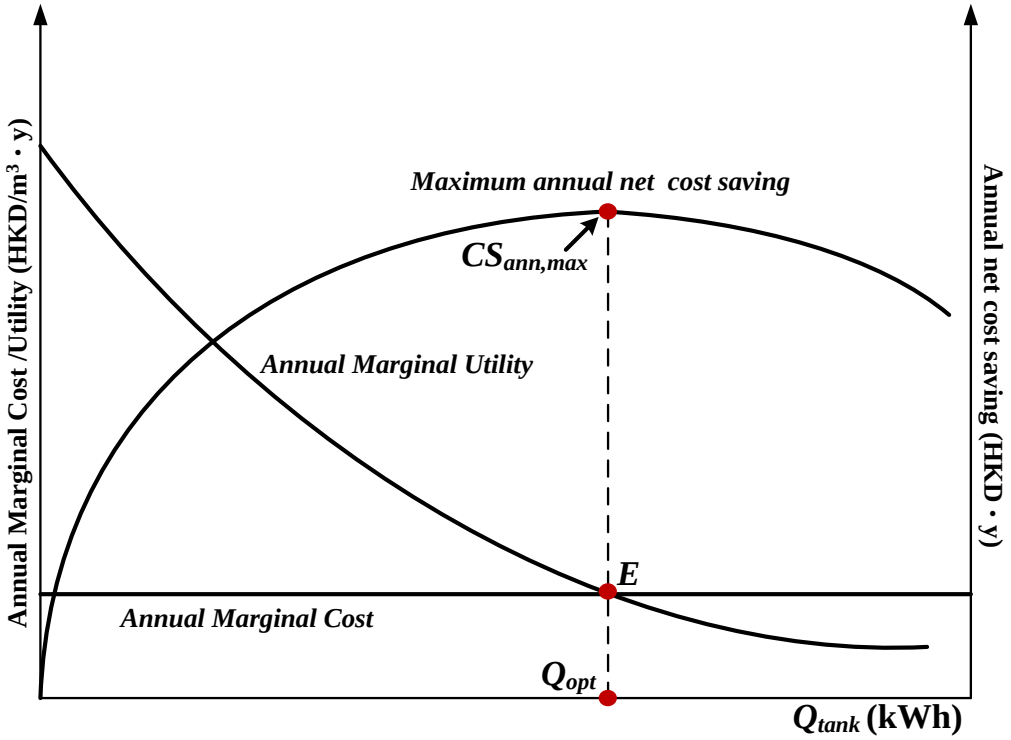

Fig.5.8 Storage capacity optimization with marginal decision rule

In this study, the above marginal decision rule is used to determine the optimal storage capacity for achieving maximum annual net cost saving under demand limiting control. As shown in Fig.5.6, annual operating cost saving increases as a slower and slower rate because cost saving from increased unit of storage capacity decreases while the average annual system cost increases almost at constant rate. The average annual system cost can be regarded as annual marginal cost. The annual operating cost saving from increased unit storage capacity is used as annual marginal utility. Therefore, the maximum annual net cost saving is achieved at the point at which the annual marginal utility equals the annual marginal cost (i.e. at Point *E*), as shown in Fig.5.8.

The annual net cost saving can be written as Eq. (1). Where, CS_{ann} is the annual net cost saving and $f(Q)$ is the corresponding function of Q (storage capacity). $f_y(Q)$ and $f_c(Q)$ are annual marginal utility and annual marginal cost respectively which are also the functions of Q. The optimal storage capacity and corresponding maximum annual net cost saving can be achieved by solving the following equation:

$$CS_{ann} = \int_0^{\mathrm{Q}} [f_y(Q) - f_c(Q)]\mathrm{d}Q = f(Q)\ (CS_{ann} \in [CS_{ann,lower}, CS_{ann,upper}]) \quad (5.1)$$

$$\frac{d(CS_{ann})}{d(Q)} = 0 \quad (5.2)$$

where, $CS_{ann,upper}$ is decided by the maximum allowable pay-back period as well as maximum allowable capital investment while $CS_{ann,lower}$ is determined by the allowable minimum annual operating cost saving.

Hence, the maximum annual net cost saving can be written in Eq. (5.3):

$$CS_{ann,max} = \int_0^{Q_{opt}} [f_y(Q) - f_c(Q)]\mathrm{d}Q = f(Q_{opt}) \quad (5.3)$$

where, $CS_{ann,max}$ is the maximum annual net cost saving as shown in Fig. 5.6. Q_{opt} is the optimal storage capacity.

The average lifespan of the major equipment in the air-conditioning system is assumed to be 10 years. The investment of unit volume storage system tank is 30000 HKD/m^3 referred to Table 4.2. The space rent is 4000 HKD/m^3·y. Therefore, the total capital investment of unit volume storage system tank is assumed as 34000 HKD/m^3 over ten-year period. The average annual system cost, namely annual marginal cost, is then 3400 HKD/m^3·y.

Because the cool storage tank mainly affects the performance of water side, the detailed configuration of air side of HVAC system is not included in the simulation. Instead, the power consumption of the air side is introduced as a major input.

One selected typical month in each of the three seasons (e.g. summer, winter and middle season) are simulated to represent the characteristics of the building annual power consumption. The annual marginal cost is the sum of monthly marginal cost. Meanwhile, the annual marginal utility is the sum of monthly marginal utility $f_m(x)$:

$$f_y(Q) = \sum_{i=1}^{12} \cdot f_{m,i}(Q) \tag{5.4}$$

where, $f_{m,i}(Q)$ is the monthly marginal utility in i_{th} month.

Generally, there are 2 main steps to obtain the optimal storage capacity:

1. By introducing actual load profiles as inputs, monthly demand limiting control with exhaustive search method, e.g. trial and error method, is used to determine the required storage capacities under different peak demand reductions in the dynamic simulation platform.
2. The optimal storage capacity and corresponding maximum annual net cost

saving can be then obtained by using the marginal decision rule. The peak demand set-points of each month are determined to maximize peak demand reduction corresponding to the optimal storage capacity.

5.3 Case Studies and Analysis

The proposed simulation-based optimal design method of small scale active storage systems was validated using the dynamic simulation platform built in chapter 3. Storage capacities required for different peak demand reductions are firstly determined in Sub-section 5.3.1. Storage capacity optimization with marginal decision rule is then done in Sub-section 5.3.2.

5.3.1 Storage capacities required for different peak demand reductions

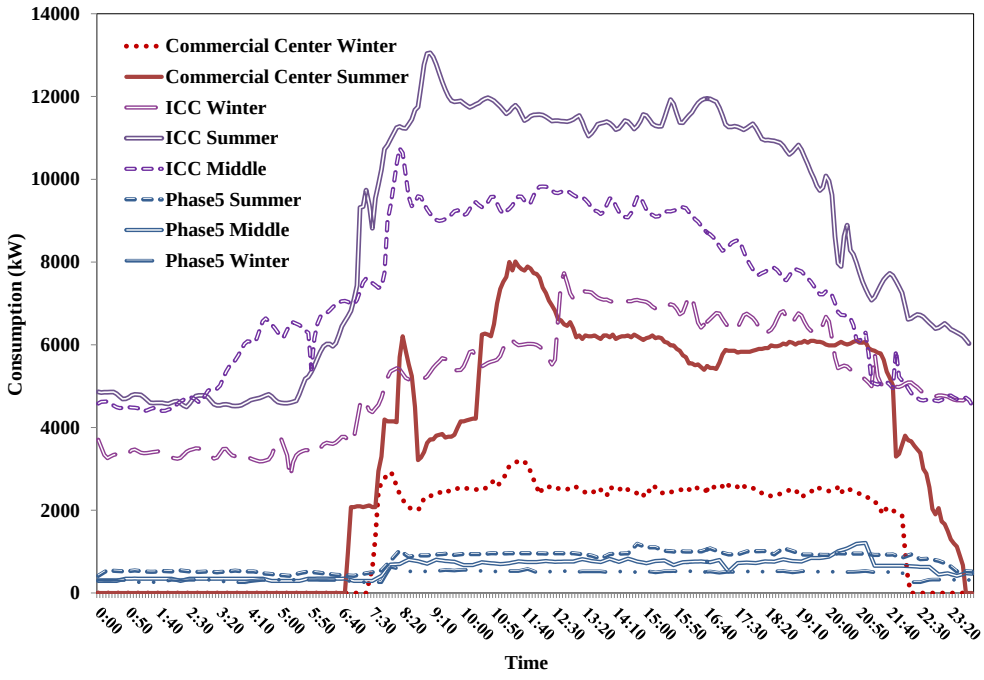

Fig.5.9 Typical daily total building power consumptions of three buildings in three seasons

To investigate the effects of using storage capacity on net cost saving, the PID demand limiting control was implemented to reduce monthly total building peak demand of three buildings in different seasons. Typical daily total building power consumptions of three reference buildings monitored in different seasons are shown in Fig.5.9. Due to the low quality of the measured data in middle season, only two seasons (summer and winter) of the commercial enter case were used.

The power spikes in the ICC building between 9:00 a.m. and 10:00 a.m. in the middle season and between 9:50 a.m. and 10:40 a.m. in the summer were not significant relatively. The spikes in the commercial center building between 10:00 a.m. and 13:00 p.m. in the summer and between 7:30 a.m. and 8:30 a.m. as well as between 11:00 a.m. and 12:00 a.m. in the winter were rather significant. The power consumption profiles have obvious impacts on the required storage capacities when certain monthly peak demand reductions were set, as shown in Fig.5.10 to Fig.5.12.

The required storage capacities used to shift cooling load in each day with different peak demand limits in a month are shown in Fig.5.10 to Fig.5.12. As the monthly peak demand reduction increased, the required storage capacity increased monotonically.

The required storage capacities in the winter case of the ICC building were larger than those in the other seasons when the expected peak demand reduction was larger than 500 kVA as shown in Fig.5.9 because the spike in winter was lower in magnitude and shorter in time as shown in Fig.5.10.

The maximum monthly peak demand reductions were around 140 and 300 kVA in the winter and the middle seasons respectively in phase 5 building because no more cooling load can be shifted if peak demand reduction increased further as shown in Fig.5.11.

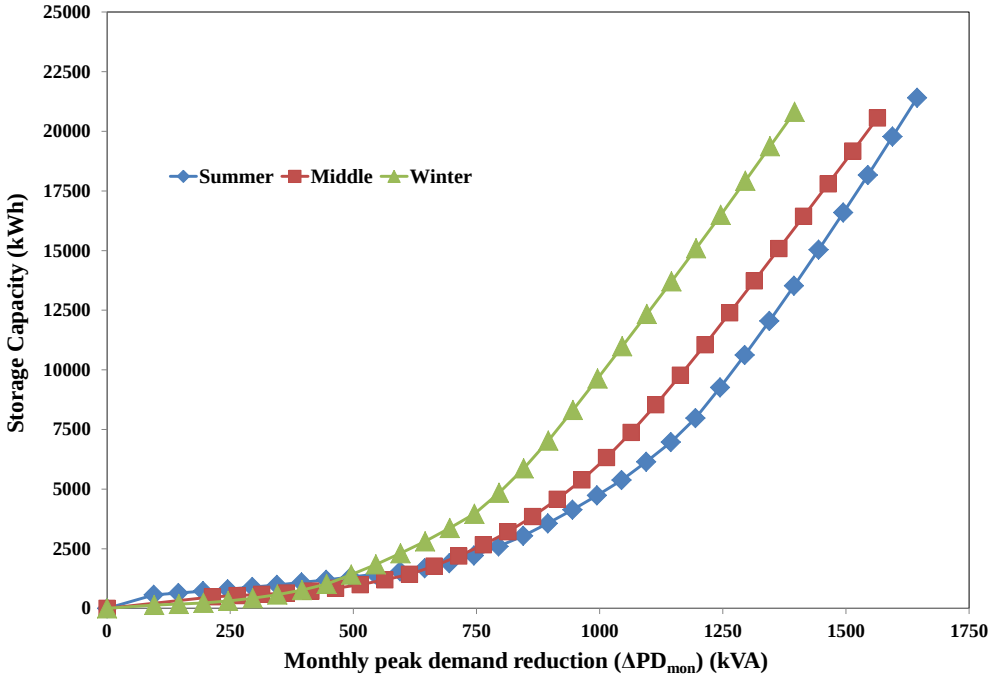

Fig.5.10 Required storage capacity for different monthly peak demand reductions in ICC

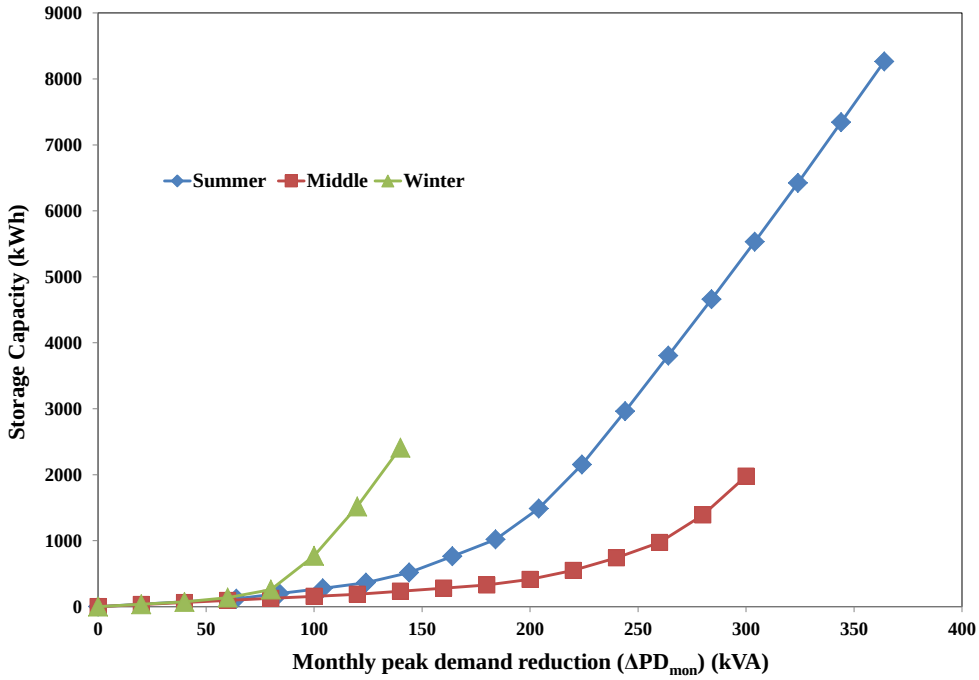

Fig.5.11 Required storage capacity for different monthly peak demand reductions in Phase 5 Building

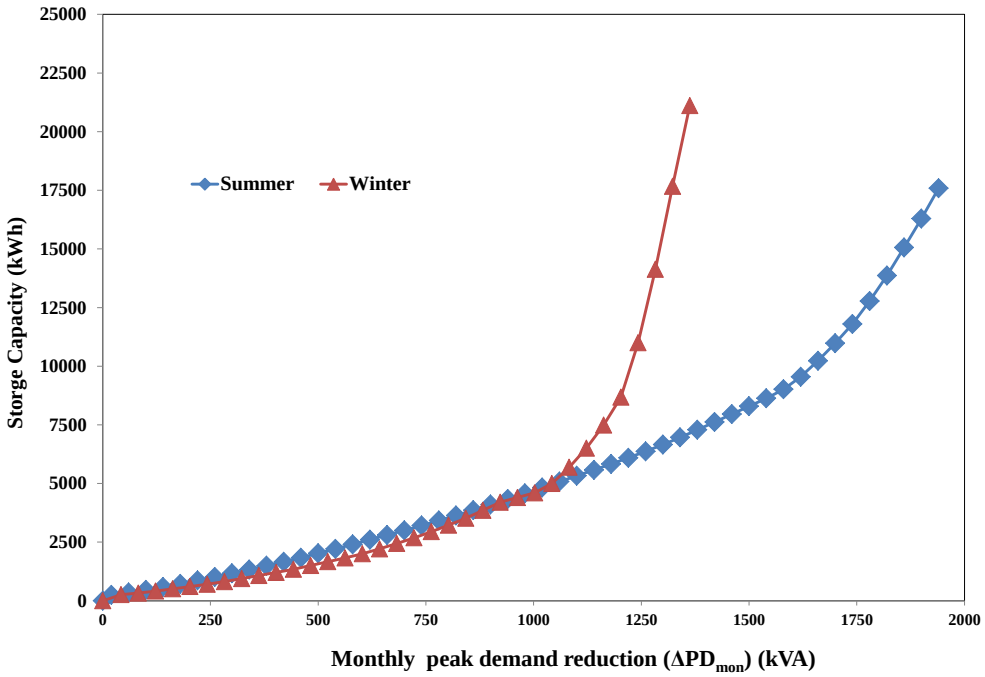

Fig.5.12 Required storage capacity under different monthly peak demand reductions in Commercial Center

Once the spikes of the commercial center building, as shown in Fig.5.9, had been shifted, the required storage capacities started to increase dramatically as the monthly peak demand exceeded about 1200 and 1600 kVA in winter and summer respectively, as shown in Fig.5.12.

Since the spikes in the ICC building were sharp, i.e., high in magnitude but short in time, the required storage capacity was smaller than that for the commercial center when the expected peak demand reduction was less than 500 kVA as shown in Table 5.1.

The required storage capacities of ICC building in different seasons were generally larger than those of the commercial center building when the peak demand reduction was over 1000 kVA. The reason was that more cooling load needed to be shifted in the ICC building if reducing the peak demand further after the spikes being shifted.

It should be noted that that the peak demands in different cases were mainly caused by the cooling load during the cool-down period at the start of the system operation. The cool-down periods appeared in the morning in all the three buildings.

Table 5.1 Required storage capacities under different monthly peak demand reductions in three buildings

Monthly peak demand reduction (kVA)	Required storage capacity (kWh)							
	ICC			Commercial Building		Phase 5		
	summer	middle	winter	summer	winter	summer	middle	winter
50	203	82	51	302	273	96	76	106
100	602	199	138	461	357	252	157	770
200	730	463	241	759	592	1398	413	-
300	903	550	431	1170	872	5510	1978	-
500	1321	950	1415	2022	1551	-	-	-
700	1903	2102	3377	3005	2555	-	-	-
1000	4799	6238	9702	4678	4703	-	-	-
1300	10620	13201	17928	6656	17281			

5.3.2 Capacity optimization

Identification of unit price for electrical demand and energy

In advance of storage capacity optimization with marginal decision rule, the unit price for electrical demand and energy should be identified firstly. The electricity price structure from China Light and Power (CLP) is depicted in Table 4. There are four different tariff types for the end-users in total. Each of them, except the first one, is mainly comprised of two items. One is the cost for the monthly peak demand and the other is the cost for the overall energy consumption in a total month. In addition, the

prices for the on-peak and off-peak periods are different. The on-peak prices are much higher than the off-peak prices, which is an attempt to encourage part of the on-peak load to be shifted into the off-peak period.

Table 5.2 Electricity price structure from CLP

<table>
<tr><td rowspan="3">Tariff type</td><td colspan="4">Composing items</td></tr>
<tr><td colspan="2">Demand part (HKD/kVA)</td><td colspan="2">Energy consumption part (Cent/kWh)</td></tr>
<tr><td>On-peak period</td><td>Off-peak period</td><td>On-peak period</td><td>Off-peak period</td></tr>
<tr><td rowspan="2">General Service Tariff</td><td rowspan="2">0.0</td><td rowspan="2">0.0</td><td>96.3(first 5000 kWh)</td><td rowspan="2">-</td></tr>
<tr><td>95.3(exceeding part)</td></tr>
<tr><td rowspan="2">Bulk Tariff</td><td>66.5(first 650)</td><td>0.0(less than on-peak)</td><td>68.9 (first 200,000)</td><td rowspan="2">61.4</td></tr>
<tr><td>63.5(exceeding part)</td><td>26.0(larger than on-peak)</td><td>67.4 (exceeding part)</td></tr>
<tr><td rowspan="2">Large Power Tariff</td><td>117.0 (first 5000)</td><td>0.0 (less than on-peak peak)</td><td>52.4 (first 200kWh/kVA)</td><td rowspan="2">42.9</td></tr>
<tr><td>112.0 (exceeding part)</td><td>33.0 (larger than on-peak peak)</td><td>50.4 (exceeding part)</td></tr>
<tr><td rowspan="2">Ice-storage Air-conditioning Tariff</td><td>66.5 (first 650)</td><td>0.0 (less than on-peak peak)</td><td>68.9 (first 200,000)</td><td rowspan="2">61.4</td></tr>
<tr><td>63.5 (exceeding part)</td><td>26.0(larger than on-peak)</td><td>67.4 (exceeding part)</td></tr>
</table>

The on-peak period in CLP refers to the time span from 9:00 a.m. to 9:00 p.m. of normal workday and the rest as well as the public holiday is the off-peak period. End-users may be qualified to take diverse tariffs according to specifications of CLP. For instance, the buildings with monthly peak demand larger than 3000 kVA can take the large power tariff, which may charge less in the electricity bill than the first two tariffs. If the buildings are equipped with the ice or chilled water-storage storage system, they are eligible to take the last tariff which appears more favorable in the monthly peak demand charge compared with that of the large power tariff.

To develop the demand limiting strategy, the large power tariff is selected. In this case, the price for the first on-peak 5000 kVA is 117 HKD/kVA; and the demand part exceeding 5000 kVA in the on-peak period will be charged 112 HKD/kVA. If the monthly peak demand in the off-peak period is larger than the monthly on-peak peak demand, extra cost will be charged for the exceeding part, i.e. 33 HKD/kVA. For the energy consumption cost, it is also divided into two parts, on-peak part and off-peak part. The load of the first 200kWh/kVA in the on-peak period charges 52.4 Cent/kWh and the exceeding part charges 50.4 Cent/kWh. All the energy consumed in the off-peak period will be charged at a constant price, i.e. 42.9 Cent/kWh.

Storage capacity optimization with marginal decision rule

The annual net cost savings with different storage capacities for three buildings are shown in Fig.5.13. - Fig.5.15. Annual marginal utility, namely annual operating cost saving from increased unit storage capacity, declined as the storage capacity increased while the annual marginal cost, namely average annual system cost, kept almost constant. The optimal storage capacity and corresponding maximum annual net cost

saving were achieved at the point at which the annual marginal utility equaled to the annual marginal cost.

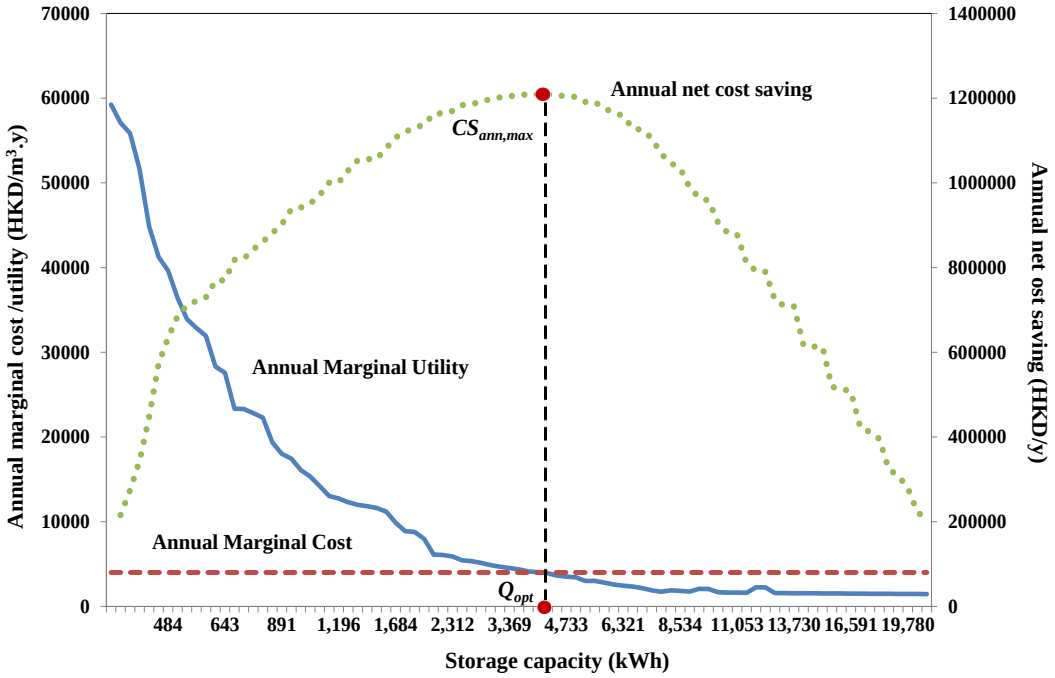

Fig.5.13 Annual net cost saving *vs* storage capacity (ICC)

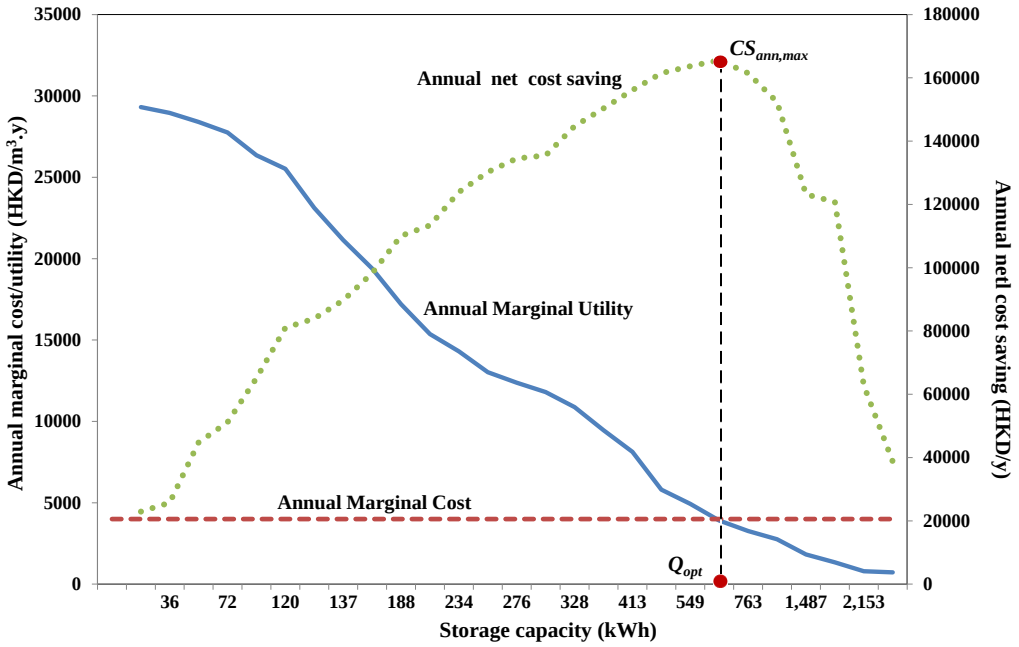

Fig.5.14 Annual net cost saving *vs* storage capacity (Phase 5)

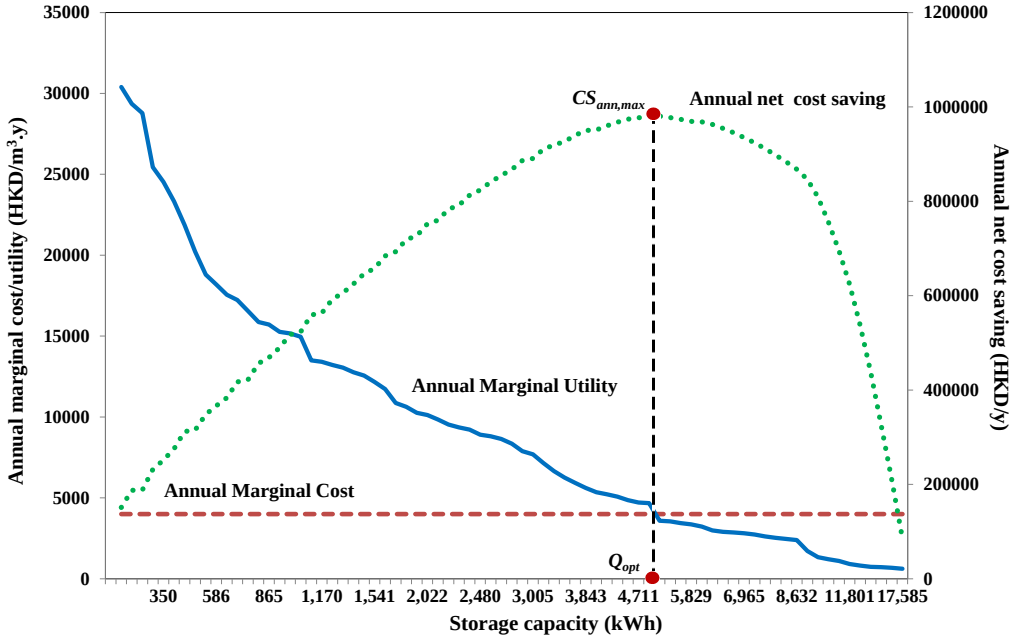

Fig.5.15 Annual net cost saving vs storage capacity (Commercial Center)

The maximum value of annual marginal utility of the commercial center building was much less than that of the ICC building because the spikes in the ICC building were sharp, i.e., high in magnitude but short in time, as explained above. However, the annual marginal utility of the ICC building declined faster the commercial center after storage capacity had increased over certain level. The intersection of annual marginal cost and annual marginal utility curves in the ICC building appeared ahead of that in the commercial center and the optimal storage capacity of the ICC building was smaller accordingly.

The results of storage capacity optimization are listed in Table 5.3. The PD_{ori} and PD_{opt} are the original monthly peak demand and optimal monthly demand set-point (kVA) respectively. It should be noted that the optimal storage capacity (Q_{opt}) was normally less than 5% of daily cooling load. The optimal peak demand set-points in different months were obtained after the Q_{opt} was determined. The CS_{ann} was significant, i.e. more

than 3% of the building annual energy cost (Co_{total}) for large and middle scale buildings. Meanwhile, the pay-back period (P_{back}) for each building was acceptable (2.7~2.8 years).

Table 5.3 Results of storage capacity optimization with marginal decision rule

Building	**ICC**			**Commercial Building**		**Phase 5**		
PD_{ori} (kVA)	12594	10209	7495	7793	3482	1144	1029	609
PD_{opt} (kVA)	11860	9360	6695	6440	2670	990	810	517
Q_{opt} (kWh)	3955			4935		595		
Q_{opt}/ Q_{daily}	1.0	1.2	1.9	3.8	6.2	1.5	2.3	3.4
V_{opt} (m^3)	113			141		17		
CS_{ann}	1,209,268			980,343		162,362		
CS_{ann}/ Co_{total}	2.9			6.5		4.6		
P_{back} (y)	2.73			3.72		2.78		

As discussed in sub-section 5.3.1, the power consumption profiles have obvious impacts on the required storage capacities. The characteristics of spikes, e.g. magnitude and duration, exist in building power consumption profiles affect the cost for given peak demand reductions. Another main factor is the electricity price structure. The electricity price structure introduced in this study comprises of two items. One is monthly peak demand charge and the other is the overall energy consumption charge over a month. Normally, there is no need to consider the demand charge during off-peak periods because the consumption of building is always much less than that in the on-peak period. The demand charge during on-peak period and the energy charge in the electricity price structure decide the effectiveness of power demand limiting control. The optimal design method is also applicable in other places where time-of-use plus peak demand charge

electricity price structure is used. Generally, it is more favorable to use active storage for limiting power demand when the demand charge is high and energy charge is low.

The Table 5.4 presents some typical time-of-use plus peak demand charge electricity price structures in USA [Henze et al, 2010]. These structures are similar to that in Hong Kong. Compared with that in Hong Kong, the higher on-peak demand charges and lower energy charges even provide greater incentives to employ the developed design method in these regions where the electricity price structures are employed.

Table 5.4 Typical time-of-use plus peak demand charge electricity price structures in USA

Location	Energy				Demand			
	Summer		Winter		Summer		Winter	
	On-Peak ($/kWh)	Off-Peak ($/kWh)	On-Peak ($/kWh)	Off-Peak ($/kWh)	On-Peak ($/kW)	Off-Peak ($/kW)	On-Peak ($/kW)	Off-Peak ($/kW)
Atlanta	0.1074	0.0194	0.0194	0.0194	8.59	4.30	-	4.30
Phoenix	0.1062	0.0410	0.0968	0.0372	4.88	-	0.31	-
Los Angeles	0.1150	0.0595	0.1027	0.0638	28.13	7.87	-	7.87
New York	0.0052	0.0052	0.0052	0.0052	14.99	9.79	6.56	2.73

5.4 Summary

A simulation-based optimal design method, which aims at achieving maximum annual net cost saving, of small scale active CTES systems for buildings peak load management is developed in this section. Substantial life-cycle cost saving can be obtained with relatively small scale active CTES. It is one more meaningful and effective design

method to optimize storage capacity concerning life-cycle cost saving involving both operational cost saving and capital cost associated to storage capacity.

The impact of the capacity of active CTES on the life-cycle cost saving is also analyzed. PID demand limiting control with exhaustive search method is used to reduce monthly total building peak demand of three buildings with different scales in different seasons. The optimal capacities of CTES and corresponding maximum annual net cost savings are then obtained using the law of marginal decision rule. Based on the results of the case studies, the following conclusions can be drawn:

1. Significant annual net cost saving, e.g. up to about 7% of total building annual electricity consumption cost, can be obtained by implementing the demand limiting control with small scale active CTES in different real buildings in Hong Kong where the power tariff is not favorable. The optimal storage capacities are normally less than 5% of daily cooling load.

2. One main factor that decides the required capacities of active CTES is the electricity price structure. The optimal design method is also applicable in other places where time-of-use plus peak demand charge electricity price structure is used. Normally, the higher on-peak demand charges and lower energy charges bring the more incentives to employ the developed design method.

3. The building power consumption profile has obvious impacts on the required storage capacities and corresponding annual net cost savings. In another word, whether or how the spikes exist in building power consumption profiles affect the cost for peak demand reductions.

4. The optimal capacity of active CTES can be determined conveniently from the

relationship between the annual net cost saving and the required capacity of CTES.

CHAPTER 6 FAST POWER DEMAND RESPONSE STRATEGIES FOR BUILDINGS INVOLVING ACTIVE AND PASSIVE COOL THERMAL ENERGY STORAGE

Two fast power demand response (DR) strategies for buildings involving both active and passive CTES for smart grid applications are developed in this section. These two control strategies provide immediate and stepped power demand reduction through shutting chiller(s) down when requested. In the basic fast DR strategy, only power demand reduction is the control objective, and the corresponding impacts on building indoor thermal comfort under different power reductions are discussed but not controlled. In the improved fast power DR strategy, the primary control objective is to restrain the building indoor temperature rise to maintain indoor thermal comfort within the expected level during the DR event while the demand reduction is the second control objective.

The introduction in Sub-section 6.1 aims to present the need for the fast power DR strategies for buildings. The outline of the developed two fast power DR strategies and the corresponding models and modules are introduced in Sub-section 6.2. The coefficients identification and validation of the used models and modules are performed in Sub-section 6.3. The case studies and analysis are proposed in Sub-section 6.4. A summary of the developed fast power DR strategies is given in Sub-section 6.5.

6.1 Introduction

As peak load and power imbalance are the critical issues which are concerned in an electrical grid, ancillary services avoiding power shortage, e.g. generator random outage and load fluctuations, become essential in power systems. The ancillary services can provide a certain generating capacity available to the grid within a short interval of time in order to meet demand when the normal power supply is insufficient. Generators have dominated supplying ancillary services through injecting power to the grid. With the arising of smart grid, the demand response resource (DRR) has become another appropriate choice. As discussed above, some Regional Transmission Operators (RTOs) and Independent System Operators (ISOs), such as Midwest ISO, New York ISO (NYISO), ISO New England (ISONE) and etc., have encouraged DRR to provide ancillary reserves.

One study [Kirby, 2006] pointed out that the HAVC system can be an ideal supplier to provide ancillary services for the grid for several reasons. For example, the HVAC loads are capable of numerous short curtailments. They can be rapidly restarted and ready to immediately respond again to another DR event. Furthermore, they do not have ramping time, minimum on time, or minimum off time limits that constrain some generators.

Chillers are the largest power consumers in an entire HVAC system and accordingly have great potential in power reduction control. One fast DR strategy, in which chiller(s) are shut down at the beginning of DR event, was developed [Xue et al, 2015]. Compared with the conventional demand limiting strategy, i.e., indoor air temperature set-point reset, the developed strategy can provide an immediate and stepped DR.

It is worth noticing that except passive CTES such as building thermal mass (BTM) discussed in sub-section 2.3, the usage of active CTES system in building for fast DR with short duration has been seldom studied. Active CTES system can actually play an important and active role in building demand response when integrated with HVAC system. The use of active CTES system can increase the capability of building demand response. In addition, the use of active CTES system also provide more controllability to modulate the power reduction profile to a more desired level, i.e. fixed power reduction.

This study therefore presents fast power demand response strategies for buildings with combined use of building passive and active CTES. Certain number of operating chiller(s) is shut down at the beginning of the DR event to generate a significant and immediate power reduction in the developed strategies.

The power reduction in the DR event is controlled under the demand reduction set-points. In the basic strategy, the discharge rate of a small scale active CTES is controlled to modulate the power reduction under the chiller power reduction set-points. In the improved strategy**,** to avoid sacrificing the indoor thermal comfort too much, the active small scale CTES is also used to limit the building indoor temperature rise under upper limits of indoor temperature set-point. Accurate demand reduction and indoor temperature prediction methods are also developed. The effectiveness of the DR strategies involving both passive and active CTES is evaluated by a set of introduced parameters.

Currently, since the opportunity to conduct validation experiments on real buildings in real smart grid is seldom, computer-based simulation is an effective mean to test and validate the strategy in a building integrated with a smart grid.

6.2 Basic Fast Power Demand Response Strategy

Unlike the existing demand response strategy by changing the indoor air temperatures, the proposed strategy can achieve fast power reduction by directly shutting down certain number of chiller(s). However, reducing the operating chiller number only cannot achieve the exact power reduction as the set-point desired and is difficult to maintain the power reduction unchanged during the whole DR event. To address this problem, the active CTES system, i.e. the PCM storage tank, is introduced to be integrated with a typical HVAC system, as shown in Fig.4.4. The active CTES has different functions in the developed fast demand response strategies. First, the power reduction can be further increased through decreasing the return chilled water temperature based on the chiller power reduction set-points. Second, the power reduction profile can be flattened during the whole DR event through modulating the discharging rate of active CTES. Third, addition cooling capacity can be provided by the active CTES to release the stress on the inadequate cooling capacity provided by the remaining operating chillers during the DR event.

It is noted that this study is conducted based on the following known conditions. First, the promissory power reduction is given by the grid managers (e.g. ISOs or RTOs), which may be a constant value or a range during the DR event. Second, the power baseline of the HVAC system (i.e. the normal power demand profile during the DR event when the demand response strategy is not activated) during the DR event can be calculated using the known method that is accepted by both the grids managers and the building owners.

6.2.1 Outline

Once the DR event occurs, the fast power demand response strategy will be activated to reduce the real-time power use by reducing the operating chiller number directly after receiving the signal from grid managers. The number of operating chillers needed to be shut down is calculated based on the maximum allowable indoor thermal loss during DR event with different durations, i.e. 2 hours. How to determine the chiller number is not the focus of this paper. The related method used can be referenced in [Xue et al, 2015], which considers the required power reduction and the space thermal comfort simultaneously. Based on the remaining operating chiller(s), this proposed strategy is to allow the actual power reductions reaching the set-points, which are larger than the power reduction in the case that only chiller(s) is shut down and no active CTES is activated, and to flatten the actual power reduction by modulating the operating capacity of the storage tank.

The proposed fast DR strategy consists of two processes: the prediction process and the control process, as shown in Fig.6.1. In the prediction process, models are developed to predict the discharge flow rates of the active storage tank during the DR event under the different power reduction set-points. In the control process, i.e. the actual operating process, the predicted discharge flow rate acts as target values for modulating the actual discharge flow rate of the storage tank.

Although a conventional feedback control can perform the real-time regulation of the discharge flow rate, the developed prediction process in this study is still necessary and has the special advantages. By using the model-based prediction process, the overall system performance during the DR event can be predicted in advance. The overall

power reduction profile and the building thermal comfort can facilitate the decision maker and the interested parties to assess the effects of the strategy comprehensively. Moreover, since the HVAC system has considerable nonlinearity and time delay properties, the conventional feedback control could cause frequent fluctuations and need a relatively long time to reach the set-point, which may fail to satisfy the requirements of fast DR. The proposed model-based predictive control could address these problems. The details of the proposed strategy are described in the following subsections. The coefficients of the modules and models are listed and discussed in Section 6.3.

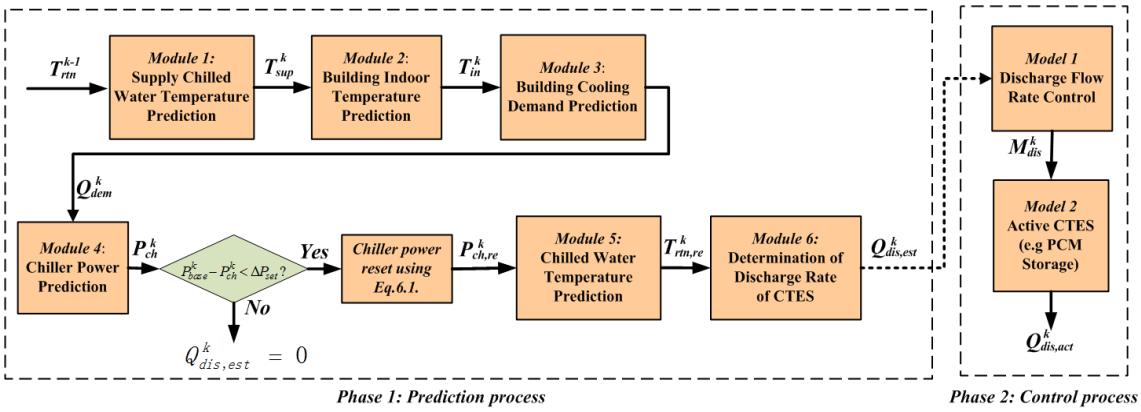

Fig.6.1 Flowchart of the developed fast demand response strategy

6.2.2 Prediction process

At the prediction process, the required discharge rate of active CTES, predicted chiller power reduction and building indoor temperature are calculated. The building indoor temperature, building cooling demand and chiller power consumption in baseline case are used as the inputs.

Flow chart of the prediction process

First, the building cooling demand (Q_{dem}) at the *k*th current sampling time is predicted

using Module 1, 2 and 3. Based on the return temperature of the chillers (T_{rtn}) at the *k-1*th sampling time), Module 1 is employed to predict the supply chiller water temperature (T_{sup}) at the *k*th sampling time. In Module 2, the building indoor temperature is calculated according to T_{sup}. By means of Module 3, the building cooling demand can be determined.

Second, the required discharge rate of the storage tank is determined according to the estimated building cooling demand using Modules 4, 5 and 6. The chiller power prediction module (Module 4) is employed to predict the required power consumption (P_{ch}) of the remained operating chiller(s) under the situation when the storage tank is not activated. The difference between the baseline (P_{base}) of the total chiller power and the predicted chiller power is compared with the chiller power reduction set-point (ΔP_{set}). If the difference (P_{base}-P_{ch}) is larger than the power reduction set-point, the required discharge rate of the storage tank is set to zero. On the contrary, if the difference is less than the chiller power reduction set-point. That means the storage tank needed to be activated. The expected chiller power will be further reduced and reset to a lower value ($P_{ch,re}$), as shown in Eq. 6.1. Based on the reset chiller power ($P_{ch,re}$), Module 5 predicts the reset chiller return water temperature ($T_{rtn,re}$) after mixed with the outlet water from the storage tank. Module 6 determines the required discharge capacity of the storage tank at *k*th sampling time.

$$P_{ch,re}^{k} = P_{base}^{k} - \Delta P_{set} \tag{6.1}$$

where, $P_{ch,re}$ is the reset chiller power.

Descriptions of modules

Module 1- Supply chilled water temperature prediction

After certain number of chiller(s) is shut down, the remaining operating chiller(s) should be overloaded, resulting both the supply and return chilled water temperatures higher than their respective set-points. The chiller supply chilled water temperature (T_{sup}) at the *k*th sampling time is determined by the chiller return chilled water temperature (T_{rtn}) at the *k-1*th sampling time for an overloaded chiller, using a simplified polynomial function, as shown in Eq. 6.2.

$$T_{sup}^{k} = a_n \cdot (T_{rtn}^{k-1})^n + a_{n-1} \cdot (T_{rtn}^{k-1})^{n-1} + \cdots + a_1 \cdot T_{rtn}^{k-1} + a_0 \qquad (6.2)$$

where, a_0 - a_n are identified by least square method using historic operation data.

Module 2- Building indoor temperature prediction

The building indoor air temperature (T_{in}) is predicted according to $T_{sup.}$ As one of the most important parameters to indicate the indoor thermal comfort level, the building indoor temperature is required to be predicted. Actually, many factors affect the building indoor temperature. For facilitating the calculation process of the whole system, the building indoor temperature is represented by a simplified polynomial function of supply chilled water temperature when the remaining operating chiller(s) is overloaded after certain number of operating chiller(s) is shut down.

A linear piecewise regression model is used to establish the relationship between the supply chilled water temperature and building indoor temperature, as shown in Eq. 6.3. Where, the coefficients A_0 - A_n and B_0 - B_n are identified by least square method using historic operation data.

$$T_{in}^{k} = A_0 + A_1 \cdot \max(T_{sup}^{k} - B_1, 0) + \cdots + A_n \cdot \max(T_{sup}^{k} - B_n, 0) \quad (6.3)$$

Module 3- Building cooling demand prediction

This module is used to predict the building cooling demand at the *k*th sampling time. The building cooling demand will be less than that in the baseline case since insufficient cooling energy is provided after certain number of operating chiller(s) is shut down. A simplified building thermal storage model [Xue et al, 2014], which can represent the thermal characteristics and the building cooling demand reduction potentials of different types of commercial buildings (e.g. light weighted, medium weighted and heavy weighted), is used to calculate the discharge rate of the building thermal mass (ΔQ_{bui}).

Eq.6.4. is used to calculate the building cooling demand (Q_{dem}) at the *k*th sampling time. Where, $Q_{dem,base}$ is the building cooling demand in baseline case. ΔQ_{dem} is the predicted building cooling demand reduction.

$$Q_{dem}^{k} = Q_{dem,base}^{k} - \Delta Q_{dem}^{k} \quad (6.4)$$

Eq.6.5. is introduced to describe the relationship between the building indoor temperature increase and the building cooling demand reduction [Xue et al, 2014]. Where, ΔQ_{bui} is the discharge rate of the building thermal mass, i.e. the passive CTES. c_{in} is the specific heat of indoor air and M_{air} is the mass of indoor air.

$$\Delta Q_{dem}^{k} = \Delta Q_{bui}^{k} + c_{in} \frac{dT_{in}}{dt} M_{air} \quad (6.5)$$

ΔQ_{bui} is determined by the simplified building thermal storage model [Xue et al, 2014], as shown in Eq.6.6:

$$\Delta Q_{bui}^{k} = \frac{T_{in}^{k} - T_{base}^{k}}{R_{bui,ou} + R_{bui,inn}} \cdot (1 + \mu \cdot e^{-\frac{t}{\tau}}) \cdot A_{bui} \quad (6.6)$$

where, T_{base} is the indoor air temperature in baseline case. $R_{bui,ou}$ and $R_{bui,inn}$ are the building outer and inner thermal resistance respectively. A_{bui} is the effective building surface area involved in the heat exchange process. τ is the time constant of building thermal mass and is defined in Eq. 6.7. α is the ratio of the building outer thermal resistance to the building inner thermal resistance as shown in Eq. 6.8.

$$\tau = \frac{R_{bui,ou} \cdot R_{bui,inn}}{R_{bui,ou} + R_{bui,inn}} \cdot C_{bui} \tag{6.7}$$

$$\alpha = \frac{R_{bui,ou}}{R_{bui,inn}} \tag{6.8}$$

where, C_{bui} is the building thermal capacitance of per square meter.

Module 4- Chiller power prediction

This module is used to predict the power consumption of the remaining operating chiller(s) (P_{ch}) after certain number of operating chiller(s) is shut down. Q_{dem} and chiller coefficient of performance (*COP*) at the *k*th sampling time are the inputs to calculate P_{ch}, as shown in Eq. 6.9. *COP* is calculated by using the regression model, as shown in Eq. 6.10.

$$P_{ch}^{k} = Q_{dem}^{k} / COP^{k} \tag{6.9}$$

$$COP^{k} = c_4 \cdot (PLR^{k})^4 + c_3 \cdot (PLR^{k})^3 + c_2 \cdot (PLR^{k})^2 + c_1 \cdot PLR^{k} + c_0 \tag{6.10}$$

where, *COP* is the chiller coefficient of performance. The coefficients c_0 - c_4 are identified with historic recorded data. The *PLR* is the part load ratio of a chiller, which is determined by Eq. 6.11. T_{rtn} at the *k*th sampling time is calculated in Eq. 6.12.

$$PLR^{k} = Q_{dem}^{k} / Q_{rated} \tag{6.11}$$

$$T_{rtn}^{k} = \frac{Q_{dem}^{k}}{c_w \cdot N_{ch} \cdot M_{ch}} + T_{sup}^{k} \quad (6.12)$$

where, the Q_{rated} is the rated cooling capacity of chiller. c_w is the specific heat of chilled water and N_{ch} is the number of remaining operating chiller(s). M_{ch} is the rated chilled water flow rate of chiller.

Module 5- Chilled water temperature prediction

The reset expected return chilled water with decreased temperature ($T_{rtn,,re}$) at *k*th sampling time is obtained by solving Eq.6.13 below.

$$T_{rtn,re}^{k} = \frac{COP_{re}^{k} \cdot P_{ch,re}^{k}}{c_w \cdot N_{ch} \cdot M_{ch}} + T_{sup}^{k} \quad (6.13)$$

where, COP_{re} is the reset chiller *COP* at the current sampling time which is calculated by Eq. 6.10.

Module 6- Determination of Active Discharge Rate of CTES

This module is used to determine the estimated discharge rate of active CTES ($Q_{dis,est}$) according to the difference between the predicted and expected values of the return chilled water temperature**.**

Q_{dis} is calculated in Eq. (6.14):

$$Q_{dis,est}^{k} = N_{ch} \cdot c_w \cdot M_{ch} \cdot (T_{rtn}^{k} - T_{rtn,re}^{k}) \quad (6.14)$$

6.2.3 Control process

The control process is the "real" operation and control process to realize the strategy through discharging the active CTES based on the expected discharge rate of active CTES predicted in the prediction process. The active CTES is used to provide additional

cooling capacity for further reducing power consumption. The control of the active CTES is based on $Q_{dis,act}$ during the "actual" DR event.

Model 1- Discharge flow rate control

During the actual operation, the actual discharge rate of active CTES is modulated by adjusting the discharge flow rate. The actual discharge rate of active CTES measurement is obtained by measuring the flow rate and the differential temperature of discharge chilled water between at outlet and inlet of the active CTES. The expected discharge rate of active CTES, which is determined in the prediction process as described above, is used as the control set-point in this step. The actual dynamic operation and control process is not included in this simulation test. A simplified model is developed to compute the real-time discharge flow rate.

The mean temperature of storage media (T_{mean}), the mass percentage of solid status storage media (Per_{solid}), the actual return chilled water temperature during the DR event ($T_{rtn,act}$) and $Q_{dis,est}$ resulted from Eq. 6.14 are used as the inputs for calculation of the required discharge flow rate (M_{dis}) of active CTES, as shown in Eq. 6.15. Where, d_0 - d_4 are the coefficients which are identified by least square method using historic operation data.

$$M_{dis}^{k} = d_0 \cdot (T_{mean}^{k})^{d_1} \cdot (Per_{solid}^{k})^{d_2} \cdot (T_{rtn,act}^{k})^{d_3} \cdot (Q_{dis,est}^{k})^{d_4} \qquad (6.15)$$

Model 2- Actual CTES

The "actual" discharge rate of the PCM storage system ($Q_{dis,act}$) is calculated according to M_{dis} and the temperature difference between the return chilled water at inlet and that at outlet of the PCM storage tank as shown in Eq. 6.16. Where, $T_{rtn,out}$ is the chilled

water temperatures at outlet of the PCM storage tank.

$$Q_{dis,act}^{k} = M_{dis}^{k} \cdot c_w \cdot \left(T_{rtn,act}^{k} - T_{rtn,out}^{k}\right) \quad (6.16)$$

6.3 Improved Fast Power Demand Response Strategy

An improved fast DR strategy is also developed in this thesis. The main improvement is that the primary control objective of the developed control strategy is to restrain the building indoor temperature rise to maintain indoor thermal comfort within certain level while the power reduction is also controlled under the power reduction set-point during the DR event. In another word, the active CTES is used not only to control chiller power reduction under chiller power reduction set-points but also to limit the building indoor temperature rise during the DR event.

More modules used in prediction step are developed while the control step is the same as that in the basic fast DR strategy. The outline of the improved fast DR strategy is introduced in Sub-section 6.3.1. In Sub-section 6.3.2, the prediction process is described to present the functions of newly added modules and procedure as well as the different objectives and formulations of the same modules, introduced in the base fast DR strategy.

6.3.1 Outline

The proposed improved fast DR strategy also consists of two processes: the prediction process and the control process, as shown in Fig.6.2. For controlling indoor thermal comfort degradation, different upper limits of indoor temperature set-point were set. In the prediction process, the developed modules are used to predict the building indoor

temperature, chiller power reduction and, most importantly, the discharge flow rates of the active storage tank during the DR event under different power reduction set-points and upper limits of indoor temperature set-point. The functions of control process are the same as that in the basic fast DR strategy.

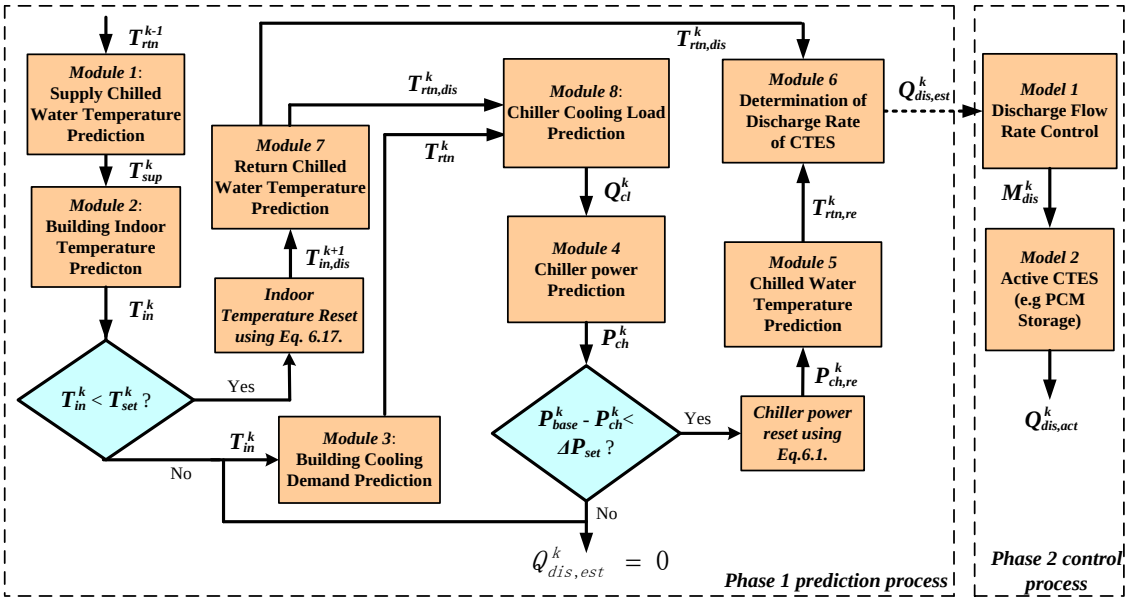

Fig.6.2 Flowchart of the developed fast demand response strategy

6.3.2 Prediction process

At the prediction process, the required discharge rate of active CTES for limiting building indoor temperature rise and keeping required power reduction, predicted chiller power reduction and building indoor temperature are calculated. The building indoor temperature, building cooling demand and chiller power consumption in baseline case are used as the inputs.

Flow chart of the prediction process

First, the building indoor temperature (T_{in}) at the kth sampling time is predicted using

Module 1 and 2. Based on the return chilled water temperature (T_{rtn}) at the *k-1*th current sampling time, the supply chiller water temperature (T_{sup}) at the *k*th sampling time is predicted in Module 1. In Module 2, T_{in} is calculated based on $T_{sup.}$

Secondly, the required discharge rate of the storage tank to limit the indoor temperature rise under certain upper limit of indoor temperature set-point is determined. The predicted T_{in} is compared with the building indoor temperature set-point. If T_{in} at the *k*th sampling time is larger than the upper limit set-point of indoor temperature (T_{set}), T_{in} at the *k+1*th sampling time will be set to a lower value ($T_{in,dis}$), shown in Eq.6.17, through activation of the active CTES to decrease the return chilled water temperature. Similar to the Module 2, the supply chilled water temperature is also represented by a simplified polynomial function of building indoor temperature. The return chilled water with decreased temperature ($T_{rtn,dis}$) at the *k*th sampling time is then predicted based on the expected supply chilled water temperature ($T_{sup,dis}$) at the *k+1*th sampling time in Module 7. $T_{rtn,dis}$ is also used as the input in Module 6 for determination of the estimated discharge rate of the storage tank ($Q_{dis,est}$) at *k*th sampling time. If T_{in} at the *k*th sampling time is not larger than T_{set}, T_{rtn} is calculated in Module 3. $T_{rtn,dis}$ or T_{rtn} is then used as inputs to calculate chiller cooling load (Q_{cl}).

$$T_{in,dis}^{k+1} = T_{set} \tag{6.17}$$

Thirdly, the required discharge rate of the storage tank to reduce the power reduction under certain chiller power reduction set-point is determined. Module 4 is employed to predict P_{ch} based on the Q_{cl}. The difference between P_{base} and P_{ch} is compared with ΔP_{set}. If the difference is less than $\Delta P_{set,}$ the expected chiller power will be further reduced and reset to a lower value ($P_{ch,re}$), as shown in Eq. 6.1. Based on the reset chiller power

($P_{ch,re}$), Module 5 predicted the reset chiller return water temperature ($T_{rtn,re}$) after mixed with the outlet water from the storage tank. The required discharge rate of the storage tank to reduce the power reduction is then calculated in Module 6. $Q_{dis,est}$ is zero when both predicted indoor temperature and chiller power fulfill the requirements of the respective set-points.

Descriptions of modules

It is worthy noticing that, in the prediction process, the inputs and outputs of some modules introduced in the basic fast DR strategy are different. Meanwhile, the new modules and procedure are developed. The following introduces the newly added modules and procedure as well as the different objectives and formulations of the same modules introduced in the base fast DR strategy.

Module 3- Building cooling demand prediction

Except building cooling demand (Q_{dem}), the return chilled water temperature (T_{rtn}) at *k*th sampling time is also predicted in this module. Q_{dem} is resulted by resolving the Eq. 6.4. to 6.8. T_{rtn} is calculated in Eq. 6.18.

$$Q_{dem}^{k} = c_w \cdot N_{ch} \cdot M_{ch} \cdot (T_{rtn}^{k} - T_{sup}^{k}) \tag{6.18}$$

Module 7- Return chilled water temperature prediction

The expected return chilled water with decreased temperature ($T_{rtn,dis}$) to limit indoor temperature at the *k*th sampling time is obtained through calculation of the corresponding expected supply chilled water temperature ($T_{sup,dis}$) at the *k+1*th sampling time in Eq.6.2.

Similar to the building indoor temperature prediction module, as shown in Eq. 6.3, the supply chilled water temperature is also represented by a simplified polynomial function of building indoor temperature. The supply chilled water temperature at the next sampling time is obtained from the Eq. 6.19, which is a polynomial function of building indoor temperature. Where, the coefficients C_0 - C_n and D_0 - D_n are identified by least square method using historic operation data.

$$T_{sup,dis}^{k+1} = C_0 + C_1 \cdot \max(T_{in,dis}^{k+1} - D_1, 0) + \cdots + C_n \cdot \max(T_{in,dis}^{k+1} - D_n, 0) \quad (6.19)$$

Module 8- Chiller cooling load prediction

Eq. 6.20 is used to calculate the chiller cooling load (Q_{cl}) at the *k*th sampling time.

$$Q_{cl}^k = c_w \cdot N_{ch} \cdot M_{ch} \cdot (T_{rtn}^k - T_{sup}^k)$$

or

$$Q_{cl}^k = c_w \cdot N_{ch} \cdot M_{ch} \cdot (T_{rtn,dis}^k - T_{sup}^k) \quad (6.20)$$

Module 4- Chiller power prediction

Eq. 6.21 is used to calculate P_{ch}.

$$P_{ch}^k = Q_{cl}^k / COP^k \quad (6.21)$$

COP is calculated by using the regression model, as shown in Eq. 6.10. The *PLR* is determined by Eq. 6.11.

Module 6- Determination of discharge rate of CTES

The estimated discharge rate of active CTES ($Q_{dis,est}$) for limiting the building indoor temperature rise or reducing the chiller power are calculated using Eq. 6.22:

$$Q_{dis,est}^{k} = N_{ch} \cdot C \cdot M_{ch} \cdot (T_{rtn}^{k} - T_{rtn,re}^{k})$$

or

$$Q_{dis,est}^{k} = N_{ch} \cdot C \cdot M_{ch} \cdot (T_{rtn}^{k} - T_{rtn,dis}^{k}) \quad (6.22)$$

6.4 Parameters Identification and Validation of Modules and Models

This sub-section aims at validating the modules and models mentioned in Sub-section 6.2 and 6.3. The identified coefficients are listed in Table 6.1. All the mean absolute error (MAE), mean absolute percentage error (MAPE) and root mean square error (RMSE) of the outputs in these models and modules are listed in Table 6.2. Identification of the parameters and validation of the thermal storage model for ICC building are showed in Appendix A.

6.4.1 Parameters identification

The coefficients of the models and modules are identified by regression using operation data generated from the simulation tests. The main coefficients are listed in Table 6.1.

Table 6.1 Identified coefficients of the modules and models

Supply chilled water temperature module in Eq.6.2.	a_0				a_1		
	-3.58				0.86		
Building indoor temperature prediction module in Eq.6.3.	A_0	A_1	A_2	A_3	B_0	B_1	B_2
	22.82	0.26	0.18	-0.44	8.61	11.39	12.59
Chiller COP model in Eq.6.10.	c_0	c_1	c_2	c_3	c_4		
	-0.0048	0.0033	-0.4352	2.3843	2.1638		
Discharge flow rate control model in Eq. 6.15.	d_0	d_1	d_2	d_3	d_4		
	0.91	1.08	0.03	-2.16	1.05		

6.4.2 Validation of modules and models

Supply chilled water temperature module in Eq.6.2: Ten hours data have been generated to validate the model in the simulation platform. It can be seen that the results calculated from Eq. 6.6 are of acceptable accuracy in estimating the supply chilled water temperature, as shown in Fig.6.3 (a).

Building indoor temperature prediction module in Eq.6.3: The data generated from the simulation platform are used to validate this model. Most predicted results have satisfactory accuracy, as shown in Fig.6.3 (b).

Chiller COP model in Eq.6.10: The data generated from the simulation platform are used to validate the chiller COP model. Most predicted results have satisfactory accuracy, as shown in Fig.6.3 (c).

Discharge flow rate control model in Eq. 6.15: The required discharge flow rates of the PCM storage tank model generated from the simulation platform are used to validate this model. Most predicted discharge flow rates have less than 10% relative errors compared with the "actual" required discharge flow rate of the PCM storage tank model, indicating that the model accuracy is acceptable, as shown in Fig.6.3 (d).

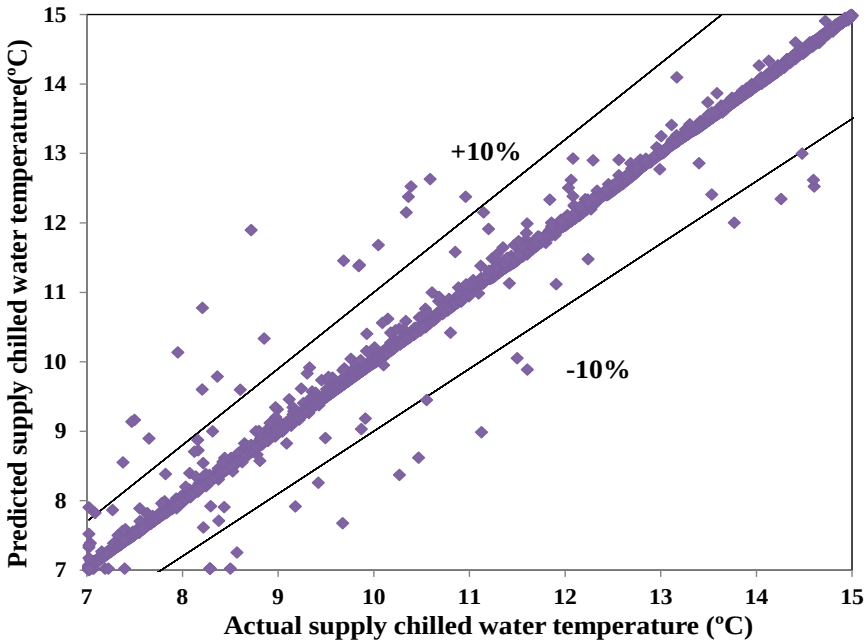

(a) Comparison between predicted and actual supply chilled water temperature

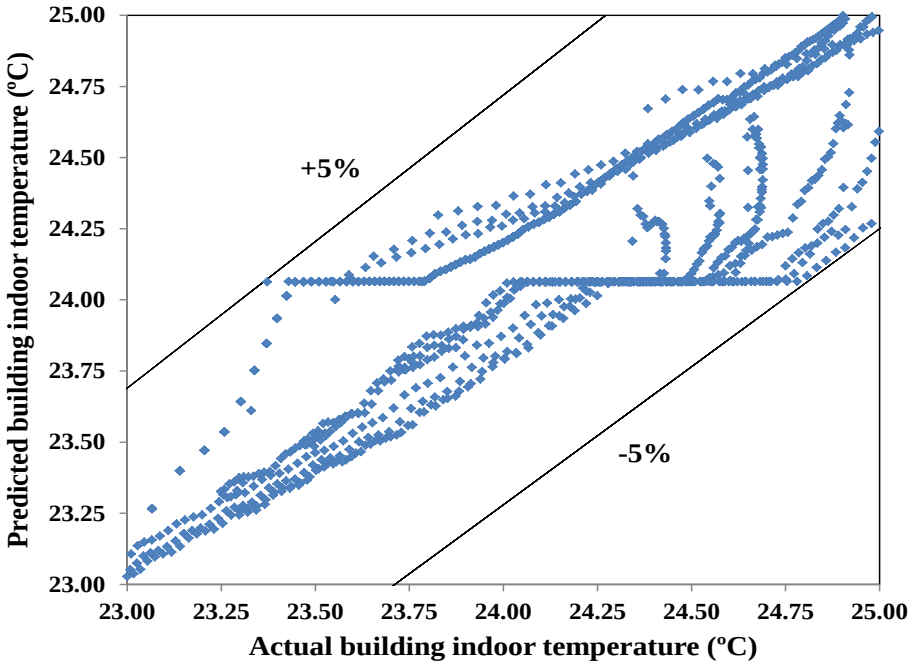

(b) Comparison between predicted and actual building indoor Temperature

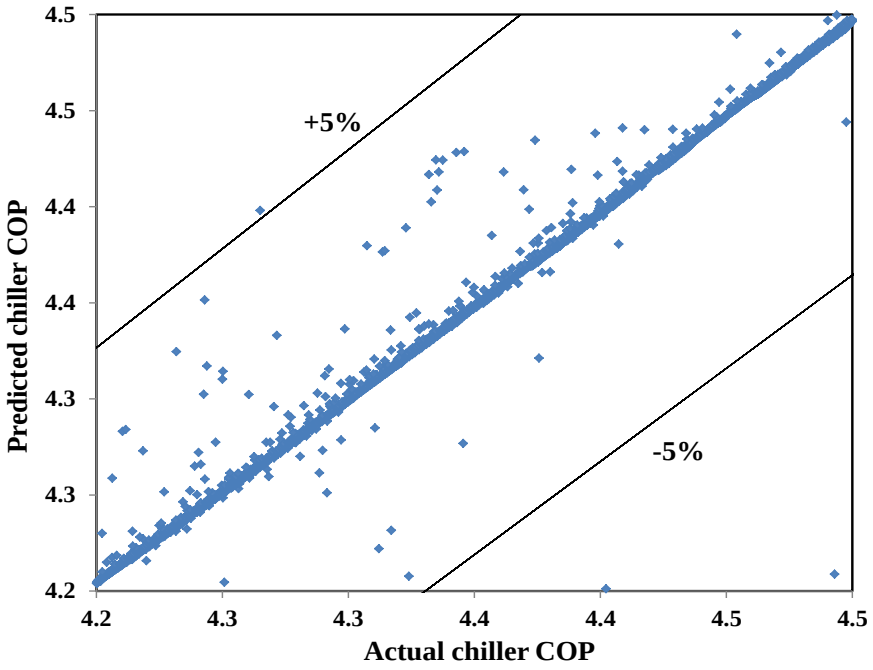

(c) Comparison between predicted and actual chiller COP

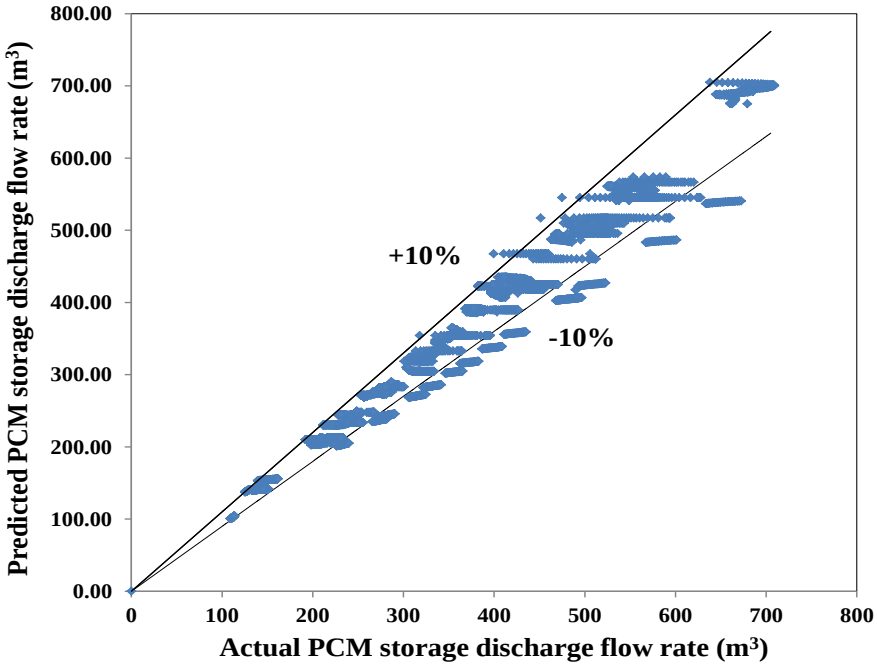

(d) Comparison between predicted and actual PCM storage discharge flow rate

Fig.6.3 Comparison between predicted and actual values of the developed modules and model

Table 6.2 lists the mean absolute error (MAE), mean absolute percentage error (MAPE) and root mean square error (RMSE) of the outputs in the above modules and models. It can be found that all the models and modules have acceptable accuracy.

Table 6.2 Accuracy indices of the developed models

	Outputs	MAE	MAPE	RMSE
Supply chilled water temperature module	T_{sup}	0.05 ˚C	1.53%	0.23 ˚C
Building indoor temperature prediction module	T_{in}	0.20 ˚C	0.86%	0.27 ˚C
Chiller COP model	*COP*	0.033	0.80%	0.10
Discharge flow rate control model	M_{dis}	17.54 m^3	5.10%	27.04 m^3

6.5 Case Studies and Analysis

The proposed fast DR response strategies for buildings involving both active and passive CTES was validated using the dynamic simulation platform built in chapter 3. The power consumption in baseline case and the test assumptions are proposed in Sub-section 6.4.1. The results and analysis of basic fast power DR strategy are described in Sub-section 6.4.2. The results and analysis of improved fast DR strategy are described in Sub-section 6.4.3.

6.5.1 Power consumption in baseline case and test assumptions

In this sub-section, the simulated building is the ICC building described in Chapter 3. The typical daily power consumption in summer, i.e. power consumption in baseline

case, is shown in Fig.6.4. A typical summer day with weather data of Hong Kong (i.e. subtropical climate) was adopted in the tests. The office hours of this building were between 08:00 a.m. and 19:00 p.m. The DR event was assumed to happen between 10:00 a.m. and 12:00 a.m. (“morning” case) or 14:00 p.m. and 16:00 p.m. (“afternoon” case). The basic fast power DR strategy was evaluated and analyzed in “morning” case study while improved fast DR strategy was evaluated and analyzed in “afternoon” case study.

The building indoor temperature set-point was set as 23°C. Initially the operating chiller number is four before the start of the DR event in both cases. Based on the maximum allowable indoor thermal loss during DR event, the number of operating chillers required to be shut down was two and the remaining operating chiller number was two accordingly in both cases.

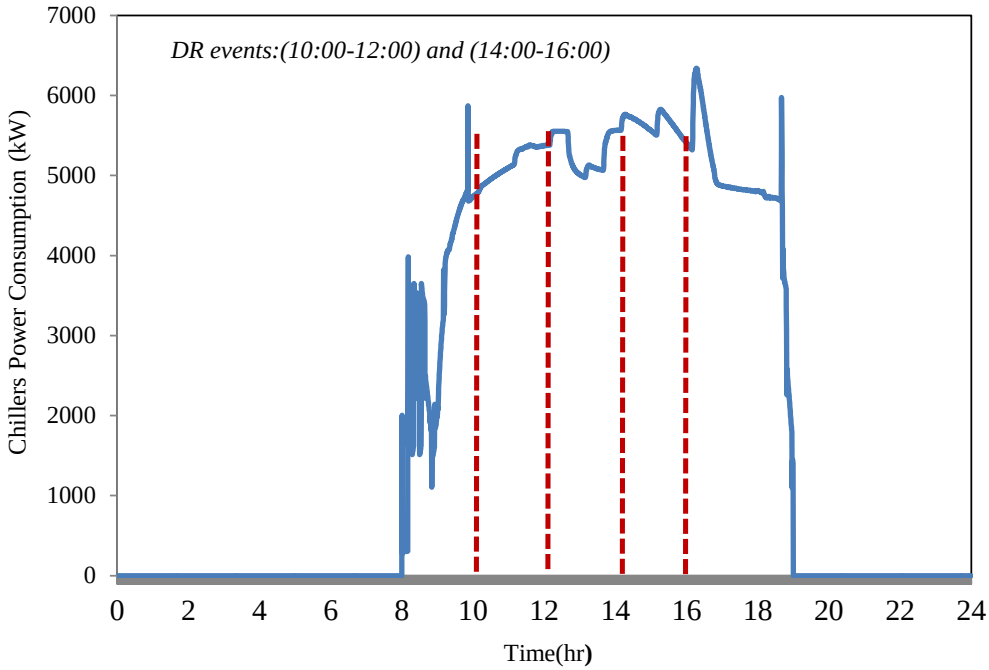

Fig.6.4 Chiller power consumption in baseline case

The DR event duration is assumed to be two hours in this study since the reliability rules typically require ancillary reserve resource to be able to sustain the demand response for two hours [Kirby, 2006]. In addition, only one DR event is assumed to happen in the test day. The simulation time step in the test platform is set to be 20 seconds to dynamically and accurately simulate the performance of the whole system as well as the building indoor heat exchange processes.

6.5.2 Results and analysis of the basic fast power demand response strategy

Chiller power reduction

The predicted and actual chiller power reduction under different power reduction set-points during the DR event are shown in Fig.6.5. The curves marked as "Actual/Without storage" were the actual power reductions when active CTES was not activated. They were the chiller power reductions when the chiller power reduction set-point was not set in the strategy.

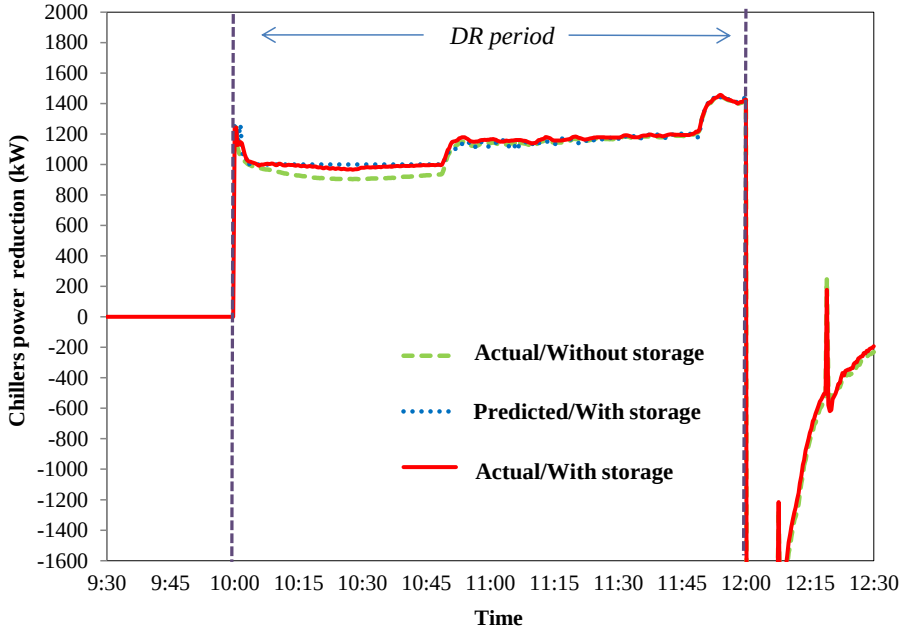

(a) Chiller power reduction set-point 1000 kW

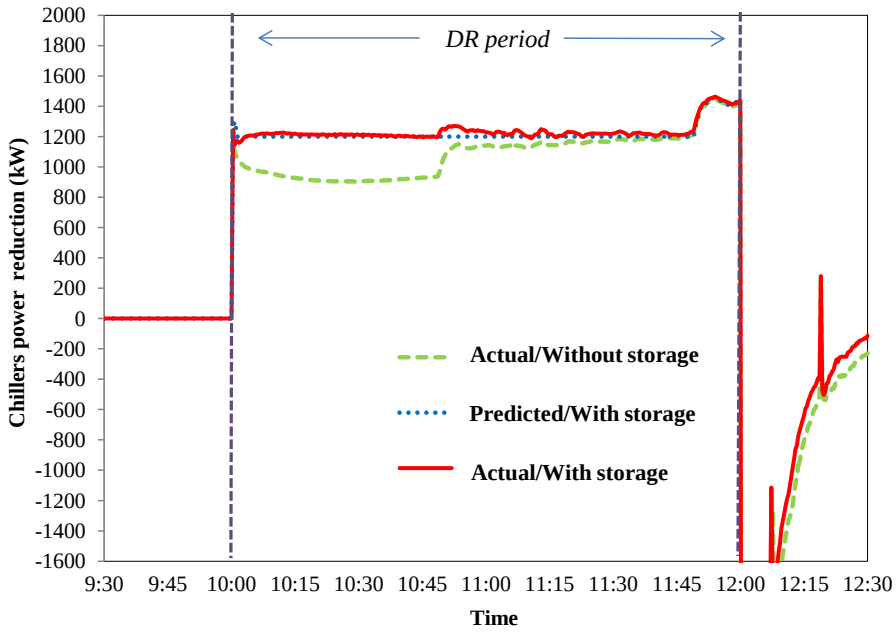

(b) Chiller power reduction set-point 1200 kW

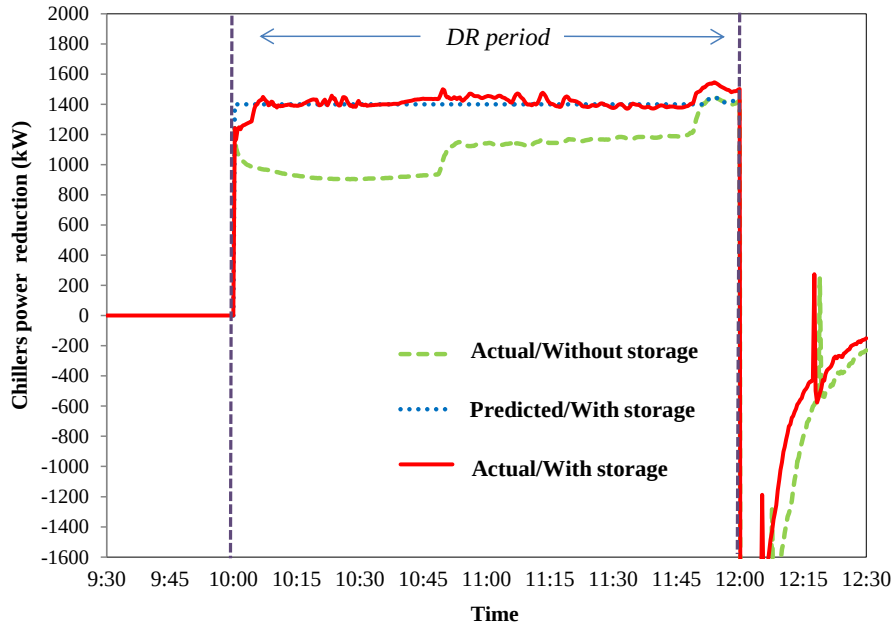

(c) Chiller power reduction set-point 1400 kW

Fig.6.5 Comparison between predicted and actual chiller power reductions (morning case)

The curves marked as “Predicted/With storage” and “Actual/With storage” were the predicted power reductions calculated in the prediction process and the actual power reductions achieved in the control process respectively, when the active CTES was activated. It is obvious that the predicted chiller power reduction was closed to the actual chiller power reduction. The mean absolute percentage error (MAPE) of predicted power reduction was less than 3.7%, which indicated that the chiller power reduction prediction was quite accurate. The accurate prediction can facilitate the grid manager to accurately estimate the power insufficiency in grid during the DR event.

At the beginning the DR event, an immediate and significant power reduction of 1243 kW, accounting for 30.2% of the original chiller power consumption, was achieved since two chillers were shut down.

With the increase of chiller power reduction set-point, the resulted power reduction increased since more cooling capacity provided by the active CTES was required. The minimum power reductions were 970 kW, 1141 kW and 1231 kW when the power reduction set-points were 1000 kW, 1200 kW and 1400 kW respectively while the minimum power reduction was 903kW only when no active CTES was activated.

In addition, the variation of the power reduction was 488 kW when the chiller power reduction set-point was 1000 kW in the test. Such variation reduced to 227 kW only when the power reduction set-point was 1400 kW, as shown in Fig. 6.5 (a) and (c). The results show that, with the increase of the chiller power reduction set-point, the power reduction profile was more flat since the operation duration of the active CTES was longer to keep the power reduction above the power reduction set-point.

Normally, the system which is affected by a demand response strategy must return to

normal operation [ASHRAE, 1993] at the end of DR events. The air-conditioning systems tend to use extra energy following DR events to bring the building indoor thermal environment to normal condition, e.g. decreasing the indoor temperature to its original set-point. Therefore, the chiller power consumption right after DR event is normally larger than that in baseline case and may result a "post DR event power spike" lasting for a certain period. This post DR event power spike is often called "rebound". To reduce the negative effects on the grid, rebound should be minimized.

With the increase of the chiller power reduction set-point, the rebound was less, as shown in Fig.6.5. It is because more cooling capacity is provided by the active CTES to release the stress on the inadequate cooling capacity provided by the chillers during the DR event.

Indoor temperature

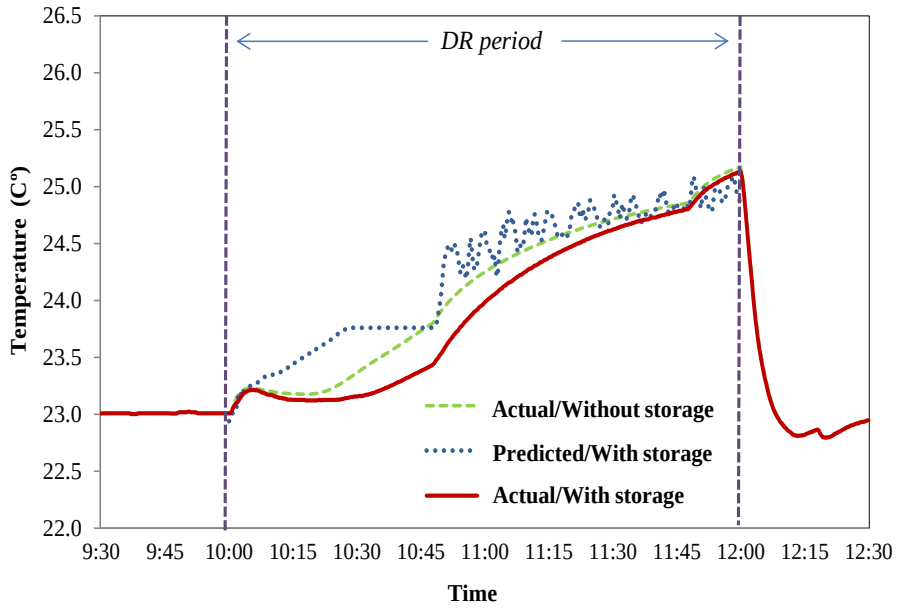

(a) Chiller power reduction set-point 1000kW

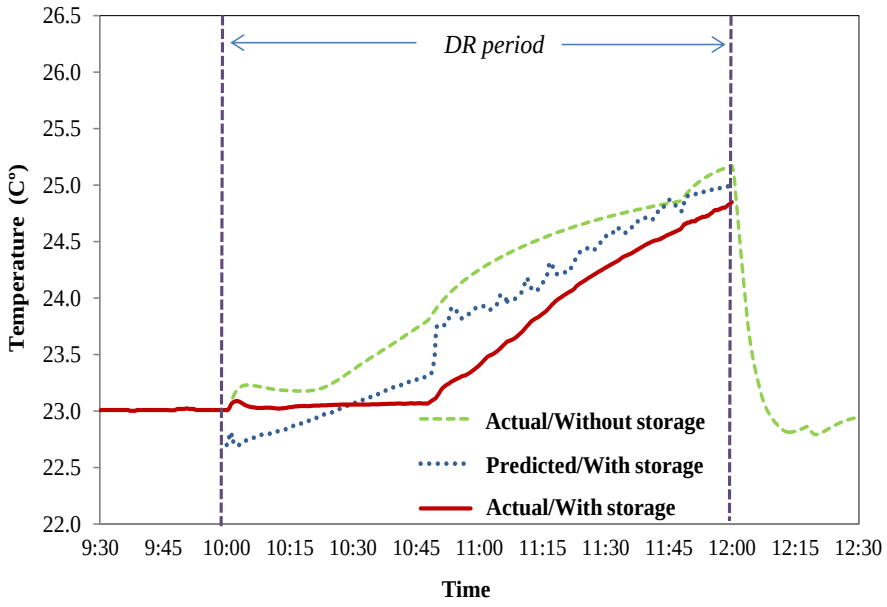

(b) Chiller power reduction set-point 1200kW

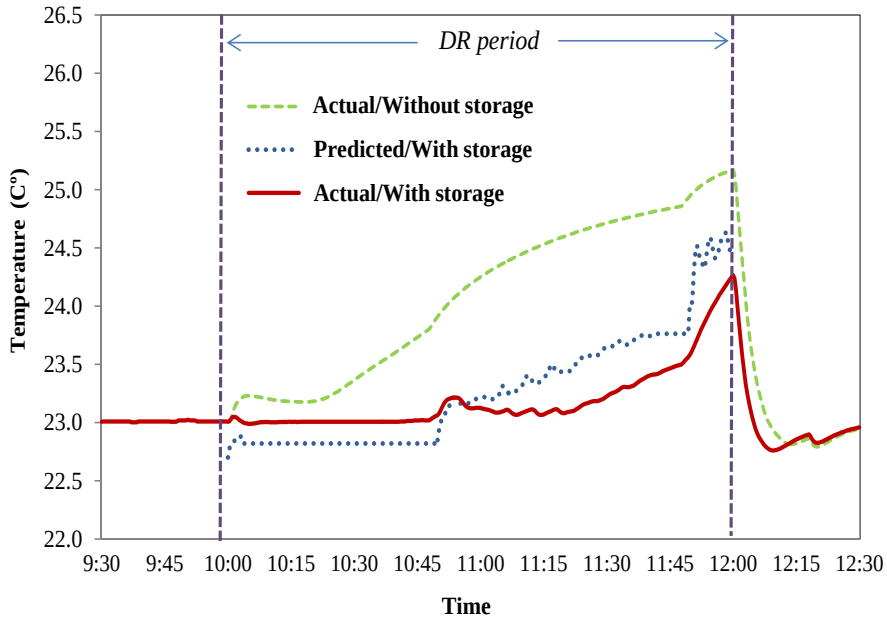

(c) Chiller power reduction set-point 1400kW

Fig.6.6 Comparison between predicted and actual indoor temperatures (morning case)

The predicted and actual building indoor temperatures under different chiller power reduction set-points during the DR event in the test are shown in Fig.6.6. Where, the marks of the curves have the same meaning as those in Fig.6.5.

It is worth noticing that indoor thermal comfort was sacrificed inevitably under control of the developed DR strategy since less cooling capacity is supplied by the remaining operating chiller(s) during the DR event. It is necessary to predict the building indoor temperature for evaluation of the effects of the power reduction on the indoor thermal comfort, since the indoor temperature is the most important parameter to characterize the indoor thermal comfort level during a DR event.

The results show that the indoor temperature kept increasing because inadequate cooling capacity was supplied by the remaining operating chillers. With the increase of the chiller power reduction set-point, the indoor temperature rise got less as more cooling capacity supplied by the active CTES. For instance, the maximum indoor temperatures were 25.1 $^{\circ}$C, 24.9 $^{\circ}$C and 24.3 $^{\circ}$C when the chiller power reduction set-points were 1000, 1200 and 1400 while the maximum indoor temperature reached 25.2 $^{\circ}$C when no active CTES was activated. The results show that the level of indoor thermal comfort degradation could be reduced when the active CTES was activated.

In addition, the test results also show that the predicted indoor air temperature was close to the actual indoor temperature, which indicates that the indoor air temperature can be predicted accurately. The accurate prediction allows decision maker to effectively assess the effects of different power reductions on the indoor thermal comfort in a particular building in advance of DR event.

Demand response effectiveness analysis

The results of the basic fast power DR strategy are summarized in Table 6.3. Average demand shed [Mathieu et al, 2011] means the average power reduction during the DR event. With the increase of the chiller power reduction set-point, the average demand

shed and the required capacity of active CTES increased. The maximum average demand shed was 1443 kW, as listed in Table 6.3, which accounted for 28.9% of the chiller power consumption in the baseline case. The maximum required capacity of active CTES is 10,680 kWh which accounts for 4.2% daily cooling load.

In this thesis, the rebound was the mean value of the chiller power rise in the hour right after the DR event. With the increase of the chiller power reduction set-point, the rebound was less, which indicated that the negative effect on grid was less, and the indoor thermal comfort degradation was lower. For instance, the maximum indoor temperature rise was 2.2 ˚C and the rebound was 799 kW, when no chiller power reduction set-point was set. The above results were reduced to 1.3 ˚C and 563 kW respectively when the demand reduction set-point was 1400 kW, as listed in Table 6.3.

Table 6.3 Results of basic fast power DR strategy

Chiller power reduction set-points (kW)	Average Demand Shed (kW)	Maximum building indoor temperature rise (˚C)	Required capacity of active CTES (kWh) /% Daily cooling load	Rebound (kW)
-	1087	2.2	-	799
1000	1121	2.1	1,346/0.53	760
1200	1235	1.9	5,183/2.0	697
1400	1443	1.3	10,680/4.2	563

6.5.3 Results and analysis of the improved fast power demand response strategy

Chiller power reduction

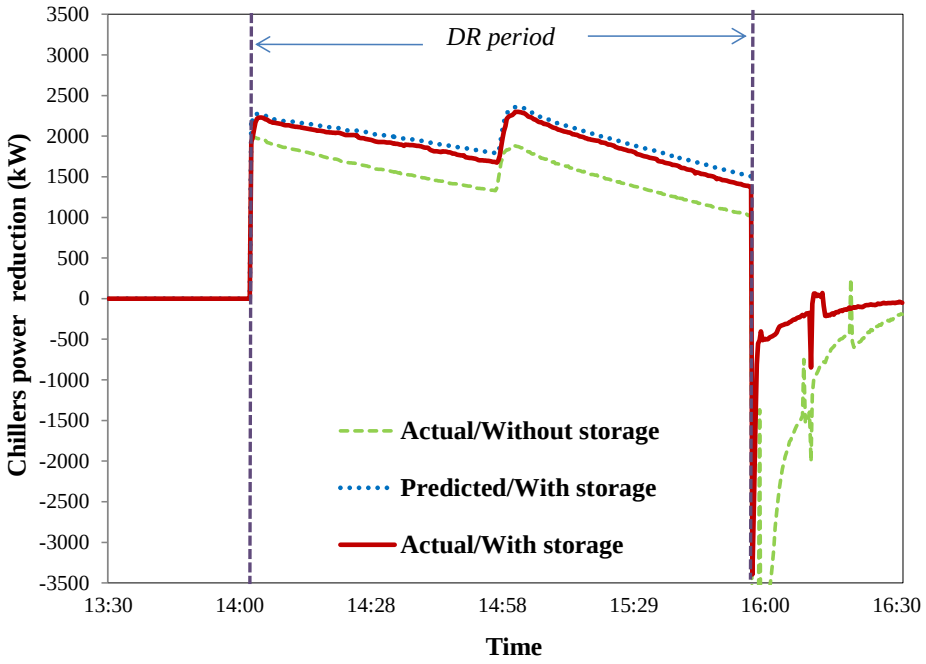

(a) Chiller power reduction set-point was not set

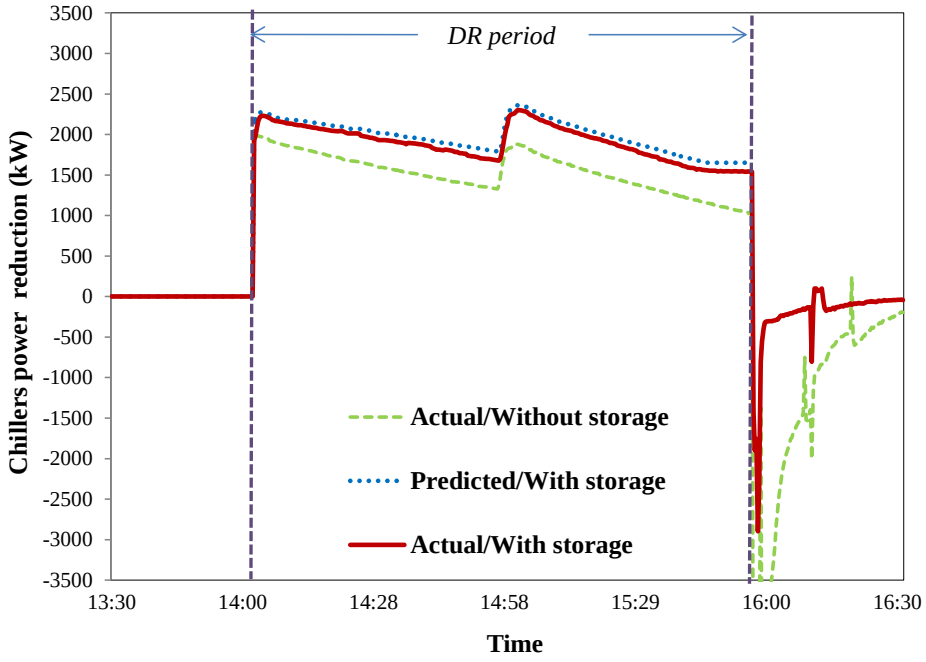

(b) Chiller power reduction set-point: 1650 kW

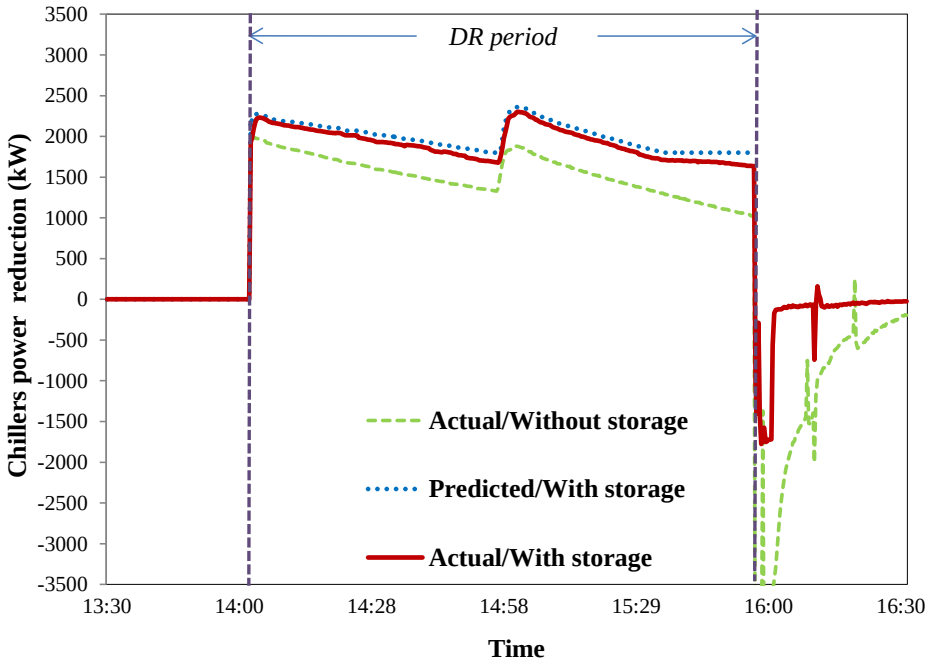

(c) Chiller power reduction set-point: 1800 kW

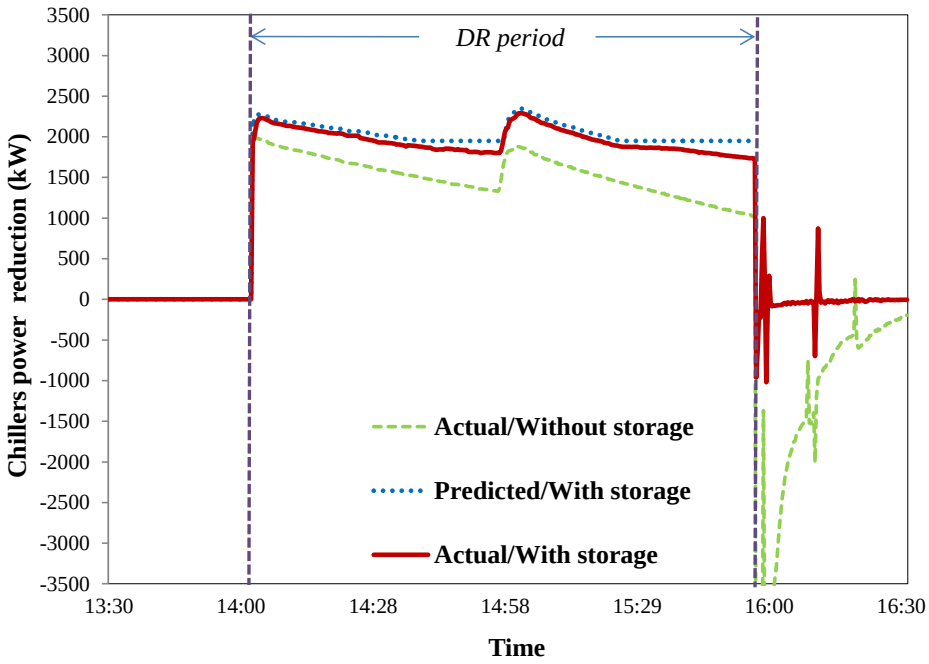

(d) Chiller power reduction set-point: 1950 kW

Fig.6.7 Comparison between predicted and actual chiller power reductions – Indoor temperature set-point upper limit of 23˚C (afternoon case)

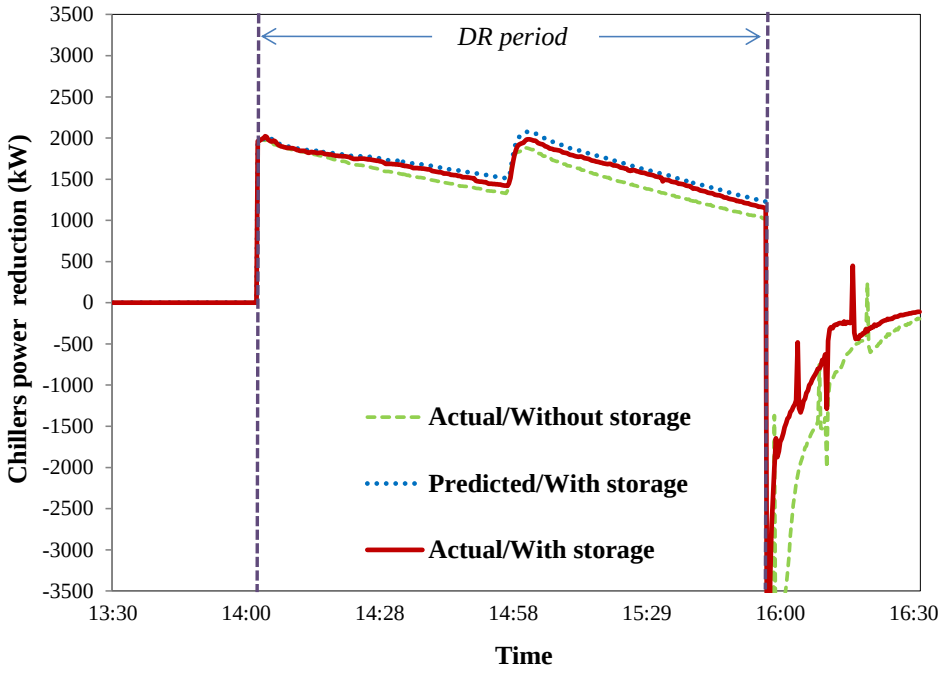

(a) Chiller power reduction set-point was not set

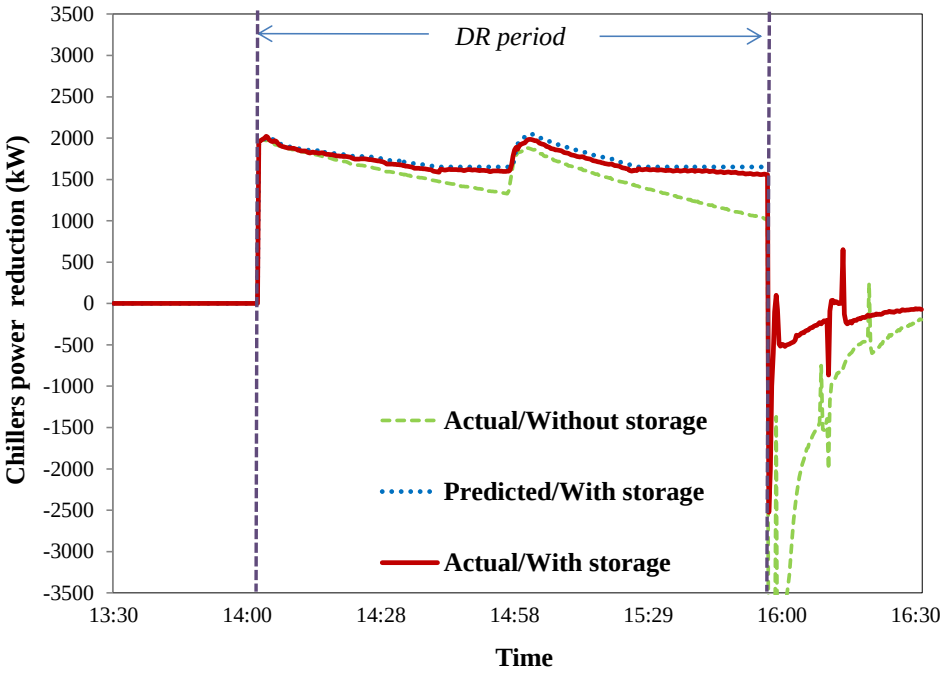

(b) Chiller power reduction set-point: 1650 kW

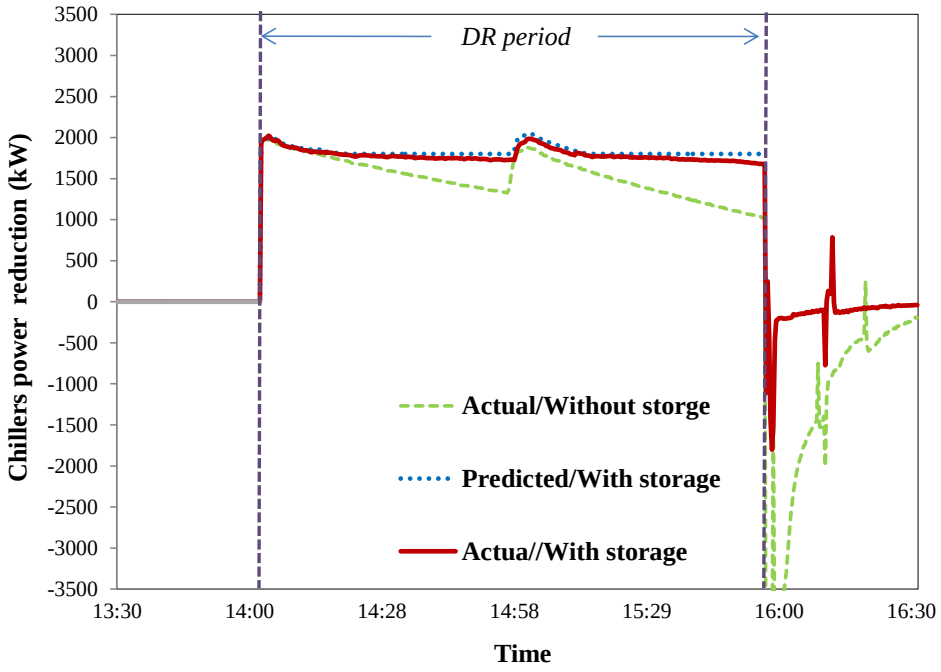

(c) Chiller power reduction set-point: 1800 kW

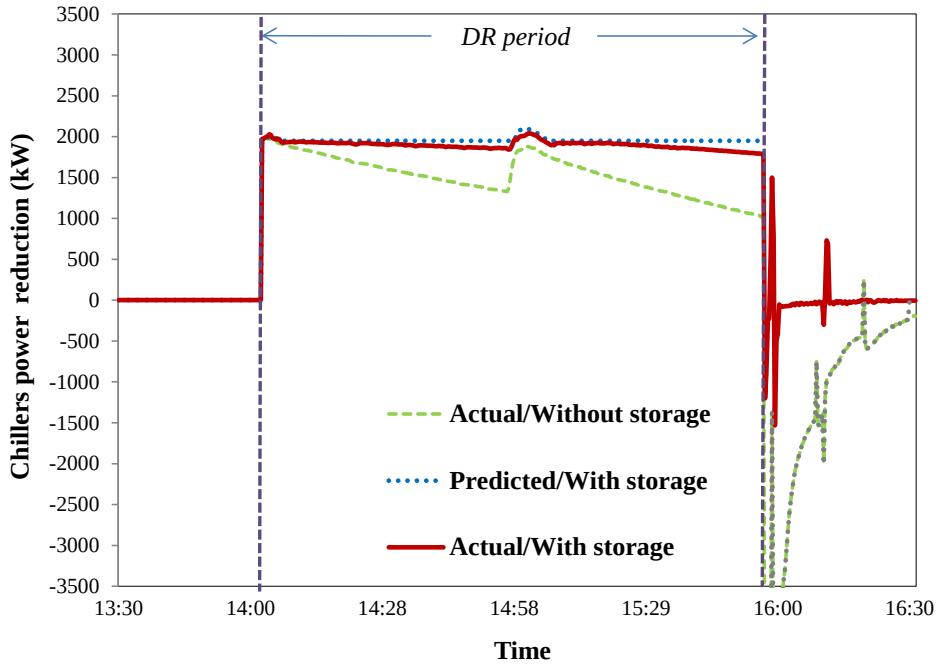

(d) Chiller power reduction set-point: 1950 kW

Fig.6.8 Comparison between predicted and actual chiller power reductions – Indoor temperature set-point upper limit of 24°C (afternoon case)

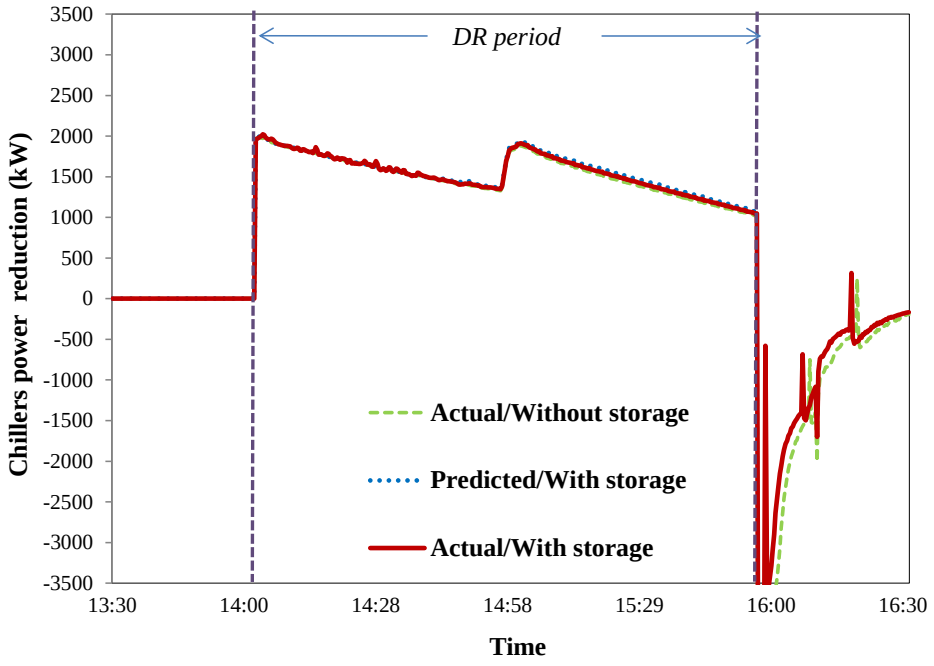

(a) Chiller power reduction set-point was not set

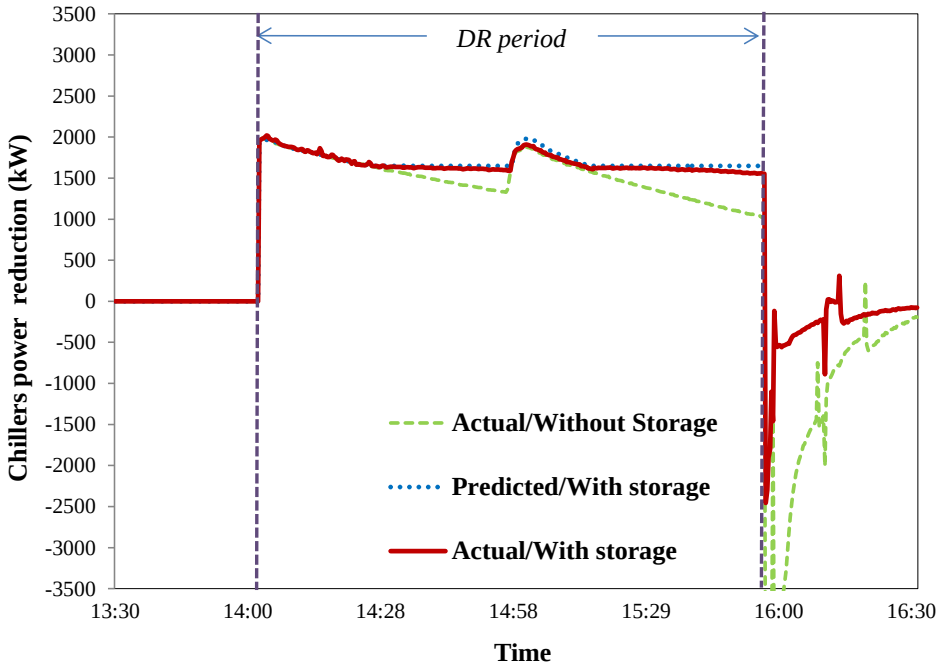

(b) Chiller power reduction set-point: 1650 kW

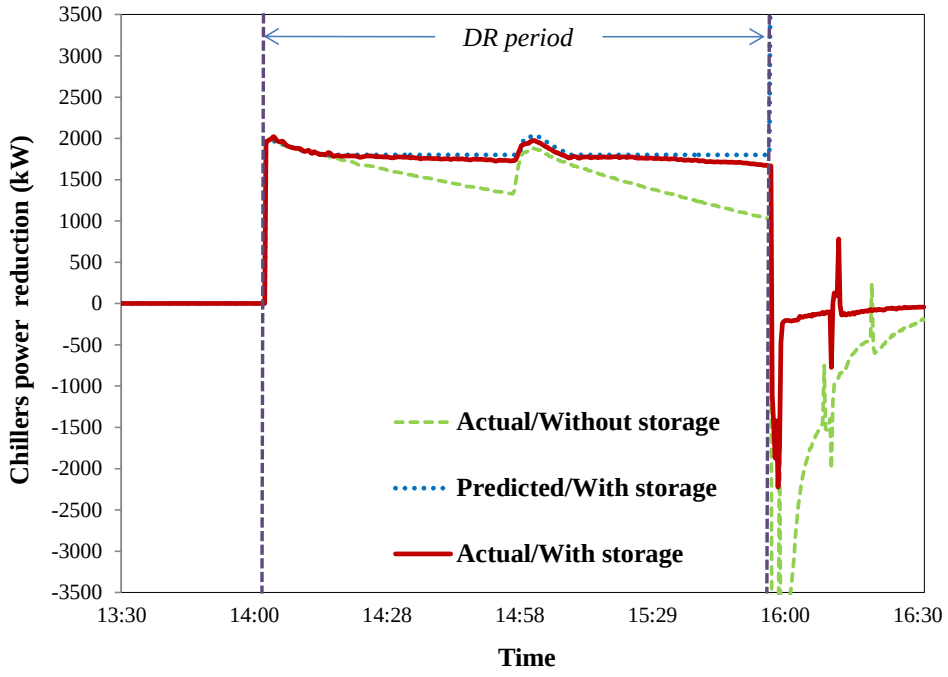

(c) Chiller power reduction set-point: 1800 kW

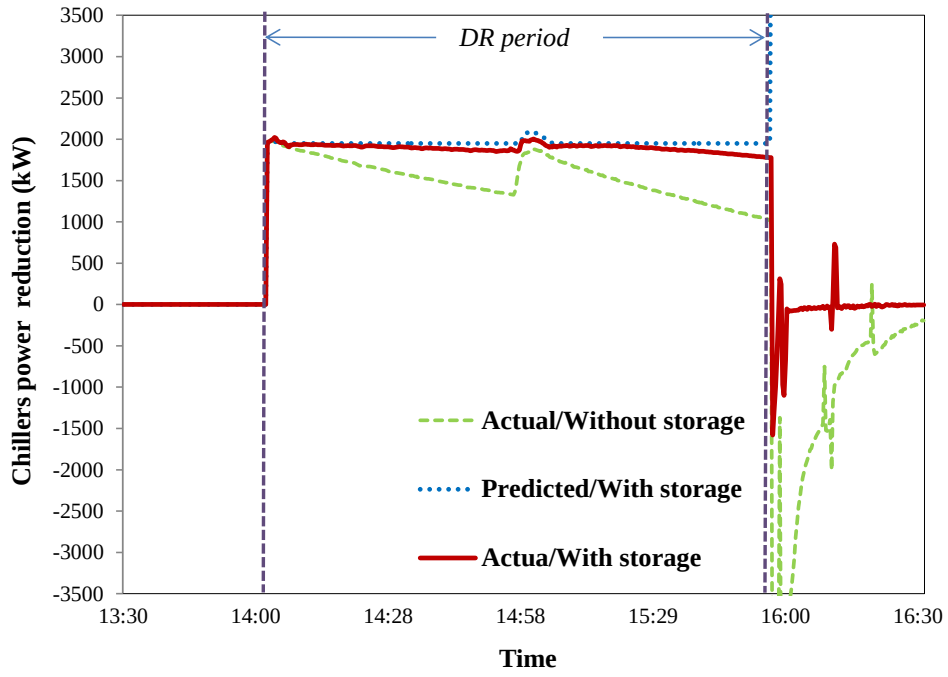

(d) Chiller power reduction set-point: 1950 kW

Fig.6.9 Comparison between predicted and actual chiller power reductions – Indoor temperature set-point upper limit of 25˚C (afternoon case)

The predicted and actual chiller power reductions under different chiller power reduction set-points and upper limits of indoor temperature set-point during the DR event are shown in Fig. 6.7 to 6.9. Where, the marks of the curves have the same meaning as those in Fig. 6.6. The curves marked as "Actual/without storage" also means the actual chiller power reductions when active CTES was not activated. They were, in fact, the chiller power reductions when neither chiller power reduction set-point nor upper limit of indoor temperature set-point was set in the control strategy in the tests.

The predicted power reduction was also close to the actual power reduction. The mean absolute percentage error (MAPE) of predicted demand reduction was less than 4.8% which indicates that the chiller power reduction prediction was accurate.

As discussed in the previous sub-sections, the indoor temperature is the most important parameter to determine the building indoor thermal comfort level, different upper limits of indoor temperature set-points were accordingly set in the tests to limit building thermal comfort loss. It is also the main advancement developed in the improved fast power DR strategy.

Once two chillers were shut down at the beginning of the DR event, an immediate power reduction of 2,005 kW was achieved, which was significant accounting for 34.5% of the original chiller power consumption.

Under the same upper limit of indoor temperature set-point, with the increase of the chiller power reduction set-point, the power reduction increased as more cooling capacity provided by the active CTES was required. In the test when the upper limit of indoor temperature set-point was 24°C, the variation of the power reduction was 838 kW when chiller power reduction set-point was not set. Such variation reduced to 250 kW

only when a chiller power reduction set-point of 1,950 kW was set, as shown in Fig. 6.8 (a) and 6.8 (d). The results show that the power reduction profile was more flat since the operation duration of active CTES was longer to keep the power reduction above the power reduction set-point.

On the contrary, under the same chiller power reduction set-point during the DR event, the power reduction decreased as less cooling capacity was required with the increase of the upper limit of indoor temperature set-point. In the test when the chiller power reduction set-point was 1,950 kW, the variation of the power reduction was 544 kW when the upper limit of indoor temperature set-point was 23°C. Such variation reduced to 250 kW when the upper limit of indoor temperature set-point was 24°C, as shown in Fig. 6.7 (d) and 6.8 (d). The results show that the power reduction profile was also more flat since the maximum power reduction under lower upper limit of indoor temperature set-point was larger than that under higher upper limit of indoor temperature set-point.

It is worth noticing that the cold energy in the active CTES was actually used for limiting the indoor temperature rise, when the upper limit of the indoor temperature set-point was set as the only objective of the modulating control during the DR event. But, in these cases, the chiller power reduction set-point was not set and the active CTES was not used to further increase the power reduction to a desired level since it was not included as an objective of the modulating control, as shown in Figs. 6.7 (a), 6.8 (a) and 6.9 (a).

Indoor temperature

The predicted and actual building indoor temperatures in the test cases using a chiller

power reduction set-point of 1,650 kW and different upper limits of indoor temperature set-point during the DR event are shown in Fig.6.10.

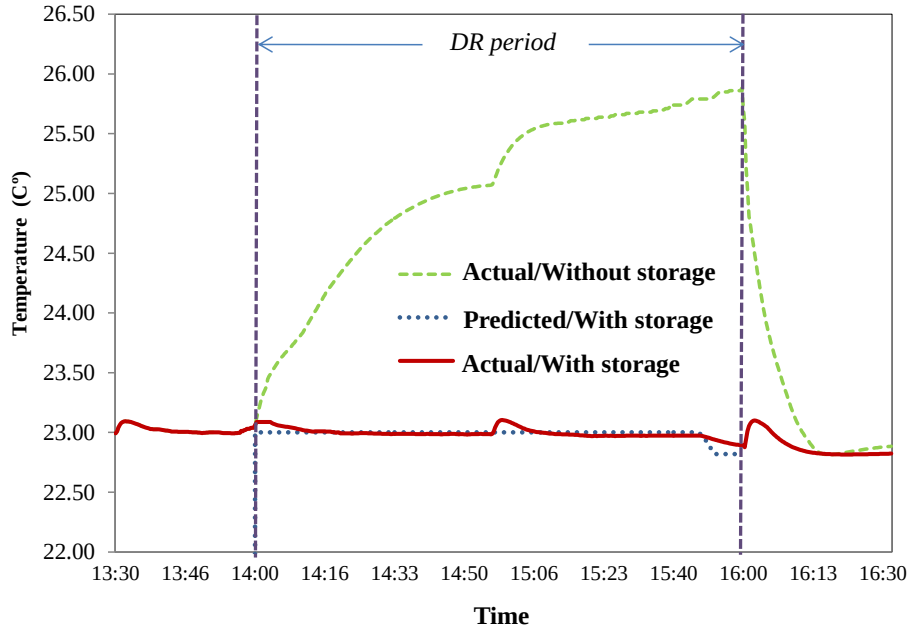

(a) Indoor temperature set-point upper limit of 23˚C

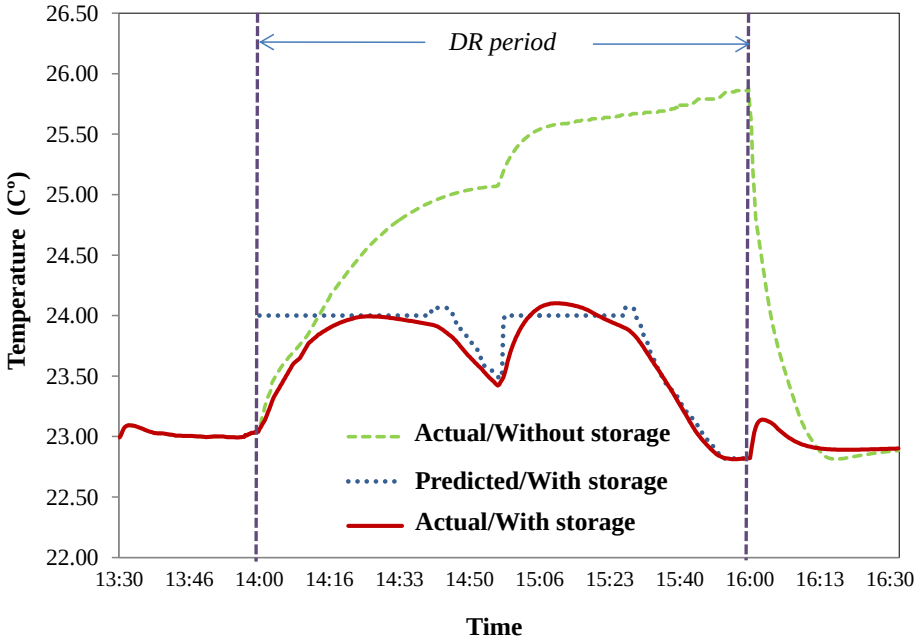

(b) Indoor temperature set-point upper limit of 24˚C

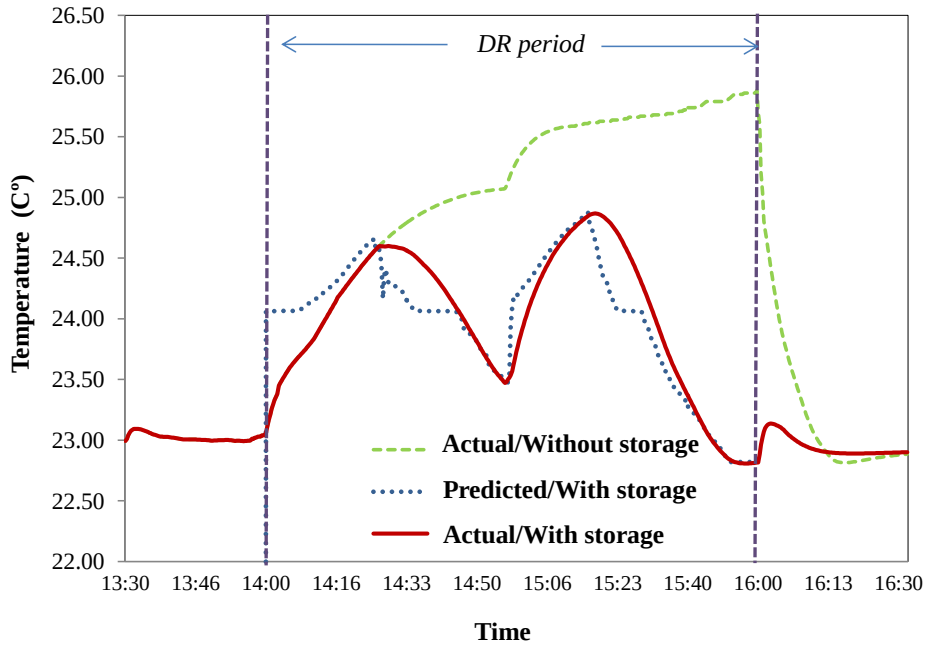

(c) Indoor temperature set-point upper limit of 25˚C

Fig.6.10 Comparison between predicted and actual indoor temperatures – chiller power reduction set-point of 1650kW (afternoon case)

The indoor temperature kept increasing as inadequate cooling capacity supplied by the remaining operating chillers if no active CTES was activated. The indoor temperature increased to 25.9˚C at the end of the DR event.

When the active CTES was activated, the level of indoor thermal comfort degradation could be controlled under preset upper limit of indoor temperature set-points during the DR event. For instance, the maximum indoor temperature rise was 0.2 ˚C when the upper limit of indoor temperature set-point was 23 ˚C, as shown in Fig.6.10 (a), and maximum indoor temperature rise was 1.8 ˚C when the upper limit of indoor temperature set-point was 25 ˚C, as shown in Fig.6.10 (c).

The test results show that the actual indoor air temperature was controlled properly below its set-point upper limits most time during DR event. In addition, the predicted

indoor air temperature was close to the actual indoor temperature, indicating that the indoor temperature prediction has acceptable accuracy. The same observations could be also drawn from the results from the test cases using different chiller power reduction set-points.

Demand response effectiveness and quantitative evaluation

The effectiveness of the developed improved fast power DR strategy is summarized in Table 6.4. The required capacities of active CTES under different chiller power reduction set-points and upper limits of indoor temperature set-point during the DR event are listed.

Table 6.4 Results of improved fast power DR strategy

Upper limits of indoor temperature set-point (˚C)	Demand reduction set-points (kW)	Average Demand Shed (kW)	Intrashed Variability (kW)	Required capacity of active CTES (kWh) /Percentage of Daily cooling load
23	-	***1,886***	***229***	***17,066/6.7***
	1,650	**1,896**	**212**	**18412/7.2**
	1,800	1,915	185	**20123/7.9**
	1,950	1,955	144	**24170/9.5**
24	-	1,634	214	7,473/3.0
	1,650	1,710	175	10,619/4.2
	1,800	1,786	72	12,907/5.1
	1,950	**1,898**	**48**	**16,604/6.5**
25	-	1,547	238	2,618/1.0
	1,650	1,680	110	9,414/3.7
	1,800	1,782	69	12,503/4.9
	1,950	***1,895***	***45***	***16,533/6.5***

The maximum average power reduction was 1,955 kW which accounts for 34.9% of the average chiller power consumption in the baseline case. Intrashed variability represents the quality of power reduction, which is the standard deviation of power reduction during the DR event [Mathieu et al, 2011]. A small intrashed variability indicates that the power reduction is steady and more predictable for the ISOs/RTOs. On the contrary, a large intrashed variability indicates that the power reduction varies frequently during the DR event. With the chiller power reduction set-point increased, the intrashed variable was reduced which indicates the quality of power reduction is better, as shown in Table 6.4.

Using different set-points, the actual indoor temperature rises and the required capacities of active CTES during the DR event can be considered as the cost concerning indoor thermal comfort degradation and the capital cost of the active CTES to support the application of the developed improved fast power DR strategy respectively. Meanwhile, the corresponding average demand reduction and its intrashed variability can be considered as the benefits of applying the developed fast power DR strategy. The results presented in Table 6.4 show the quantitative relation between costs and benefits.

For instance, the average demand reduction and the required capacity of active CTES were 1,886 kW and 17,066 kWh respectively, when the upper limit of indoor temperature set-point was 23°C and demand reduction set-point was not set. They were 1,895 kW and 16,533 kWh respectively (similar to that in the above first case) when the upper limit of indoor temperature set-point was 25°C and demand reduction set-point was 1,950 kW. But the corresponding indoor thermal comfort deterioration and the intrashed variability were very different. If the indoor thermal comfort was given a

higher weighting by a decision maker, the first case was better. If the quality of power reduction is given a higher weighting, the second case was better. Therefore, the quantitative relation between costs and benefits can facilitate the decision maker and the interested parties to assess the effects of the strategy comprehensively and to make proper choices concerning their interests.

In addition, the average demand shed was 1,896 kW, when the upper limit of indoor temperature set-point was 23°C and demand reduction set-point was 1650 (third case). It was close to 1,898 kW when the upper limit of indoor temperature set-point was 24°C and the demand reduction set-point was 1,950 kW (fourth case). But the required capacity of active CTES (18,412 kWh) in the third case was much larger than that (16,604 kWh) in the fourth case while the indoor thermal comfort degradation was lower in the third case. Therefore, the decision makers can also make their choices by compromising the cost concerning indoor thermal comfort degradation and the capital cost of the active CTES.

6.6 Summary

Along with the development of smart grid, critical issues, such as peak load and power imbalance, need more efforts from power demand side, e.g., buildings. This chapter presents two fast power DR strategies for buildings involving both active and passive CTES for smart grid applications. The investigation on the power demand reduction potential in buildings is also proposed.

It is worth noticing that the on-line feed-back control of discharging storage will be also used as an effective correction and supplement way in the actual implementation of the

developed DR strategy since uncertainty is inevasible in the prediction process and is a key issue for building demand management.

Based on the results of the case studies, the following conclusive remarks can be drawn:

For both the developed fast DR strategies:

- The developed strategies can provide immediate and significant power demand reduction through shutting chiller(s) down during the DR event when a relatively small CTES is used. For instance, 28.9% of chiller power can be reduced when an active CTES with capacity accounting for 4.2% of daily cooling load is used in the morning case. 34.9% of chiller power is reduced when the required capacity of active CTES accounts for 7.3% of daily cooling load in the afternoon case.
- With the increase of the chiller power reduction set-points, the rebound decreases. For instance, the rebound is 760 kW when the capacity of active CTES is 1.3% of the daily cooling load in morning case. The rebound reduced to 563 kW when the capacity of active CTES increases to 4.2% of the daily cooling load.
- Accurate prediction of chiller power reduction and indoor temperature during the DR event can be calculated in advance, e.g. the mean absolute percentage errors of predicted demand reduction in the basic and improved fast power DR strategies are less than 3.7% and 4.8% respectively. The accurate prediction of power reduction can also facilitate the grid managers to accurately estimate the power insufficiency during the DR event and accordingly schedule the supply to meet the demand effectively.

For the improved fast DR strategy:

- Under the same upper limit of indoor temperature set-point, with the increase of the

chiller power reduction set-point, the intrashed variability decreases under control of the improved fast power DR strategy since the operation duration of active CTES is longer to keep the power reduction above the set-point. Meanwhile, under the same chiller power reduction set-point, with the increase of the upper limit of indoor temperature set-point, the intrashed variability also decreases since the maximum power reduction under lower upper limit of indoor temperature set-point was larger than that under higher upper limit of indoor temperature set-point.

- After using a small scale active CTES, the level of indoor thermal comfort degradation during the DR event can be controlled under different upper limits of indoor temperature set-point of the improved fast power DR strategy. For instance, the indoor temperature rise can be limited to less than 0.3 $^{\circ}$C only when the capacity of active CTES is 6.7% of the daily cooling load and the indoor temperature rise can be limited to less than 1.7 $^{\circ}$C when the capacity of active CTES is 3.7% of the daily cooling load only.
- The quantitative analysis on the improved fast power DR strategy concerning the required capacity of active CTES, the indoor thermal comfort and the quantity as well as quality of the power reduction during the DR event is also presented. The quantitative relation can facilitate the decision makers to evaluate the effects of the strategy for a particular building under certain electricity pricing/incentive policy. The decision makers can also make their choices by compromising the costs concerning indoor thermal comfort degradation and the capital cost of the active CTES.

CHAPTER 7 LIFE-CYCLE COST SAVING ANALYSIS AND OPTIMAL DESIGN OF ACTIVE COOL THERMAL ENERGY STORAGE FOR BUILDING DEMAND MANAGEMENT

As discussed in Chapter 5 and 6, the benefits of using CTES for the building demand management mainly come from two aspects: building peak load management (PLM) and demand response (DR). During the DR event, the active storage can help to achieve fast demand response by reducing the power demand. When in the normal periods without the DR event, the active storage also can be employed to reduce the peak demand so as to reduce the higher charge for the peak demand.

In this chapter, life-cycle cost benefit analysis and optimal design of active CTES for building demand management is presented. Firstly, the combined benefits of the active CTES implemented in both fast DR and PLM are analyzed based on one existing DR program and one electricity price structure. Secondly, the simulation-based optimal design method (presented in Section 5) is employed to optimize the capacity of active CTES and to determine the corresponding life-cycle cost saving potentials.

In Sub-section 7.1, the life-cycle cost analysis of the capacity of active CTES is conducted. The storage-priority control strategy as well as the economic incentives for fast power DR and PLM is firstly introduced. The optimal design of active CTES for building demand management is then implemented in Sub-section 7.2. A summary is given in Sub-section 7.3.

7.1 Life-cycle Cost Saving Analysis

As analyzed in Chapter 5, significant annual net cost saving can be achieved by implementing the demand limiting control with small scale active CTES in different real buildings in Hong Kong. Actually, the active storage also can bring significant cost benefits when it is used for supporting the fast demand response (DR). Incentives due to participating in a DR program provided by grid manager can be achieved by using active CTES. Therefore, it is necessary to analyze the combined benefits of the active CTES implemented in both fast DR and PLM during the life-cycle.

When conducting the economic analysis, the annual cost savings were calculated based on different tank capacities which are required to fulfill the fast DR strategy under different chiller power reduction set-points (mentioned in sub-section 6.5 and Table 6.4). Both the benefits from shifting peak demand under an electricity price structure and participating in a DR program provided by ISOs/RTOs to provide fast DR are concerned.

The benefits of active CTES used in PLM and the corresponding control method of active CTES are proposed in Sub-section 7.1.1.The incentive mechanism of DR is introduced to assess the cost benefit from implementation of active storage in fast DR in Sub-section 7.1.2. Based on the given DR program and electricity price structure, the life-cycle cost saving analysis is conducted in Sub-section 7.1.3.

7.1.1 Cost benefits calculation for peak load management

Nowadays, the time-of-use (TOU) pricing policy has been adopted in many countries to discourage the use of electricity under peak load conditions.

An electricity price structure in Guangzhou in South China, as listed in Table 7.1 is selected as the example to demonstrate the economic benefits from PLM. The whole pricing duration is divided into three periods: high price period, moderate price period and low price period.

Table 7.1 An electricity price structure in Guangzhou in South China

	Electricity price (USD/kWh)		
Location	High price period (14:00 a.m.to 17:00 p.m.)	Moderate price period (8:00 a.m. to 14:00 a.m.; 17:00 p.m. to 24:00 p.m.)	Low price period (0:00 a.m. to 8:00 a.m.)
Guangzhou	0.13	0.09	0.05

The storage-priority control is used for PLM because it is one of the most common active CTES operation modes. The storage-priority control means the storage media of active CTES is melted as much as possible during peak demand period. It aims at fully discharging the available capacity of active CTES to reduce chiller power. The principle is described in Sub-section 2.2.

The storage-priority control is also implemented in the dynamic simulation platform built in Section 3. During the discharging period, the valve *B* is fully opened to allow maximum discharging flow rate to the PCM tank, as shown in Fig. 4.4 (b). The tank is fully charged during night when the electricity price is the lowest in a day under the electricity price structure.

7.1.2 Incentive mechanism of the fast demand response

Normally the benefits for demand response largely depend on the financial structure of

the DR program [Rahimi and Ipakchi, 2010] which is provided by ISOs/RTOs (grid management). An existing DR program of ISO New England (NEISO) [ISO New England Inc, 2009], called Real-time Demand Response (RTDRP), as listed in Table 7.2, in U.S. is employed in this thesis to demonstrate the economic benefits of fast demand response.

Table 7.2 A demand response program of NEISO

Program	Response time	Duration of DR event	Minimum reduction	Incentive	
				Energy payment	Capacity payment
Real-Time Demand Response (RTDRP)	30 minutes	2 hours	100 kW	500 USD/MWh	$4.1/kW per month

The response time, duration of DR event and minimum reduction are the specific requirements of the DR program. The response time refers to the duration from the time when a change in power is requested to the time when a power change is done by demand response resource (DRR) [Oldewurtel et al, 2013]. Obviously, the speed, amount and duration of the power reductions, resulted under control of the developed fast DR strategy, can meet the above requirements. The incentive paid to customers consists of two parts: One is the energy payment and the other is the (monthly) capacity payment.

The benefits can be calculated by the given energy payment and capacity payment in Table 7.2. For instance, if the predetermined power reduction capacity is 400 kW, the capacity payment to the customer is 1640 (400×4.1) USD per month at least even

though no DR event actually happens. If the required reduction is 300 kW and the duration is 2 hours in one DR event, the energy payment is 300 USD (300×2×0.5) per event. Therefore, the total monthly payment is 1940 USD if the DR event happens once in this month.

7.1.3 Life-cycle cost saving analysis

For exploration of the relationship between the cost saving and capital cost of the active CTES for building demand management, the quantitative analysis on the life-cycle cost saving potentials of the active CTES with different capacities was conducted, as listed in Table 7.3.The capacities of the active CTES, percentage of daily cooling load and average demand shed determined by the improved fast power DR strategy as well the corresponding chiller power reduction set-points and upper limits of indoor temperature set-point during the DR event are introduced from Table 6.4. Average demand shed [Mathieu et al, 2011] means the average power reduction during the DR event.

It was assumed that the required demand reduction in each event was the same as the average demand shed. The annual income from fast DR was accordingly calculated. For instance, the maximum annual income from fast DR was 59,823 USD (1955×6×4.1+1955×6×2×0.5) and the corresponding required capacity of active CTES was 24,170 kWh (i.e. 9.5% of daily cooling load) when the chiller power reduction set-point was 1,950 kW and the upper limits of indoor temperature was 23°C in the improved fast DR strategy.

The storage-priority control for load shifting was activated during the normal days (359 days in one year) when no DR event happened. The active CTES was activated to shift power consumption from the high price period (14:00 a.m.to 17:00 p.m.) to the low

price period (0:00 a.m. to 8:00 a.m.). The annual cost saving comes from the differences of electricity prices between high price period and low price period. Total annual cost saving was the sum of annual income from fast demand response and annual cost saving from peak load management.

As discussed is Section 5, average annual system cost was the sum of annualized capital cost of the active CTES system and the annual space rent. The average lifespan of the major equipment in the air-conditioning system was also assumed to be 10 years. The total capital investment of unit volume storage tank was assumed as 4350 USD/m3 (34000 HKD/ m3) over ten years period. The average annual system cost was then 435 USD/m3·y. The life-cycle cost saving was the annual net cost saving which was the difference between the total annual cost saving and the average annual system cost.

The pay-back periods for fast DR, PLM or total annual cost saving of each resulted capacity of active CTES were listed.

Table 7.3 Quantitative analysis on the life-cycle cost saving potentials of the active CTES with different capacities

Upper limits of indoor temperature set-point (˚C)		23				24				25			
Chiller power reduction set-points (kW)		-	1,650	1,800	1,950	-	1,650	1,800	1,950	-	1,650	1,800	1,950
Average Demand Shed (kW)		1,886	1,896	1,915	1,955	1,634	1,710	1,786	1,898	1,547	1,680	1,782	1,895
Required active storage capacity (kWh)		17,066	18,412	20,123	24,170	7,473	10,619	12,907	16,604	2,618	9,414	12,503	16,533
Percentage of Daily cooling load (%)		6.7	7.2	7.9	9.5	3.0	4.2	5.1	6.5	1.0	3.7	4.9	6.5
Annual Income from fast DR (USD·y)		57,712	58,018	58,599	59,823	50,000	52,326	54,652	58,079	47,338	51,408	54,529	57,987
Annual cost saving from PLM (USD·y)		196,054	211,517	231,173	277,665	85,850	121,991	148,276	190,747	30,076	108,148	143,634	189,931
Total annual cost saving (USD·y)		253,766	269,535	289,772	337,488	135,850	174,317	202,927	248,826	77,414	159,556	198,164	247,918
Life-cycle cost saving (USD·y)		41,221	40,226	39,154	36,468	42,779	42,065	42,180	42,035	44,808	42,311	42,448	42,011
Pay-back period (year)	For DR	36.8	39.5	42.8	50.3	18.6	25.3	29.4	35.6	6.9	22.8	28.6	35.5
	For PLM	10.8	10.8	10.8	10.8	10.8	10.8	10.8	10.8	10.8	10.8	10.8	10.8
	For total	8.4	8.5	8.6	8.9	6.9	7.6	7.9	8.3	4.2	7.3	7.9	8.3

It can be found that the required capacities active CTES as well as the corresponding percentages to the daily cooling load increased with the increase of the chiller power reduction or the decrease of upper limit of indoor temperature set-point. Both the annual income from fast DR and annual cost saving from peak load management, which was calculated based on the DR program in U.S. and the electricity price structure in Guangzhou in South China discussed above respectively, increased accordingly.

The annual income from fast DR accounted for 61% of the total annual cost saving when the chiller power reduction set-point was not set and upper limit of indoor temperature was 25°C. The proportion reduced to 32%, 28% and 23% when the chiller power reduction set-points were 1650 kW, 1800 kW and 1950 kW respectively. The results show that the annual income from fast DR accounted for a significant proportion of the total annual cost saving. In addition, under the same upper limit of indoor temperature set-point, the percentage of the annual income from fast DR to the total annual cost saving decreased with the increase of chiller power reduction set-point.

Meanwhile, under the same chiller power reduction set-point, the annual income from fast DR accounted for a smaller proportion of total annual cost saving with the decrease of the upper limit of building indoor temperature set-point. For instance, when the chiller power reduction set-point was not set, the annual income from fast DR accounted for 37% and 23% only when the upper limits of building indoor temperature were 24°C and 23°C respectively. It is because, compared with the increase of income form fast DR, the cost saving from PLM increased as a faster rate since the capacity of active CTES, resulted under control of the improved fast DR strategy, grew progressively with the increase of the chiller power reduction set-point or with the decrease of upper limit

of indoor temperature set-point.

This above observations also show that the fast DR is necessary for a relatively small scale active CTES to achieve the remarkable economic benefit while for a relatively large scale active CTES, the PLM which can bring significant cost saving should be paid a higher weighting.

The life-cycle cost was 42,311 USD·y with the storage capacity of 9,414 kWh when the power reduction set-point was 1650 kW and the upper limit of indoor temperature set-point was 25°C. The life-cycle cost was 40,226 USD·y with the storage capacity of 18,412 kWh when the power reduction set-point was the same and the upper limit of indoor temperature set-point was 23°C. Meanwhile, the life-cycle cost was 41,221 USD·y with the storage capacity of 17,066 kWh when power reduction set-point was not set and the upper limit of indoor temperature set-point was 23°C. The life-cycle cost was 36,468 with the storage capacity of 24,170 kWh when power reduction set-point increased to 1950 kW and the upper limit of indoor temperature set-point was the same. The results show that although the cost saving from PLC increased fast, the required active CTES and the corresponding average annual system cost also increased dramatically with the increase of chiller power reduction set-point or the decrease of upper limit of indoor temperature set-point. Therefore, the resulted annual net cost saving did not increased.

The pay-back period for total annual cost saving of each resulted capacity of active CTES were acceptable (4.2~8.9 years). The pay-back period for fast DR increased dramatically since the annual income from fast DR increased as a low rate while the required active capacity of active storage increased progressively with the increase of

the chiller power reduction set-points or the decrease of upper limit of indoor temperature set-point. For instance, the pay-back period exceeded 22 years when the chiller power reduction set-point was larger than 1650 kW and the decrease of upper limit of indoor temperature set-point was 25°C. Meanwhile, the pay-back period for PLM kept stable, i.e. 10.8 year, since annual cost saving from PLM was proportional to the required capacity of active CTES.

As discussed above, the active CTES can bring significant annual cost saving through supporting the fast DR and PLM. Under different chiller power reduction set-points, the required active storage capacities and the corresponding life-cycle cost saving are different. Therefore, it is necessary to optimize the storage capacity which can result the maximum life-cycle cost saving for building demand management.

7.2 Optimal Design of Active Cool Thermal Energy Storage

In this sub-section, in order to achieving maximum annual net cost saving, the optimal capacity of active CTES for building demand management, including fast DR and DLR, is resulted through introducing the optimal design method presented in Chapter 3. Based on different indoor thermal comfort requirements of building users, i.e. different upper limits of indoor temperature, the optimized capacities of active CTES, the life-cycle cost saving potentials and the chiller power reduction set-points in the developed fast power DR strategy are resulted and analyzed. The main factor that determine the optimal capacities of active CTES are summarized.

The required active CTES capacities under different upper limits of indoor temperature set-points and chiller power reduction set-points are shown and analyzed in Sub-section

7.2.1. Based on the given DR program and electricity price structure, the optimal capacities under different upper limits of indoor temperature are resulted in Sub-section 7.2.2. The impact of the capacities of active CTES on the life-costs saving is also analyzed in this sub-section.

7.2.1 Required capacities for different indoor thermal comfort requirements

Since the cost saving from PLM was proportional to the capacities of active CTES, determined under control of the improved fast DR strategy, it is necessary to investigate the effects of different upper limits of indoor temperature set-point and chiller power reduction set-points on the required capacities of active CTES first. The developed improved power DR control with exhaustive search method was accordingly used to determine the required capacities.

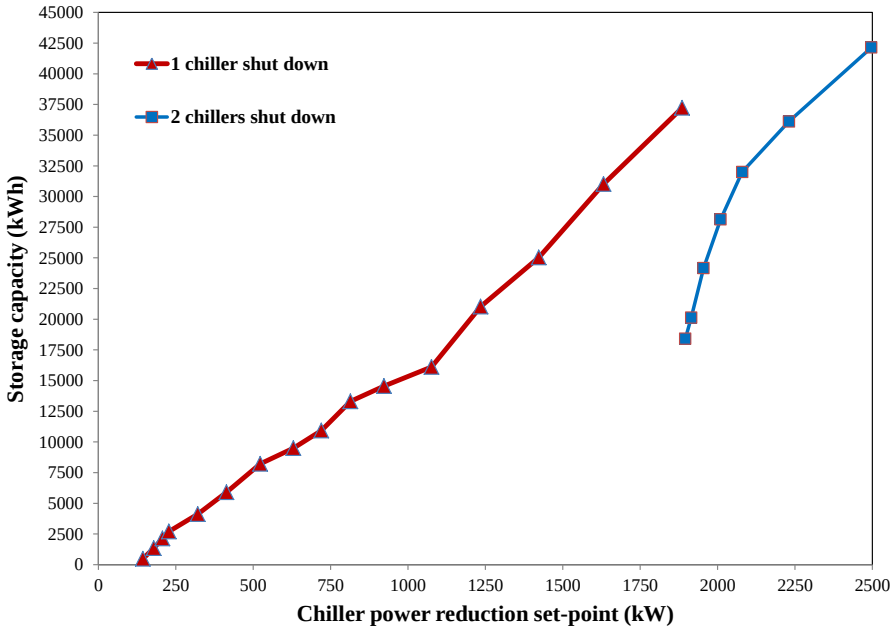

Fig.7.1 Required capacity of active CTES for different chiller power reduction set-point – Indoor temperature set-point upper limit of 23˚C

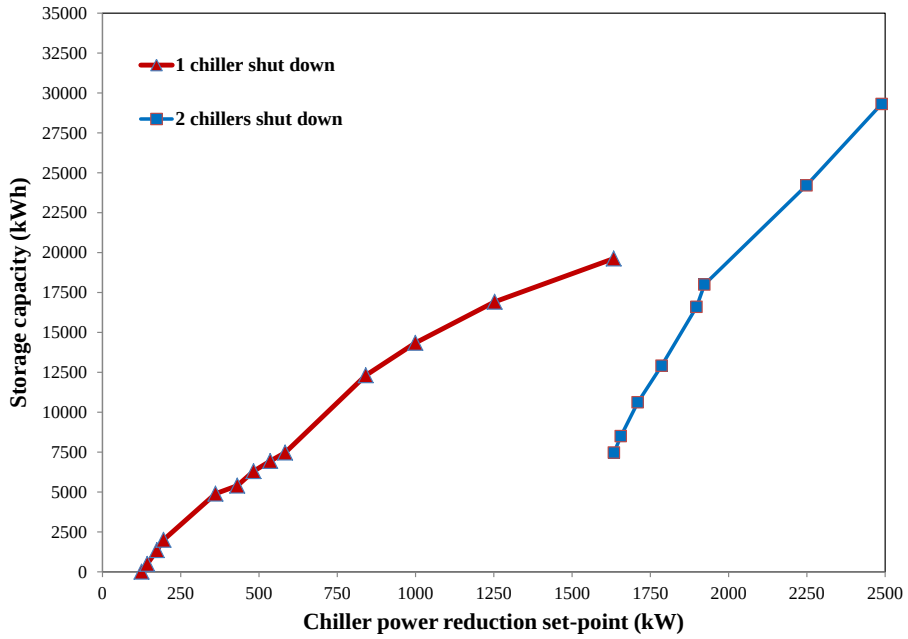

Fig.7.2 Required capacity of active CTES for different chiller power reduction set-point – Indoor temperature set-point upper limit of 24˚C

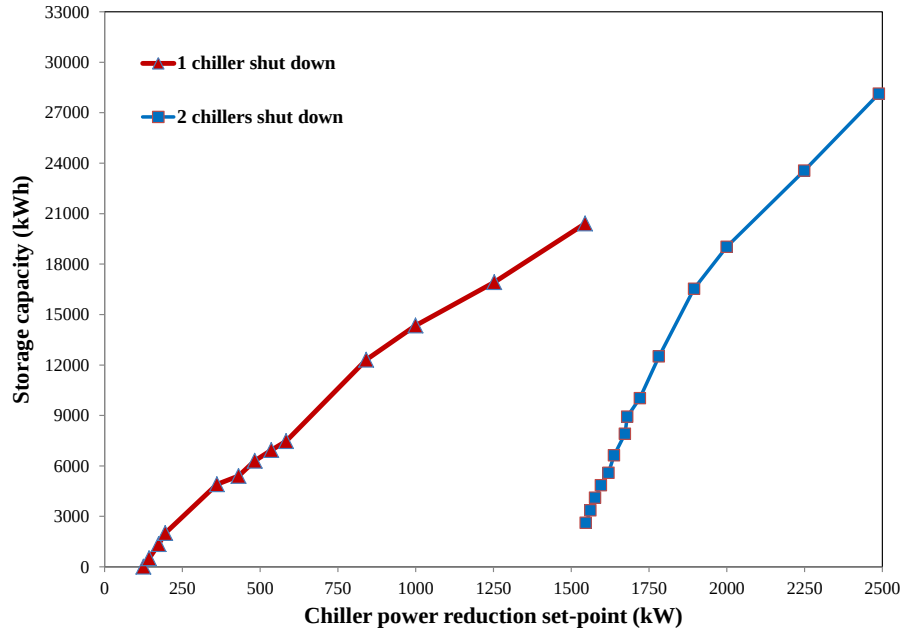

Fig.7.3 Required capacity of active CTES for different chiller power reduction set-point – Indoor temperature set-point upper limit of 25˚C

The required capacity of active CTES for different chiller power reduction set-point under different upper limits of indoor temperature set-point during the DR event are shown in Fig. 7.1 to 7.3. As the chiller power reduction set-points increase, the required capacities of active CTES increased when the number of chiller required to be shut down was the same.

When the chiller power reduction set-point increases to a certain value, the number of the chillers required to be shut down increased and the corresponding required capacities of active CTES were quite different. For instance, when the upper limit of indoor temperature set-point was 23°C and the power reduction were the same, i.e. 1886 kW, the required capacity of active storage are 37,222 kWh and 17,066 kWh when one chiller was shut and two chillers were shut down respectively. The reason for the different required capacities of active CTES was that, compared to that when two chillers were shut down, much more cooling capacity from the active CTES was required to reduce to power reduction to same level, e.g. 1886 kW, when only one chiller was shut down. Therefore, for the same chiller power reduction, the required capacities of active storage may be quite different when the numbers of chillers required to be shut down were different. It is quite different from the required capacities of the active CTES under the demand limiting control, as shown in Fig. 5.8 to 5.10 of Section 5.

In addition, for the same chiller power reduction, the required storage capacity is larger when the upper limit of indoor temperature set-point is lower. For instance, when the power reduction was 500kW, the required capacities of active CTES were around 7600 kWh, 6500 kWh and 6100 kWh when the upper limits of indoor temperature set-point

were 23°C, 24°C and 25 °C respectively. It was because that more cooling capacity of active CTES was required when the allowable indoor thermal comfort loss was less.

The resulted capacities of active CTES as well as the annual income from fast DR and cost saving from PLM under different upper limits of indoor temperature set-point were summarized in Table 7.4.

Table 7.4 Capacities of active CTES under different upper limits of indoor temperature and chiller power reduction set-points

Average Demand Shed (kW)	Annual Income (USD·y) from fast DR	Upper limits of indoor temperature set-point (°C)											
		23				24				25			
		Number of chillers shut down	Required active storage capacity (kWh)	Average annual system cost (USD·y)	Annual cost saving from PLM (USD·y)	Number of chillers shut down	Required active storage capacity (kWh)	Average annual system cost (USD·y)	Annual cost saving from PLM (USD·y)	Number of chillers shut down	Required active storage capacity (kWh)	Average annual system cost (USD·y)	Annual cost saving from PLM (USD·y)
144	4,962	1	480	5,978	5,514	1	470	5,854	5,399	1	470	5,854	5,399
414	12,668		5,900	73,480	67,779		5166	64,339	59,347		5166	64,339	59,347
1076	32,864		16,111	200,651	185,083		15213	189,467	174,767		15213	189,467	174,767
1547	47,338		28,410	353,826	326,374		18,631	232,036	214,033	2	2618	32,605	30,076
1634	50,000		31,063	386,867	356,852	2	7,474	93,083	85,850		6577	81,912	75,557
1886	57,712	2	17,066	212,545	196,054		16,103	200,551	184,991		15873	197,687	182,349
2010	61,506		28,140	350,464	323,272		20,431	254,454	234,711		19,777	246,308	227,198
2231	68,269		36,111	449,737	414,843		28,314	352,631	325,271		28,011	348,857	321,790
2497	76,408		42,141	524,836	484,116		37,999	473,250	436,533		37,773	470,436	433,936

7.2.2 Capacity optimization

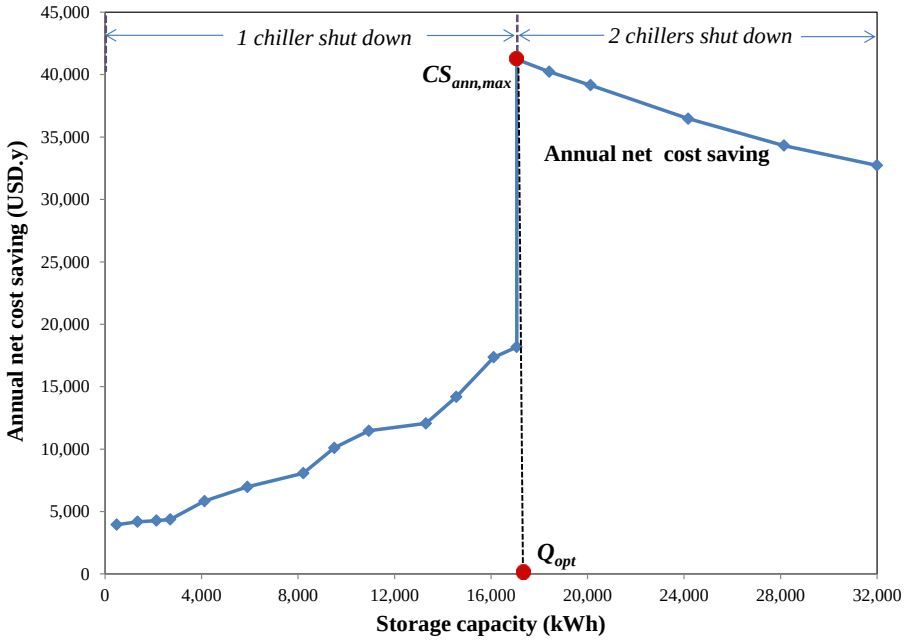

Fig.7.4 Annual net cost saving of active CTES – Indoor temperature set-point upper limit of 23˚C

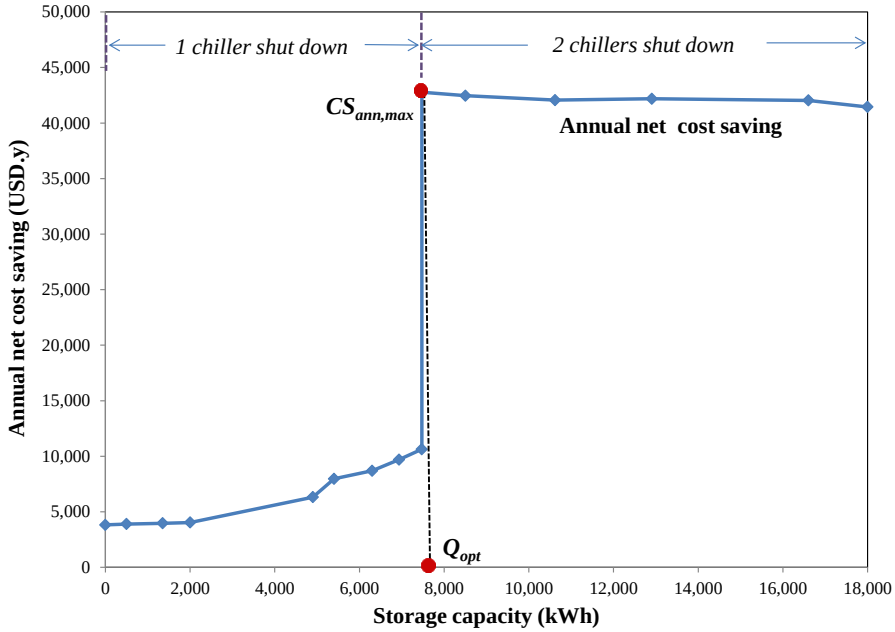

Fig.7.5 Annual net cost saving of active CTES – Indoor temperature set-point upper limit of 24˚C

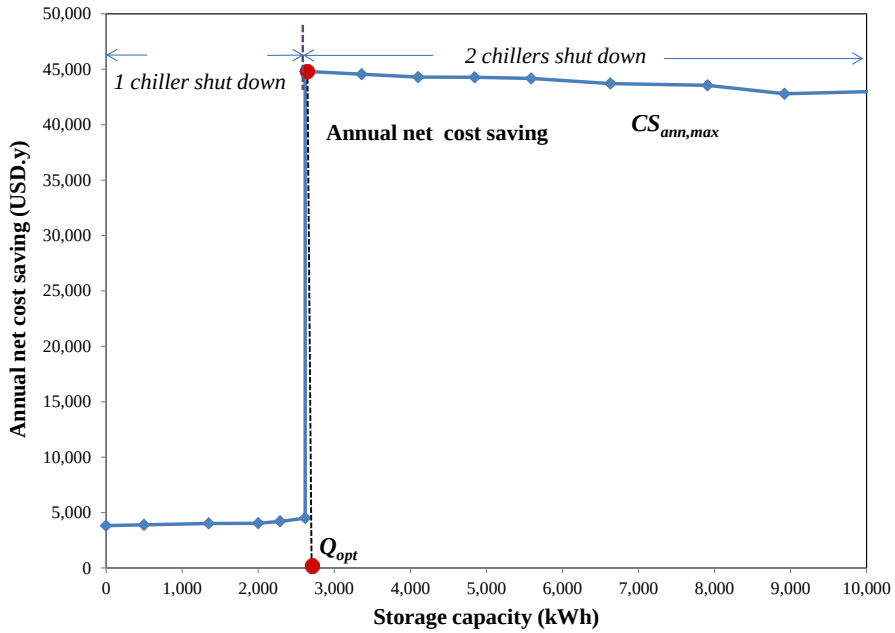

Fig.7.6 Annual net cost saving of active CTES – Indoor temperature set-point upper limit of 25˚C

The annual net cost savings of active CTES for building demand management under different upper limits of indoor temperature set-point are shown in Fig. 7.4 to 7.6. $CS_{ann,max}$ is the maximum annual net cost saving and Q_{opt} is the optimal capacity of active CTES.

With the increase of the required capacity of active CTES, the annual net cost saving increases when one chiller was shut down. The main reason is that, with increase of the required capacity of active CTES, the required capacity of active CTES increased largely although the ratio of annual income from fast DR to the average annual system cost decreased and the ratio of annual cost saving from PLM annual to the average annual system cost kept constant, i.e. 92%. For instance, the ratio of annual income from fast DR to the average annual system cost was 83% and the storage capacity was 480 kWh only, as shown in Table 7.4, when the upper limit of indoor temperature set-point

was 23 ˚C and the average demand shed was 144 kW (first case). The ratio of annual income from fast DR to the average annual system cost reduced to 13% but the storage capacity was 31,063 kWh, which was 65 times of that in the first case when the average demand shed increased to 1634 kW (second case) and the upper limit of indoor temperature set-point was the same. Therefore, the total annual cost saving kept increasing with the increase of the required capacity of active CTES.

When the number of chiller required to be shut down increased, the total annual cost saving had a stepped increase because the annual income from fast DR largely increased. When two chillers were shut down, on the contrary, the annual net cost saving decreased with the increase of the required capacity of active CTES. The reason is that the ratio of annual income from fast DR to the average annual system cost decreased as a faster rate while the required capacity of active CTES increased as a lower rate. For instance, the ratio of annual income from fast DR to the average annual system cost was 145% and the storage capacity was only 7474 kWh, as shown in Table 7.4, when the upper limit of indoor temperature set-point was 24 ˚C and the average demand shed was 1634 kW (third case). The ratio of annual income from fast DR to the average annual system cost reduced to 16% but the storage capacity is 37,999 kWh, which was only 5 times of that in the third case, when average demand shed increased to 2497 kW (fourth case).

Given the above observations, the maximum annual net cost saving ($CS_{ann,max}$) is achieved where two chillers are shut down and chiller power reduction set-points are not set, at shown in Fig. 7.4, 7.5 and 7.6. The optimal capacity increased with the increase of the upper limit of indoor temperature set-point. The results of storage capacity

optimization and the corresponding optimal chiller power reduction set-point are listed in Table 7.5. It should be noted that the optimal capacity of active CTES (Q_{opt}) is normally less than 7% of the typical daily cooling load.

Table 7.5 Results of storage capacity optimization for different indoor thermal comfort requirements

	Upper limits of indoor temperature set-point (°C)		
	23	24	25
Optimal Chiller power reduction set-points (kW)	-	-	-
Optimal capacity of active CTES (kWh)	17,066	7,473	2,618
Percentage of daily cooling load (%)	6.7	3.0	1.0
Maximum annual net cost saving (USD·y)	41,221	42,779	44,808

7.3 Summary

The life-cycle cost benefit analysis and optimal design of active CTES for building demand management is proposed in this section. The active storage is beneficial to both fast DR response and PLM. During the DR event, income from fast DR can be achieved through activation of the active CTES. During the normal days, the active CTES can be also used to shift peak load for reducing the high charge of peak demand. For demonstrating the economic benefits of active CTES used in the fast DR and PLM, one existing DR program and one electricity price structure are introduced. The optimal design method, presented in Section 5, is then used to optimize the capacity of active CTES and to determine the corresponding life-cycle cost saving potentials for building demand management.

Based on the results of the case studies, the following conclusions can be drawn:

- The annual income from fast DR accounts for a significant proportion of the total annual cost saving, as listed in Table 7.3. Compared with the increase of income from fast DR, the cost saving from PLM increases as a faster rate with the progressive increase of the capacity of active CTES resulted under control of the improved fast DR strategy, when the chiller power reduction set-point increases or the upper limit of indoor temperature set-point decreases. This observation suggests that the fast DR is necessary for a relatively small scale active CTES to achieve the remarkable economic benefit while for a relatively large scale active CTES, the PLM which brings significant cost saving should be paid a higher weighting.
- The results, shown in Fig. 7.4 to 7.6, show that, with the increase of the required capacity of active CTES, the annual net cost saving increases when only one chiller is shut down. While the annual net cost saving decreases, with the increase of the required capacity of active CTES, when two chillers are shut down. Based on the different indoor thermal comfort requirements, i.e. different upper limits of indoor temperature, the maximum annual net cost savings, maximum life-cycle cost saving, are accordingly achieved where two chillers are shut down and the chiller power reduction set-points are not set.
- The results of storage capacity optimization show that substantial life-cycle cost saving can be obtained with relative small scale active CTES, i.e. 6.7%, 3,0% and 1.0% daily cooling load based on the different indoor thermal comfort requirements. With the decrease of the upper limit of indoor temperature set-point, the optimal capacity of active CTES largely increases.

CHAPTER 8 CONCLUSIONS AND RECOMMEDATIONS

In this thesis, optimal design and control strategies of cool thermal energy storage (CTES) systems for building demand management are proposed. Buildings can have considerable flexibility in power demand when CTES are used. The CTES can effectively shift building peak load and provide more capabilities of building power demand response (DR) due to the significant thermal storage. An optimal design method of active CTES for building peak load management is developed. Two fast power DR strategies for building involving both active and passive CTES for smart grid applications are also developed. Furthermore, the life-cycle cost benefit analysis and optimal design of active CTES for building demand management are proposed.

This section is organized as follows: Sub-section 8.1 presents the summary of main contributions of the research presented in this thesis. The conclusion of the all researches presented in this thesis is summarized in Sub-section 8.2. The recommendations for future work are presented in Sub-section 8.3.

8.1 Summary of Main Contributions

The main contributions in this thesis are summarized as following:

1. A simplified PCM storage tank model is developed to test the performance of optimal design and control strategies of CTES for building demand management. The model concerns computation speed and program size when implemented in large scale system simulations. The validation results demonstrate that the model

have acceptable accuracy and reliable performance.

2. A simulation-based optimal design method of active CTES for building peak load management is developed. The results of case studies show that significant annual net cost saving can be obtained by implementing demand limiting control with small scale storage tanks in different real buildings in Hong Kong. The optimal storage capacity can be determined conveniently from the relationship between the annual net cost saving and the required storage capacity. Except the original power consumption profiles, another main factor affecting the optimal capacity is the electricity price structure on the required capacities of active CTES.

3. Two fast power DR strategies for buildings involving both active and passive CTES for smart grid applications are developed. Compared with traditional HVAC DR strategies, these two control strategies provide immediate and stepped power demand reduction through shutting chiller(s) down when requested. The active CTES is used to enhance the capacity of power reduction or to provide additional cooling capacity for improving indoor thermal comfort level. Through controlling the discharging rate of active CTES, the chiller power reduction is modulated based on its set-point in the basic fast power DR strategy while both the chiller power reduction and the indoor temperature are the control objectives in the improved fast power DR strategy. In addition, chiller power reduction and indoor temperature during the DR event can be accurately predicted.

4. The life-cycle cost benefit analysis and optimal design of active CTES for building demand management are also proposed. Two main benefits of using CTES, including peak load management (PLM) and DR are considered simultaneously.

Based on different indoor thermal comfort requirements, i.e. different upper limits of indoor temperature, the optimized capacities of active CTES for building demand management is determined by the optimal design method. The results show that the annual income from fast DR accounted for a significant proportion of the total annual cost saving and substantial life-cycle cost saving can be obtained with relative small scale active CTES.

8.2 Conclusions

On PCM storage tank model

For dynamically and accurately simulating the system performance, a reliable CTES model is an important basis for the thermodynamic characteristic and energy performance analysis. A simplified physical dynamic model, with acceptable accuracy and good reliability, of coils storage tank is accordingly developed. The computation speed and program size of the developed model is highly concerned for implementation in large scale system simulations. The design and the corresponding mathematical equations of the model are introduced.

The validation of the model is conducted through comparing the two main outputs of the model, including the discharge rate and the mean PCM temperature in tank, with the results from an experimental study. The validation results show that the model has acceptable accuracy and reliable performance.

For testing the performance of the developed optimal design and control strategies of CTES, the simulated active CTES system using the developed PCM storage tank model are then constructed. The thermal-physical properties and price of PCM and PCM tank

are also introduced.

On the optimal design method of active CTES for building peak load management

A simulation-based optimal design method of small scale active CTES used for building peak load management (PLM) is developed. This method, aiming at achieving maximum life-cycle cost saving, i.e. maximum annual net cost saving, is one more effective and meaningful design method to optimize the storage capacity concerning both operational cost saving and the capital cost of used active CTES.

There are two main steps to obtain the optimal storage capacity. The first one is that by introducing actual load profiles as inputs, monthly demand limiting control with exhaustive search method is implemented to determine the required storage capacities under different peak demand reductions. In the second step, the optimal storage capacity and the corresponding maximum annual net cost saving are obtained by using the marginal decision rule. The peak demand set-points of each month are accordingly determined.

The results of case studies shown that significant annual net cost saving, accounting for about 7% of total building annual electricity consumption cost, can be achieved by implementing the demand limiting control with small scale active CTES (e.g. less than 5% of daily cooling load) in different real buildings in Hong Kong where the power tariff is not favorable.

Whether or how the spikes exist in original building power consumption profiles has significant impacts on the required storage capacities and corresponding annual net cost savings. Another main factor that decides the required capacities of active CTES is the

electricity price structure.

<u>On the fast power demand response strategies for buildings involving active and passive CTES for smart grid applications</u>

Two fast power demand response (DR) strategy involving both active and passive CTES are developed. Certain number of operating chiller(s) is shut down at the beginning of the DR event to achieve a significant and immediate power reduction. In the basic fast DR strategy, only power demand reduction is the control objective while in the improved fast power DR strategy, to control indoor thermal comfort degradation, the building indoor temperature during the DR event is the second control objective. Two processes are included in the strategies: prediction process and control processes.

The active CTES has different functions in the developed fast demand response strategies. First, the actual power reduction can be flattened, i.e. less intrashed variability, during the DR event through modulating the discharging rate of the storage tank. Secondly, the demand reduction potential can be further increased through decreasing the return chilled water temperature based on the chiller power reduction set-points. Third, additional cooling capacity can be supplied by the active storage to release the stress on the inadequate cooling capacity provided by the remaining operating chillers during the DR event.

The test results show that developed strategies can provide immediate and significant power demand reduction through shutting chiller(s) down during the DR event when a relatively small CTES is used. The degradation of indoor thermal comfort during the DR event can be controlled under different upper limits of indoor temperature set-point by using a small scale active CTES. Accurate prediction of chiller power reduction during

the DR event can be calculated in advance, which facilitates the grid managers to accurately estimate the power insufficiency during the DR event and accordingly to schedule the power supply to meet the demand effectively. The quantitative analysis on the improved fast power DR strategy concerning the required capacity of active CTES, the indoor thermal comfort and the quantity as well as quality of the power reduction during the DR event is presented to facilitate the decision makers to evaluate the effects of the strategy for a particular building under certain electricity pricing/incentive policy.

On the life-cycle cost benefit analysis and optimal design of active CTES for building demand management

The life-cycle cost benefit analysis and optimal design of active CTES for building demand management is proposed. The active CTES can bring benefits through helping to achieve fast demand response by reducing power demand during the DR event and also shifting peak demand to reduce the high charge of the peak demand. In this research, the active CTES is under control of the fast power DR strategy during the DR event. Meanwhile, during the normal days, the active CTES is under control of the storage-priority control to shift peak demand. One existing DR program in US and one electricity price structure in south China are introduced to calculate the detailed economic benefits of the active CTES in terms of the fast DR and PLM.

The life-cycle cost saving analysis of the resulted capacities of active CTES from the improved fast power DR strategy is first conducted. The results show that the annual income from fast DR is significant. While compared with the income increase from fast DR, the cost saving from PLM increases as a faster rate and accounts for a larger proportion of the total annual cost saving with the progressive increase of the capacity of

active CTES, resulted under control of the improved fast DR strategy, when the chiller power reduction set-point increases or the upper limit of indoor temperature set-point decreases. This suggests that small scale active CTES to is more suitable for supplying fast DR to achieve the remarkable economic benefit while for large scale active CTES, the PLM which brings significant cost saving should be implemented.

Based on the different indoor thermal comfort requirements, the optimized capacities of active CTES, the corresponding life-cycle cost saving potentials and the chiller power reduction set-points in the developed fast power DR strategy are then identified by the optimal design method introduced in Chapter 5. The resulted maximum life-cycle cost savings are achieved where two chillers are shut down and the chiller power reduction set-points are not set. In addition, the optimal capacity of active CTES largely increases with the decrease of the upper limit of indoor temperature set-point.

8.3 Recommendations for Future Work

Major efforts of this thesis have been made on the development of the optimal design and control strategies of CTES for building demand management. It would be very desirable and valuable to make further efforts on the following aspects to improve the quality of the research and to bring these methods into practical applications.

- For the optimal design of active CTES for PLM, the operating performance and cost saving potential of active CTES using ice as storage media, should be evaluated according to their higher energy storage density and lower cost. In addition, control of passive CTES, i.e. pre-cooling and building indoor temperature set-point reset, could be added to further enlarge the cost saving.

- In-situ implementation and validation of the developed fast power DR strategy and the corresponding modules/models is needed when the conditions are available. The feedback information is quite valuable for updating them to obtain desirable and satisfactory performances in practice. It is a time and energy consuming task to validate the proposed strategies in the practical buildings. Therefore, a lot of efforts need to be paid in the future studies.
- Currently, the chiller power is set as the power control objective in the developed fast power DR strategies. For more comprehensive and applicable control of the DR supplied by the whole HVAC system, the power of whole HVAC system should be considered as the power control objective. Therefore, the power of other main components in HVAC system, such as AHU and pumps, should be counted during DR events. While the AHU and pumps will be run at full speed to strive more chilled water and cooling energy to achieve the indoor air temperature set-point, since the cooling capacity provided the remaining operating chiller is less than that in baseline case.
- The rebound after DR events should be estimated and controlled. The partial capacity of the active CTES can be used to limit the power rise during rebound period. In addition, the combined usage of the developed fast DR and indoor air temperature set-point reset strategies could be also preferable to enhance the DR capabilities of buildings for different response time needs.

APPENDIX A-SIMPLIFIED BUILDING THERMAL STORAGE MODEL

Based on the equivalence principle, the simplified building energy model, i.e. 3R2C&2R2C as shown in Fig.A.1, was developed in [Wang and Xu, 2006]. This simplified building thermal storage model was further modified to simplified building thermal storage model, 2R1C model [Xue et al, 2014], as shown in Fig.A.2.

As a simplified building energy model, 3R2C model is used to represent building envelope, including external walls, windows, roofs and etc., and 2R2C model is employed to represent building internal mass, including internal walls, floors, partitions, furniture, ceilings and etc. For the simplified building thermal storage model, a building is simplified to a lumped thermal mass, consists of internal and external masses, and it is assumed to be homogeneous. An equivalent temperature (T_{bui}) is used to represent the energy status of the building. In the thermal storage model, heat gains achieved in convection, radiation, sensible and latent heat processes, etc., are assumed to be constant even the building indoor temperature is changed. Building thermal environment characteristic can be accordingly represented by the overall building thermal capacitance (C_{bui}), the outer thermal resistance ($R_{bui,ou}$) and the inner thermal resistance ($R_{bui,inn}$). The thermal mass of the air volume is ignored as it is too small compared with the thermal mass of building structures.

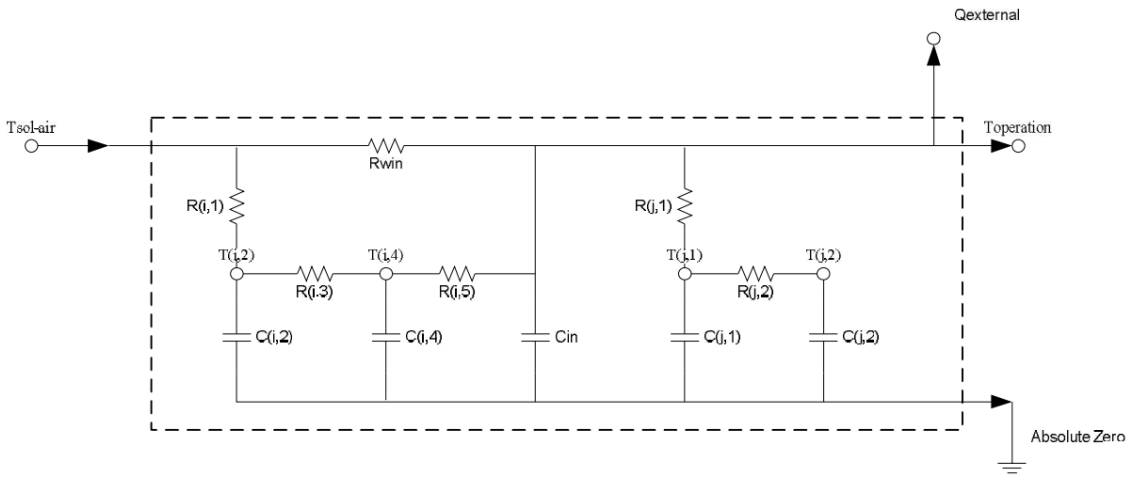

Figure A.1 Restructuring of the simplified building energy model

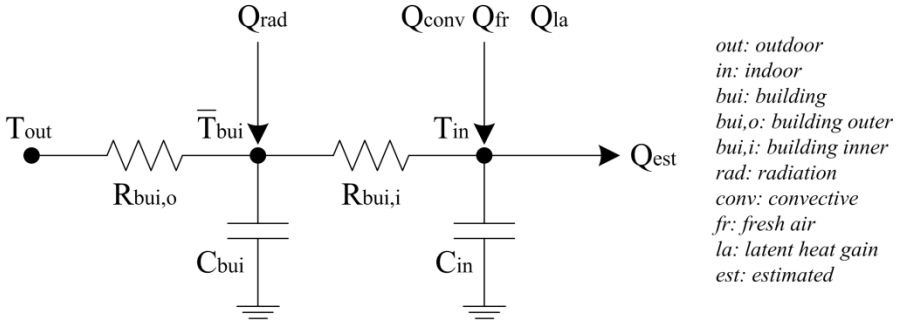

Figure A.2 The simplified building thermal storage model based on equivalence principle

A differential equation is established according to energy balance in the simplified thermal storage model, as shown in Eq.A.1. A function indicating the energy status of the building thermal masses is then written as Eq.A.2 by solving the Eq.A.1.

$$C_{bui}\frac{dT_{bui}(t)}{dt}A_{bui} = \frac{T_o(t)-T_{bui}(t)}{R_{bui,ou}}A_{bui} - \frac{T_{in}(t)-T_{bui}(t)}{R_{bui,inn}}A_{bui}+Q_{rad} \qquad (A.1)$$

$$T_{bui}(t) = T_{eqt}\left(1-e^{\frac{-t}{\tau_{bui}}}\right) + T_{bui}(0)e^{\frac{-t}{\tau_{bui}}} \qquad (A.2)$$

where,

$$T_{eqt} = \left(\frac{T_o}{R_{bui,ou}} + \frac{T_{in}}{R_{bui,inn}} + \frac{Q_{rad}}{A_{bui}}\right) R_{bui} \quad \text{(A.3)}$$

$$\tau_{bui} = R_{bui} \cdot C_{bui} \quad \text{(A.4)}$$

$$R_{bui} = \frac{R_{bui,ou} \cdot R_{bui,inn}}{R_{bui,ou} + R_{bui,inn}} \quad \text{(A.5)}$$

where, $T_{bui}(0)$ is the initial equivalent temperature of building thermal masses. T_{eqt} is the equivalent temperature of external heat sources, i.e. radiation gains (Q_{rad}), the outdoor and indoor air and etc. T_o and T_{in} are the outdoor and indoor temperatures. τ_{bui} is the time constant of the building thermal mass. A_{bui} is the effective building surface area involved in the heat exchange process.

The heat exchange between the indoor air and the building is particularly concerned since heating/cooling load alteration potential of building is determined by the processes of thermal energy store/release. By combining the Eq.A.1 and 2, the heat flux between the indoor air and the building and can be written as Eq.A.6.

$$Q_{bui}(t) = \frac{|T_{eqt} - T_{bui}(0)|}{R_{bui,inn}} e^{\frac{-t}{\tau_{bui}}} A_{bui} + \frac{T_{in}(t) - T_o(t)}{R_{bui,ou} + R_{bui,inn}} A_{bui} - \frac{Q_{rad} R_{bui}}{R_{bui,inn}} \quad \text{(A.6)}$$

Similar to the simplified building energy model mentioned above, the predicted building heating/cooling load can be represented in Eq. A.7 according to energy balance. The alteration potential of the building heating/cooling load can be then represented by Eq. A.8. It is worth noticing that, as the gains of a building are assumed to be constant in the altered cases and the reference case, the gains due to convection, radiation, sensible and latent heat processes, etc. can be canceled and do not appear in the mathematical formula of the thermal storage model.

$$Q_{dem} = Q_{con} + Q_{fr} + Q_{infil} - Q_{bui} - C_{in} \frac{dT_{in}}{dt} A_{in} \quad \text{(A.7)}$$

$$\Delta Q_{dem} = -\Delta Q_{bui} \tag{A.8}$$

where, Q_{dem} is the predicted heating/cooling demand of the building. Q_{fr}, Q_{conv}, Q_{infil} are the heat gains from fresh air induction, convective heat gains, and air infiltration respectively. T_{in}, C_{in}, A_{in} are temperature of indoor air, thermal capacitance (per square meter) and effective area of indoor air respectively. ΔQ_{bui} and ΔQ_{dem} are the changing/discharging rate of the building thermal masses and the alteration of the building demand load respectively.

The key function of the simplified thermal storage model is to predict the charging/discharging rate of a building as shown in Eq. A.9. The charging/discharging rate (i.e., the heating/cooling load alteration potential) of building thermal masses can be summarized in Eq. A.9 to 13.

$$\Delta Q_{bui}(t) = \begin{cases} \Delta Q_{pre,c}(t) & t \in [0, t_{char}] \\ \Delta Q_{pre,c}(t) + \Delta Q_{set,d}(t) & t \in [0, t_{dis}] \end{cases} \tag{A.9}$$

where,

$$\Delta Q_{pre,c}(t) = \frac{\Delta T_{in,char}}{R_{bui,ou}+R_{bui,inn}}(1 + \alpha e^{\frac{-t}{\tau_{bui}}})A_{bui} \tag{A.10}$$

$$\Delta Q_{set,d}(t) = \frac{\Delta T_{in,dis}}{R_{bui,ou}+R_{bui,inn}}(1 + \alpha e^{\frac{-t}{\tau_{bui}}})A_{bui} \tag{A.11}$$

$$\Delta Q_{pre,h}(t) = -\alpha \frac{\Delta T_{in,char}}{R_{bui,ou}+R_{bui,inn}}(1 - e^{\frac{-t_{char}}{\tau_{bui}}})e^{\frac{-t}{\tau_{bui}}}A_{bui} \tag{A.12}$$

$$\alpha = \frac{R_{bui,ou}}{R_{bui,inn}} \tag{A.13}$$

where, $\Delta Q_{pre,c}$, $\Delta Q_{pre,h}$ and $\Delta Q_{set,d}$ are the heating/cooling load alterations corresponding to the precooling, preheating and the temperature set-point reset strategies during the

charging and discharging periods respectively. $\Delta T_{in,char}$ and $\Delta T_{in,dis}$ are the temperature set-point differences between the altered cases and the reference case during the charging and discharging periods respectively. α is the ratio of the building outer thermal resistance to the inner thermal resistance. t_{char} and t_{dis} are the durations of charging and discharging.

It is worth noticing that the thermal storage model is considered to be too simple to represent the full characteristics of building heating/cooling load accurately. Therefore, it is not suitable for predicting building heating and cooling loads. In this thesis, this simplified building thermal storage model is only used for prediction of building cooling load alternations, i.e. the changes of the cooling load referring to corresponding reference.

Although different types of buildings, e.g. light weighted, medium weighted and heavy weighted, have different storage capabilities and energy performances [Xue et al, 2014]. The heating/cooling load alternation potentials and thermal characteristics of different types of buildings can be accordingly represented by the same thermal storage model as well. In the simplified building thermal storage, C_{bui}, $R_{bui,ou}$ and $R_{bui,inn}$ of a building and the overall COP of the HVAC system are the key coefficients to be identified.

Table A.1 Identified parameters of the thermal storage model

Building type	$R_{bui,ou}$ (m^2K/W)	$R_{bui,inn}$ (m^2K/W)	R_{bui} (m^2K/W)	α	τ (hour)
Medium weighted	0.32	0.28	0.15	1.14	10.97

Identification of the parameters and validation of the thermal storage model for ICC building are conducted by using building historical operation data such as the daily

cooling demand in the baseline case. A genetic algorithm-based (GA-based) method is used to identify these parameters for the simulated building [Xue et al, 2014], as listed in Table A.1. The medium weighted building in this study follows the definition of ASHRAE, which is defined mainly based on concrete thickness of the structure. The main part of medium weighted external wall is the concrete of thickness which is 100 mm. The building envelope is medium weighted as normally defined.

REFERENCES

US, Energy Information Administration, Office of Energy Markets and End Use, 2010 Department of Energy, Annual Energy Review.

Xiao F., Wang S.W.. 2009. Progress and methodologies of lifecycle commissioning of HVAC systems to enhance building sustainability. Renewable and Sustainable Energy Reviews 13(5): 1144-9.

Motegi N., Piette M.A., Watson D.S., Kiliccote S., Xu P. 2005. Introduction to Commercial Building Control Strategies and Techniques for Demand Response. Berkeley: Lawrence Berkeley National Laboratory: LBNL-59975.

Arteconi A., Hewitt N.J., Polonara F. 2012. State of the art of thermal storage for demand-side management. Applied Energy 93: 371-89.

Escrivá-Escrivá G. 2011. Basic actions to improve energy efficiency in commercial buildings in operation. Energy and Buildings 43(11):3106-3111.

Wang S.W., Ma Z.J.. 2008. Supervisory and Optimal Control of Building HVAC Systems: A Review. HVAC&R Research 14(1):3-32.

ASHRAE Design Guide for Cool Thermal Storage, 1993, American Society of Heating, Refrigerating, and Air-Conditioning Engineers, Inc. 1791 Tullie Circle, N.E., Atlanta, GA 30329, U.S.A.

Sun Y.J., Wang S.W., Xiao F., Gao D.C.. 2013. Peak load shifting control using different cold thermal energy storage facilities in commercial buildings: A review. Energy Conversion and Management 71: 101-14.

Watson D.S., Kiliccote S., Motegi N., Piette M.A. 2006. Strategies for demand response in commercial buildings. Proceedings of 2006 ACEEE Summer Study on Energy

Efficiency in Buildings, Pacific Grove, USA.

Kirby B.. 2006. Demand Response for Power System Reliability: FAQ. Oak Ridge National Laboratory 2006: Technical Report ORNL/TM-2006/565.

Soares L.J., Medeiros M.C. 2008. Modeling and forecasting short-term electricity load: A comparison of methods with an application to Brazilian data. International Journal of Forecasting 24(4): 630-44.

Elleson J.S. 1997. Successful cool storage projects: from planning to operation. American Society of Heating, Refrigerating and Air-conditioning Engineers, Inc. 1791 Tullie Circle, N.E., Atlanta, GA 30329, U.S.A.

Hasnain SM. 1998. A review on sustainable thermal, energy storage technologies, part II: cool thermal storage. Energy Conversion and Management 39(11):1139-53.

Henze G. P., Felsmann C., and Knabe G. 2004. Evaluation of optimal control for active and passive building thermal storage. International Journal of Thermal Sciences 43(2): 173–83.

Zhu N., Ma Z.J. and Wang S.W. 2009. Dynamic characteristics and energy performance of buildings using phase change materials: A review. Energy Conversion and Management 50: 3169-81.

Ibrahim D, Rosen M.A. 2002. Thermal energy storage: systems and applications. New York: Wiley Ltd.

Mackie E.I, Reeves G. 1998. Stratified chilled water storage tank design guide. PaoloAlto, CA: Electric Power Research Institute.

Yau Y.H., Rismanchi B. 2012. A review on cool thermal storage technologies and operating strategies. Renewable and Sustainable Energy Reviews 16 (1): 787 – 797.

Chan A.L.S., Chow T.T., Fong S.K.F., Lin J.Z. 2006. Performance evaluation of district

cooling plant with ice storage. Energy 31(14): 2750-62.

Lee A.H.W., Jones J.W. 1996. Modeling of an ice-on-coil thermal energy storage system. Energy Conversion and Management 37 (10):1493-507.

Shi W., Wang B., Li X. 2005. A measurement method of ice layer thickness based on resistance-capacitance circuit for closed loop external melt ice storage tank. Applied Thermal Engineering 25(11-12): 1697-707.

Zhu Y.X., Zhang Y. 2001. Modeling of thermal processes for internal melt ice-on-coil tank including ice-water density difference. Energy and Buildings 33(4): 363-70.

Erek A., Dincer I. 2009. Numerical heat transfer analysis of encapsulated ice thermal energy storage system with variable heat transfer coefficient in downstream. International Journal of Heat and Mass Transfer 52(3):851-59.

Pasupathy A., Velraj R., Seeniraj R. 2008. Phase change material-based building architecture for thermal management in residential and commercial establishments. Renewable and Sustainable Energy Reviews 12(1): 39–64.

Oró E., Gracia A., Castell A., Farid M.M., Cabeza L.F. 2012. Review on phase change materials (PCMs) for cold thermal energy storage applications. Applied Energy 99: 513–33.

Braun J.E. 2003. Load control using building thermal mass. Journal of solar energy engineering 125:292-301.

Zhu N., Xu X.H., Wang S.W., Ma Z.J. 2010. A simplified dynamic model of building structures integrated with shaped-stabilized phase change materials. International Journal of Thermal Sciences 49(9):1722-31.

Huang S.J., Huang C.C. 2000. An adaptive load shedding method with time-based design for isolated power systems. Electrical Power and Energy Systems 22 (1): 51 – 58.

Henze G.P., Krarti M., Brandemuehl M.J. 1997. A simulation environment for the analysis of ice storage controls. HVAC&R Research 3(2):128–48.

Henze G.P., Dodier R.H., Krati M. 1997. Development of a predictive optimal controller for thermal storage system. HVAC&R Research 3 (3) (1997):234-64.

Lee W.S., Chen Y.T., Chen T.H. 2009. Optimization for ice-storage air-conditioning system using particle swarm algorithm. Applied Energy; 86(9): 1589-95.

Drees K.H., Braun J.E. 1996. Development and evaluation of a rule-based control strategy for ice storage systems. HVAC&R Research 2(4):332-35.

Braun J.E. 2007. A near-optimal control strategy for cool storage systems with dynamic electric rates. HVAC&R Research 13(4): 557- 80.

Massie D., Curtiss P., Kreider J.K. 2004. Neural network optimal controller for commercial ice thermal storage system. ASHRAE Transactions 110(2):361-69.

Ma Y., Borrelli F., Hencey B., Packard A., Bortoff S. 2009. Model predictive control of thermal energy storage in building cooling systems. In the proceeding of 48th IEEE Conference on Decision and Control held jointly with 28th Chinese Control Conference. Shanghai, P.R. China, December 16-18.

Ashok S., Banerjee R. 2003. Optimal cool storage capacity for load management. Energy 28(2):115-26.

Arkin H., Navon R., Burg I. 1997. HVAC with thermal energy storage: optimal design and optimal scheduling. Journal of Building Services Engineering Research and Technology 18(1):31-38.

Navon R., Arkin H. 1997. Economic evaluation of HVAC systems with ice storage designed using an optimization technique. Construction Management and Economics 15(5): 429-39.

Chen C.S., Sheen J.N. 1993. Cost benefit of a cooling energy storage system. IEEE Transactions on Power Systems 8(4): 1504-10.

Yin R.X., Xu P., Piette M.A., Kiliccote S. 2010. Study on auto-DR and pre-cooling of commercial buildings with thermal mass in California. Energy and buildings 42(7): 967–75.

Ma J.R., Qin J., Salsbury T., P. Xu. 2012. Demand reduction in building energy systems based on economic model predictive control. Chemical Engineering Science 67(1):92–100.

Sun Y.J., Wang S.W., Xiao F., Huang G.S. 2012. A study of precooling impacts on peak demand limiting in commercial buildings. HVAC&R Research 18(6): 1098-11.

Sun Y.J., Wang S.W., Huang G.S. 2010. A demand limiting strategy for maximizing monthly cost saving of commercial buildings. Energy and Building 42 (11): 2219- 30.

Xu P., Haves P., Braun J.E., Hope L.T. 2004. Peak demand reduction from pre-cooling with zone temperature reset in an office building. In proceedings of 2004 ACEEE summer study of energy efficiency in buildings, Pacific Grove, CA.

Lee K.H., Braun J.E. 2008. Development of methods for determining demand-limiting set-point trajectories in buildings using short-term measurements. Building and Environment 43 (10): 1755–68.

Lee K.H., Braun J.E. 2008. Evaluation of methods for determining demand-limiting setpoint trajectories in buildings using short-term measurements. Building and Environment 43 (10): 1769–83.

Braun J.E., Montgomery K.W., Chaturvedi N. 2001. Evaluating the Performance of Building Thermal Mass Control Strategies. HVAC&R Research 7(4): 403- 2.

Cheng H., Brandemuehl M.J., Henze G.P., Florita A.R., Felsmann C. 2008. Evaluation

of the primary factors impacting the optimal control of passive thermal storage. ASHRAE Transactions 114: 57–64.

Ma Y., Kelman A., Daly A., Borrelli F. 2012. Predictive control for energy efficient buildings with thermal storage: modeling, stimulation, and experiments. IEEE Control Systems 32 (1): 44 – 64.

Zhu N., Wang S.W., Ma Z.J., Sun Y.J. 2011. Energy performance and optimal control of air-conditioned buildings with envelopes enhanced by phase change materials. Energy Conversion and Management 52(10): 3197-205.

Halford C.K., Boehm R.F. 2007. Modeling of phase change material peak load shifting. Energy and Buildings 39(2): 298–305.

Kondo T., Ibamoto T. 2006. Research on thermal storage using rock wool phase change material ceiling board. ASHRAE Transactions 112(1): 526–31.

Stetiu C., Feustel H.E. 1998. Phase Change Wallboard and Mechanical Night Ventilation in Commercial Buildings. Berkeley: Lawrence Berkeley National Laboratory.

Henze G.P., Kalz D., Felsmann C., Knabe G. 2004. Impact of forecasting accuracy on predictive optimal control of active and passive building thermal storage inventory. HVAC&R Research 10(2):153–78.

Liu S.M., Henze G.P. 2004. Impact of modeling accuracy on predictive optimal control of active and passive building thermal storage inventory. ASHRAE Transactions 110(1):151–63.

Henze G.P. 2005. Energy and Cost Minimal Control of Active and Passive Building Thermal Storage Inventory. Journal of Solar Energy Engineering, Transaction of the ASME 127(3):343-51.

Liu S.M., Henze G.P. 2007. Evaluation of reinforcement learning for optimal control of building active and passive thermal storage inventory. Journal of Solar Energy Engineering 129 (2):215–25.

Zhou G., Krarti M., Henze G.P. 2005. Parametric analysis of active and passive building thermal storage utilization. Journal of Solar Energy Engineering –Transaction of the ASME 127(1):37-46.

Henze G.P., Kalz D., Liu S.M., Felsmann C. 2005. Experimental analysis of model-based predictive optimal control for active and passive thermal storage inventory. HVAC&R Research 11 (2): 189–213.

Department of Energy, U.S. 2006. Benefits of demand response in electricity markets and recommendations for achieving them: report to U.S. Congress pursuant to section 1252 of the Energy Policy Act of 2005. Washington D.C.: U.S. Department of Energy. See also http://eetd.lbl.gov/ea/EMP/reports/congress-1252d.pdf.

Federal Energy Regulatory Commission. U.S. 2011. Demand Response Compensation in Organized Wholesale Energy Markets. Issued March 15, 2011. http://www.ferc.gov/EventCalendar/Files/20110315105757-RM10-17-000.pdf

Surles W., Henze G.P. 2012. Evaluation of automatic priced based thermostat control for peak energy reduction under residential time-of-use utility tariffs. Energy and Buildings 49: 99-108.

EMSD. 2012. Hong Kong Energy End-use Data. The Energy Efficiency Office, EMSD, Hong Kong.

Zhou K.L., Yang S.L., and Shen C. 2013. A review of electric load classification in smart grid environment. Renewable and Sustainable Energy Reviews 24:103-110.

Xu P., Haves P. 2006. Case study of demand shifting with thermal mass in two large commercial buildings. ASHRAE transactions 112(1): 572-80.

Yin R.X., Xu P., Piette M.A., Kiliccote S. 2010. Study on auto-DR and pre-cooling of commercial buildings with thermal mass in California. Energy and Buildings 42(7): 967-75.

Xu P., Haves P., Piette M.A., Zagreus L. 2005. Demand shifting with thermal mass in large commercial buildings: field tests, simulation and audits. Berkeley: Lawrence Berkeley National Laboratory: LBNL-58815.

Kiliccote S., Piette M.A., Warson D.S. 2006. Dynamic controls for energy efficiency and demand response: Framework concepts and a New Construction study case in New York. Proceedings of the 2006 ACEEE Summer study on energy efficiency in buildings, Pacific Grove, CA, August.

Erickson V.L., Cerpa A.E. 2010. Occupancy Based Demand Response HVAC Control Strategy. Proceedings of the 2nd ACM Workshop on Embedded Sensing Systems for Energy-Efficiency in Building, BuildSyst '10, ACM, New York, NY, USA 2010:7–12.

Katipamula S., Lu N. 2006. Evaluation of residential HVAC control strategies for demand response programs. ASHRAE Transactions 112(1): 535-546.

Chen Y.H., Li J. 2011. Comparison of security constrained economic dispatch formulations to incorporate reliability standards on demand response resources into Midwest ISO co-optimized energy and ancillary service market. Electric Power Systems Research 81: 1786– 95.

Hao Y H., Middelkoop T., Barooah P., and Meyn S. 2012. How demand response from commercial buildings will provide the regulation needs of the grid. In Communication, Control and Computing (Allerton), 50th Annual Allerton Conference on, 2012:1908-13.

Kiliccote S., Piette M.A., Koch E., Hennage D. 2010. Utilizing automated demand response in commercial buildings as non-spinning reserve product for ancillary services markets. In IEEE conference on decision and control (CDC), Atlanta, USA, 2010.

Kiliccote S. 2013. Field testing of automated demand response for integration of renewable resources in California's ancillary services market for regulation products. Berkeley: Lawrence Berkeley National Laboratory: LBNL-5556E.

Eto J., Nelson-Hoffman J., Torres C., Hirth S., Yinger B., Kueck J., Kirby B., Bernier C., Wright R., Barat A., Watson D. 2006. Demand response spinning reserve demonstration. Berkeley: Lawrence Berkeley National Laboratory: LBNL-62761.

Lu N. 2012. An evaluation of the HVAC load potential for providing load balance service. IEEE Transactions on Smart Grid 3(2): 1263-70.

Lin Y., Barooah P., and Meyn S. 2013. Low-frequency power-grid ancillary services from commercial building HVAC systems. In proceedings of the IEEE international conference on Smart Grid Communications. Oct, 2013: 169-74.

Yan C.C., Xue X., Wang S.W., Cui B.R. 2014. A novel air-conditioning system for proactive power demand response to smart grid. Energy Conversion and Management 2014; http://dx.doi.org/10.1016/j.enconman.2014.09.072.

Wang S.W., Wang J., Burnett J. 2000. Mechanistic model of centrifugal chillers for HVAC system dynamics simulation. Buildings Services Engineering Research & Technology 21(2):73-83.

Braun J.E., Klein S.A. and Mitchell J.M. 1989. Effectiveness models for cooling towers and cooling coils. ASHRAE Transactions 95(2):164-74.

Wang S.W. 1998. Dynamic simulation of a building central chilling system and evaluation of EMCS on-line control strategies. Building and Environment 33(1): 1-20.

Wang S.W., Xu X.H. 2006. Parameter estimation of internal thermal mass of building dynamic models using genetic algorithm. Energy Conversion and Management 47(13-14):1927-1941.

Xue X., Wang S.W., Sun Y.J., Xiao F. 2014. An interactive building power demand management strategy for facilitating smart grid optimization. Applied Energy 116: 297-310.

Wu S.W., Fang G.Y., Chen Z. 2012. Discharge characteristics modeling of cool thermal energy storage system with coil pipes using n-tetradecane as phase change material. Applied Thermal Energy 37:336-43.

Castell A., Belusko M., Bruno F., Cabeza L.F. 2011. Maximisation of heat transfer in a coil in tank PCM cold storage system. Applied Energy 88(11): 4120-7.

PCM Products Ltd. Sales Literature, www.pcmproducts.net

Samuelson P.A., Nordhaus W.D. 2010. Economics. 19 th ed. New York: McGraw-Hill.

Rittenberg L, Tregarthen T. 2009. Principles of Microeconomics. Irvington, NY: Flat World;

Henze G.P., Felsmann C., Cheng H., Florita A.R., Brandemuehl M.J. 2010. Advances in near-optimal control of passive building thermal storage. Journal of Solar Energy Engineering 132(2):271–80.

Xue X., Wang S.W., Yan C.C., Cui B.R. 2015. A fast chiller power demand response control strategy for buildings connected to smart grid. Applied Energy 137: 77-87.

Mathieu J.L., Price P.N., Kiliccote S., Piette M.N. 2011. Quantifying changes in building electricity use, with application to demand response. IEEE Transactions on Smart Grid 2011 2 (3): 507–18.

Cui B.R., Wang S.W., Sun Y.J. 2014. Life-cycle cost benefit analysis and optimal

design of small scale active storage system for building demand limiting. Energy 73: 787-800.

Rahimi R., Ipakchi A. 2010. Demand response as a market resource under the smart grid paradigm. IEEE Transactions on Smart Grid 2010 1(1): 82 – 88.

ISO New England Inc. 2009. Technical feasibility and value to the market of smaller demand response resources providing ancillary services. ISO New England Inc. Oct 28, 2009.

Oldewurtel F., Borsche T., Bucher M., Fortenbacher P., Haring M.G.V.T., Mathieu J.L., Megel O., Vrettos E., Andersson G. 2013. A framework for and assessment of demand response and energy storage in power systems. 2013 IREP Symposium-Bulk Power System Dynamics and Control -IX (IREP), August 25-30, 2013, Rethymnon, Greece.